Protection of Different Configured Transmission Lines and Frequency Control of Microgrid Using Artificial Intelligent Techniques

Submitted in partial fulfilment of the requirements

for the award of the degree of

DOCTOR OF PHILOSOPHY
in
Electrical Engineering

By
Gotte Vikram Raju
(Roll No. 718124)

Supervisor:

Dr. N.V. Srikanth
Professor

DEPARTMENT OF ELECTRICAL ENGINEERING
NATIONAL INSTITUTE OF TECHNOLOGY, WARANGAL
(An Institute of National Importance)
HANUMAKONDA, TELANGANA STATE, INDIA – 506004
April – 2024

APPROVAL SHEET

This Thesis work entitled **"Protection of Different Configured Transmission Lines and Frequency Control of Microgrid Using Artificial Intelligent Techniques"** by **Gotte Vikram Raju**, bearing **Roll No: 718124**, is approved for the degree of **Doctor of Philosophy** in **Electrical Engineering** from **National Institute of Technology, Warangal**.

Examiners

_____

_____

_____

Supervisor

_____

Dr. N. V. Srikanth
Professor
Department of Electrical Engineering
NIT Warangal

Chairman

_____

Dr. Ch. Venkaiah
Professor
Department of Electrical Engineering
NIT Warangal

Date : _____
Place : NIT Warangal

DEPARTMENT OF ELECTRICAL ENGINEERING
NATIONAL INSTITUTE OF TECHNOLOGY, WARANGAL
HANUMAKONDA, TELANGANA STATE, INDIA – 506 004

CERTIFICATE

This is to certify that the thesis entitled **"Protection of Different Configured Transmission Lines and Frequency Control of Microgrid Using Artificial Intelligent Techniques"** which is being submitted by **Mr. Gotte Vikram Raju (Roll No. 718124)**, is a bonafide work submitted to National Institute of Technology, Warangal in partial fulfilment of the requirements for the award of the degree of **Doctor of Philosophy** in Department of Electrical Engineering. To the best of my knowledge, the work incorporated in this thesis has not been submitted elsewhere for the award of any degree.

Dr. N.V. Srikanth
(Supervisor)
Professor
Department of Electrical Engineering
National Institute of Technology, Warangal

Date:

Place: NIT Warangal

DECLARATION

This is to certify that the work presented in the thesis entitled "**Protection of Different Configured Transmission Lines and Frequency Control of Microgrid Using Artificial Intelligent Techniques"** is a bonafide work done by me under the supervision of **Dr. N. V. Srikanth**, Professor, Department of Electrical Engineering, National Institute of Technology, Warangal, India and was not submitted elsewhere for the award of any degree.

I declare that this written submission represents my ideas in my own words and where others' ideas or words have been included; I have adequately cited and referenced the original sources. I also declare that I have adhered to all principles of academic honesty and integrity and have not misrepresented or fabricated or falsified any idea/date/fact/source in my submission. I understand that any violation of the above will be a cause for disciplinary action by the institute and can also evoke penal action from the sources which have thus not been properly cited or from whom proper permission has not been taken when needed.

Gotte Vikram Raju
(Roll No: 718124)

Date:
Place: NIT Warangal

ACKNOWLEDGEMENTS

It gives me immense pleasure to express my deep sense of gratitude and thanks to my supervisor **Dr. N. V. Srikanth,** Professor, Department of Electrical Engineering, National Institute of Technology Warangal, for his invaluable guidance, support, and suggestions. His knowledge, suggestions, and discussions helped me to become a capable researcher. He has shown me the interesting side of this wonderful and potential research area. His encouragement helped me to overcome the difficulties encountered in my research as well as in my life.

I am very much thankful to **Prof. B. L. Narasimharaju,** Head, Department of Electrical Engineering for his constant encouragement, support and cooperation.

I would like to express my sincere gratitude to **Dr. D. M. Vinod Kumar (HAG),** Professor (Retd.), Department of Electrical Engineering for his constant technical suggestions, encouragement, support and cooperation during the progress of this research work.

I thank all my Doctoral Scrutiny Committee members, **Dr. Ch. Venkaiah,** Professor, Department of Electrical Engineering, **Dr. A. V. Giridhar,** Associate Professor, Department of Electrical Engineering, **Dr. Altaf Q. H. Badar,** Assistant Professor, Department of Electrical Engineering and **Dr. N. Bheema Rao,** Professor, Department of Electronics and Communication Engineering for their detailed review, constructive suggestions and excellent advice during the progress of this research work.

I also appreciate the encouragement from teaching and non-teaching members, and the fraternity of Department of Electrical Engineering of NIT Warangal. They have always been encouraging and supportive.

I wish to express my sincere thanks to **Prof. Bidyadhar Subudhi**, Director, NIT Warangal for his official support and encouragement.

I convey my special thanks to the contemporary Research Scholars Mr. Anil Kumar A, Mr. Laxman B, Mr. Lokesh V, Mr. Dinesh Kumar Ambati and Mr. Ravi Kumar G. I acknowledge my gratitude to all my teachers and colleagues at various places for supporting me to complete the work.

My special thanks, sincere acknowledgement, heartfelt gratitude and indebtedness are due to my parents **Shri. Gotte Yellaiah** & **Smt. Gotte Aruna,** my wife (Gotte Moukthika), my brothers (Dr. Gotte Ramesh and Gotte Vamshi Krishna) and other family members for their sincere prayers, blessings, constant encouragement, shouldering the responsibilities and moral support rendered to me throughout my life, without which my research work would not have been possible.

Above all, I express my deepest regards and gratitude to "**ALMIGHTY**" whose divine light and warmth showered upon me the perseverance, inspiration, faith and enough strength to keep the momentum of work high even at tough moments of research work.

Gotte Vikram Raju

Ж

ABSTRACT

Protection and control are crucial to maintain the stable operation of the power systems. Growth in global electricity consumption due to urbanization and industrialization, demands enhanced generation and transmission capacities with higher order network configurations. Power transmission network plays a vital role in transmitting power to distant areas or load centres. Often, renewable energy integration into power systems is encouraged due to low carbon emissions. There is a steady growth in the amount of renewable energy generation every year. The geographically dispersed nature and intermittent generation of renewables require increased transmission capabilities to move excess energy to distant load centres. Rising power demand and renewable integration are a challenge to the power system's protection and control. In order to have improved system stability, reduced service disruptions, and enhanced power delivery efficiency, the protection of transmission lines and frequency control of the system are vital. This work focuses on artificial intelligent protection schemes for various transmission line configurations (double circuit three-phase, single circuit six-phase, and single circuit three-phase), to ensure reliable and secure power transmission and control strategy for frequency control of microgrid. The main aim of the transmission line protection scheme is to identify and isolate the fault as quickly as possible to maintain the stability of the system. The quick detection and classification of faults help the repairmen or maintenance crew to improve the service restoration time.

An intelligent protection scheme is proposed based on a single fuzzy inference system and discrete Fourier transform towards the faulty phase detection and classification on the mutually coupled double circuit lines. This proposed protection technique uses the magnitude of the pre-processed current information measured at the sending end bus only. This is implemented in the MATLAB/Simulink environment on a 400 kV, 50 Hz, and 300 km double circuit transmission line model. The efficacy of the proposed scheme has been tested by performing a wide range of simulation studies concerning different types of faults viz. common short circuit faults, cross-country and evolving faults, and high impedance faults. Typical fault scenarios viz. current transformer saturation, noisy environment, and faults occurring during power swing scenarios with variations in different fault parameters and operating conditions were also studied. The results presented confirm that the proposed method detects/classifies all types of faults within one cycle time and is reliable with a detection/classification accuracy of 99.75%. It is found immune to the variations in fault

parameters and for varying operating conditions. Also, it is not affected by the zero-sequence mutual impedance of the line and does not require any training and communication link. Furthermore, the performance is also appraised with other training-based protection schemes.

The enhanced power transfer capability is possible with the six-phase transmission system but it did not gain popularity due to the lack of a proper protection scheme to secure the line for 120 types of different possible short circuit faults. This work presents a comprehensive protection scheme utilizing discrete wavelet transform (db4 mother wavelet) and artificial neural networks (ANNs). Levenberg-Marquardt algorithm is used for training the ANNs. This protection scheme requires only pre-processed current information of the sending end bus. For fault detection and classification of all 120 types of faults, a single ANN module is implemented with six inputs and six outputs. For the estimation of fault location in each phase, 11 ANN modules with six outputs are used viz. one for each of the 11 types of combination of faults. The proposed protection scheme is implemented on a six-phase Allegheny power transmission system using MATLAB/Simulink platform. The simulation results prove its efficiency and effectiveness in detecting and classifying all types of faults with varying parameters. All fault types are detected/classified within one cycle time and the detection/classification accuracy is found to be 99.76%. It is found that the performance of the fault location estimation modules is better with the training data and moderate with the testing data.

The integration of renewable energy sources (RES), such as solar and wind power, into power systems presents unique challenges for transmission line protection. Traditional distance protection schemes may not be adequately sensitive or adaptable to the dynamic characteristics of RES-connected lines. To address these challenges, this work proposes an intelligent novel protection scheme that combines the fuzzy logic system for fault detection/classification with regression-based bagged ensemble learning for fault location estimation. The proposed scheme utilizes voltage signals of the bus connected to renewable energy sources processed with discrete Fourier transform (DFT) to extract relevant features for fault diagnosis. A Mamdani based fuzzy inference system is implemented to analyze the DFT-extracted features and make decisions regarding fault occurrence and type. A bagged ensemble learning approach, incorporating multiple regression trees, is employed to accurately estimate the fault location along the transmission line. The performance and efficacy of the proposed protection scheme are verified through extensive

MATLAB/Simulink simulations on the transmission line model integrated with renewable energy sources (solar and wind). The simulations were carried out considering the variations in fault parameters with different solar irradiations and wind speeds. The results demonstrate that the scheme effectively detects and classifies various fault types in one cycle time, even under dynamic RES generation conditions. The proposed scheme achieved 99.56% accuracy in fault detection/classification confirming its reliable operation. Further, the proposed fault location estimation approach approximates the fault location within ±5% error band and the Chi-square test is performed to assess its reliability.

However, apart from the protection of transmission lines, there is another equally concerned issue as much as protection i.e., frequency control of microgrid. Microgrid (MG) is a combination of diesel engine generators, renewable energy sources, loads and various energy storage systems. The low inertia of the microgrid system, stochastic loads and intermittent/discontinuous generation of renewables create complications in the frequency control of microgrid. Massive frequency deviations will cause stability and reliability problems and sometimes may lead to microgrid blackouts.

A more rugged and efficient control action is needed to ameliorate the frequency stability of the microgrid. Therefore, a multi-stage PID controller whose parameters are optimized by the moth flame optimization (MFO) algorithm is proposed to control the frequency of an islanded Bella Coola microgrid. This microgrid has renewable energy sources and coordinated control of plug-in hybrid electric vehicles with diesel engine generators. Some popular meta-heuristic based PID control techniques viz. PSO-PID, TLBO-PID, and GOA-PID are also applied to assess the superior performance of the MFO algorithm. The effectiveness of the proposed control method is evaluated on the Bella Coola microgrid to obtain its dynamic response considering the simultaneous changes in renewable energy sources, load, and parametric uncertainties. The dynamic response of the microgrid is enhanced significantly which is confirmed through MATLAB/Simulink simulation results. Moreover, the proposed multi-stage PID controller is robust towards parametric uncertainties of microgrid and plug-in hybrid electric vehicles as compared to other PID controllers. The stability and comparison analysis prove that the proposed method works efficiently.

*****

Contents

Page No.

List of Figures

List of Tables

List of Abbreviations and Symbols

AFL	Actual fault location
AGC	Automatic generation control
AI	Artificial intelligence
ANFIS	Artificial neuro fuzzy inference system
ANN	Artificial neural network
ANN_FDC	Artificial neural network_Fault detection and classification
ANN_FLE	Artificial neural network_Fault location estimation
CCF	Cross-country fault
CSA	Cuckoo search algorithm
CT	Current transformer
D	Damping coefficient of microgrid load
DCTL	Double circuit transmission lines
DEG	Diesel engine generator
DFIG	Doubly fed induction generator
DFT	Discrete Fourier transform
DWT	Discrete wavelet transform
E_{fl} (or) EFL	Estimated fault location
EHV	Extra high voltage
ELM	Extreme learning machine
ESS	Energy storage systems
FACTS	Flexible alternating current transmission system
FD	Fault detection
FDC	Fault detection and classification
FFA	Firefly algorithm
FI	Fault index
FIA	Fault inception angle
FIS	Fuzzy inference system
FIT	Fault inception time
FLE	Fault location estimation
FPS	Fault during power swing
FSA	Future search algorithm

Δf	Frequency deviation of microgrid
GA	Genetic algorithm
GOA	Grasshopper optimization algorithm
GPR	Gaussian process regression
GRC	Generation rate constraint
GSC	Grid side converter
GWO	Grey wolf optimization
HIF	High impedance fault
HPF	High-pass filter
HSA	Harmony search algorithm
HVDC	High voltage direct current
ITAE	Integral time absolute error
K_{EV}, K_{PV}, K_{WTG}	Gain constants of EV's participation, PV and WTG systems
K_t	Temperature coefficient of PV
L_a	Actual fault location
L_f	Fault location
LD	Load disturbance power
LFC	Load frequency control
LG	Line to ground
LL	Line to line
LLG	Line to line to ground
LLL	Line to line to line
LMA	Levenberg-Marquardt algorithm
LPF	Low-pass filter
M	Moment of inertia of microgrid
MF	Membership function
MFO	Moth flame optimization
MFCC	Magnitude of the fundamental component of current
MFCV	Magnitude of the fundamental component of voltage
MG	Microgrid
MODWT	Maximal overlap discrete wavelet transform
MPID	Multi-stage PID controller
MPPT	Maximum power point tracking

mse	Mean squared error
NF	No-fault
NFL	No free lunch
N_{EV}	Number of electric vehicles
N_{sf}	Number of non-simultaneous short circuit faults
OF	Objective value of flame
OM	Objective value of moth
PD	Proportional derivative
PFC	Primary frequency control
PHEVs	Plug-in hybrid electric vehicles
PI	Proportional integral
PID	Proportional integral derivative
PLL	Phase locked loop
P&O	Perturb and observe
POS	Peak overshoot
PS	Power swing
PSB	Power swing blocking
PSO	Particle swarm optimization
PUS	Peak undershoot
PV	Photovoltaic
PVD	Photovoltaic disturbance power
PWM	Pulse width modulation
P_{solar}	Rated power of solar panel at standard operating conditions
ΔP_{DEG}	Change in DEG output power
ΔP_{PHEV}	Change in PHEV output power
ΔP_{L}	Change in load power of microgrid
ΔP_{PV}	Change in PV output power
ΔP_{WTG}	Change in WTG output power
R	Speed regulation constant of DEG
R_{av}	Droop coefficient of PHEV
RES	Renewable energy sources
R_f	Fault resistance
RMS	Root mean square

RSC	Rotor side converter
SCC	Short circuit capacity
SFC	Secondary frequency control
SNR	Signal to noise ratio
SOC	State of charge
SSO	Social spider optimization
ST	Settling time
STC	Standard test conditions
std	Standard deviation
SVM	Support vector machine
TCSC	Thyristor-controlled series capacitor
TF	Transfer function
T_a	Ambient temperature
T_{EV}, T_{PV}, T_{WTG}	Time constants of electric vehicle battery, PV and WTG systems
T_f	Fault inception time or time of fault
T_1, T_2,T_3	Time constants of the governor, transport delay and DEG
T_{STC}	Temperature at standard test conditions
TLBO	Teaching learning based optimization
TPIC	Three phase instantaneous currents
VSI	Voltage source inverter
WD	Wind disturbance power
WTG	Wind turbine generator
ZSC	zero sequence current
β	Blade pitch angle
Φ	Fault inception angle
$\Delta\delta$	Power flow angle
φ	Solar irradiance

Chapter 1

Introduction

1.1 Introduction

Protection and control of power systems are the thrust of research areas in the present era. In recent times, due to urbanization, industrialization and population growth, the world has witnessed a drastic rise in electrical energy/power consumption. The electrical energy consumption has reached approximately 23643 Terra Watt hour globally in the year 2022 [1]. To meet the growing demands, the generation and transmission capacities must be increased. The power transmission network plays a vital role in meeting the growing electrical demand. Transmission lines are the backbone of the electrical grid, carrying electricity from power plants to consumers over long distances. They facilitate electricity trading between different regions and countries. Also, facilitates the integration of renewable energy sources. To have enhanced power transmission capabilities with better efficiencies, higher order power transmission network configurations are preferred. Furthermore, nations across the world have aimed towards reducing the carbon emissions by encouraging renewable energy sources to generate clean energy. Despite the global economic crisis in 2020, there is a considerable rise in global renewable energy generation with capacity reaching 260 GW during COVID 2019 pandemic. Solar (127 GW) and wind (111 GW) dominated this capacity expansion by 91% [2]. Higher levels of renewable energy penetration have been witnessed in the distribution levels and installation of renewable energy sources has also creeped into the sub-transmission levels. In the next few years, it is presumed that the penetration of renewables may also take place at the transmission levels. This penetration of renewable energy sources in the transmission and distribution sectors poses challenges to protection and control, especially towards the load frequency control of the microgrid. However, due to the terrestrial and environmental conditions, renewable energy generation is not possible at all the locations. The excess renewable energy generated is to be transmitted to the load centres wherever it is required. The resulting intermittent generation and centralized demand require increased transmission capabilities.

In view of the above, to handle the power, the most viable configurations of the transmission networks are required. The transmission lines spread over long distances are exposed to different weather conditions and are easily prone to fault conditions as insulation is not provided. Faults on transmission lines are inevitable. A reliable protection scheme ensures the safe and secure operation of the transmission network with minimal interruption and early restoration of the quality power supply. The main aim of the transmission line

protection scheme is to identify and isolate the fault as quickly as possible to maintain the stability of the system. The quick detection and classification of faults help the repairs/maintenance crew to improve the service restoration time. However, apart from the protection of transmission lines which transfer the generated electrical power, there is another equally concerned issue as much as protection i.e., frequency control of the microgrid. Microgrid (MG) is a combination of diesel engine generators (DEG), renewable energy sources (RES), loads and various energy storage systems (ESS). The frequency control task is quite simple in conventional power systems because the disturbances arise only due to the stochastic loads. However, the frequency control problem in an islanded microgrid is always a concerning challenge for the operators. The low inertia of the system, stochastic loads and intermittent/discontinuous generation of renewables create complications in the frequency control of the microgrid. Massive frequency deviations will cause stability and reliability problems and sometimes may lead to microgrid blackouts. In this regard, this thesis presents the protection of double circuit three-phase transmission lines, single circuit six-phase transmission lines, and single circuit three-phase transmission lines connected to renewable energy sources. Also, the frequency control of an islanded microgrid having renewable energy sources and plug-in hybrid electric vehicles (PHEV) is presented.

1.1.1 Types of Short Circuit Faults in Three-phase and Six-phase Transmission Lines

The primary job of transmission lines is to transfer the electrical power from the generation units to the distribution units or the load centres. The vast existence of transmission lines over several kilometres exposed to different terrestrial weather conditions makes them vulnerable to inevitable fault situations. The transmission line faults are broadly classified into two categories: open circuit faults (series faults, where one or more conductors are open-circuited) and short circuit faults (shunt faults, where one or more conductors are short-circuited). The short circuit faults are characterized by an increase in current and a decrease in voltage. The short circuit faults are further classified as symmetrical (LLL/LLLG: triple line/triple line to ground faults) and unsymmetrical (LG/LLG/LL: single line to ground/double line to ground/double line faults) faults in case of three-phase transmission system [3]. Broadly, there are about 11 types of short circuit fault combinations that can possibly occur in a three-phase transmission system. However, there are about 120 types of short circuit fault combinations that can possibly occur in a six-phase transmission system.

These 120 fault combinations are grouped into 11 categories of faults. Table 1.1 gives the 11 categories of faults and Fig. 1.1 presents the flowchart of the segregation of 120 fault types of a six-phase transmission system [4, 5].

Table 1.1 Types and no. of short circuit faults on six-phase transmission line

Fault type	1-LG	2-L	2-LG	3-L	3-LG	4-L	4-LG	5-L	5-LG	6-L	6-LG
No. of faults	6	15	15	20	20	15	15	6	6	1	1
Total						120					

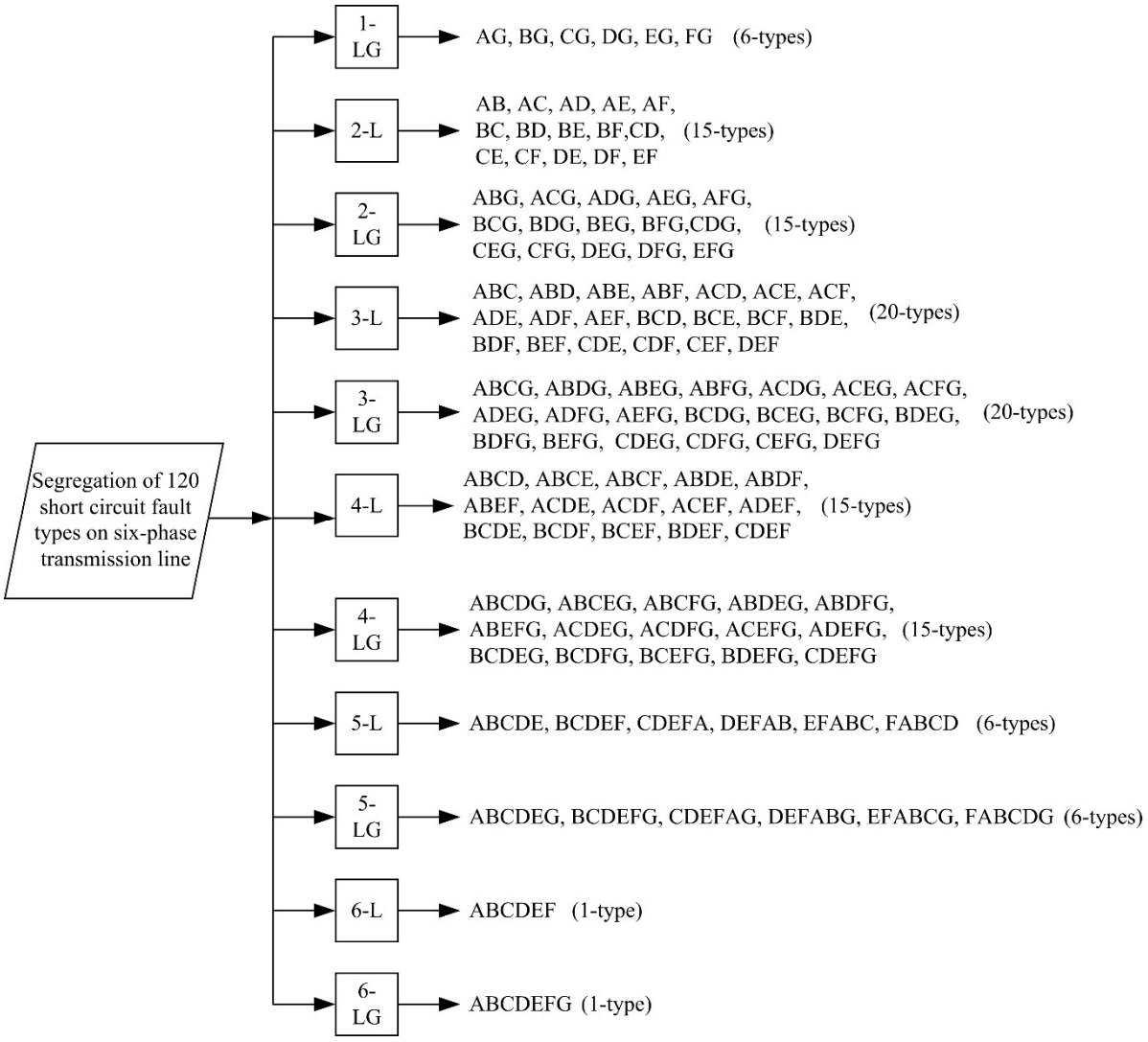

Fig. 1.1 Flowchart of segregation of 120 types of short circuit faults

The number of non-simultaneous short circuit faults *(N_{sf})* for the '*k*' phase transmission system is given in Eq. (1.1) [6]. For ex., $k = 3$, $N_{sf} = 3+2(3)+2(1) = 11$ and for $k = 6$, $N_{sf} = 6+2(15)+2(20)+2(15)+2(6)+2(1)=120$.

$$N_{sf} = \binom{k}{1} + 2\sum_{i=2}^{k}\binom{k}{i} \tag{1.1}$$

Protection of transmission of lines is crucial because:

- Maintaining a safe, reliable, and stable power supply.
- Faults on these lines can disrupt service, causing outages and economic losses. Also affects the homes, businesses, and critical infrastructure.
- Transmission lines carry high-voltage electricity, which can be dangerous if not properly protected. Faults can lead to arcing, fires, and even electrocution. Protecting transmission lines helps to prevent these accidents and keep people safe.
- Transmission lines are expensive to build and maintain. Faults can damage equipment, such as transformers, switchgear, and other expensive equipment, requiring costly repairs and replacements. Protecting transmission lines helps to extend the life of equipment and reduce maintenance costs and equipment damage.

Effective protection systems quickly isolate the fault, minimizing damage and preventing the hazardous situation from escalating.

1.2 Brief Overview of Artificial Intelligent Techniques

The rise of artificial intelligence (AI) has revolutionized its application to solve power system problems. Fuzzy logic, artificial neural networks, decision trees, and evolutionary optimization techniques are now employed in developing sophisticated power system protection and control schemes. The advancements in AI techniques opened doors to extensive research in power system protection and control, paving the way for more robust and intelligent solutions. The main computational AI philosophies include fuzzy logic, neural networks, evolutionary computation, machine learning, and probabilistic reasoning. These computational methods are encouraged due to their ability to solve complex problems (achieve solutions) at a lower cost than conventional computing methods.

1.2.1 Fuzzy Logic Systems

In 1965, Lotfi Zadeh, the “father of fuzzy logic,” introduced this revolutionary concept. Fuzzy logic, unlike traditional binary logic with its strict true/false (1/0) values, embraces the notion of vagueness and uncertainty. Fuzzy logic that is based on fuzzy set theory allows for degrees of truthfulness between these extremes. This makes it ideal for handling uncertainty and imprecision, i.e. common in real-world situations. Fuzzy logic can be defined as a form of knowledge representation suitable to define imprecise/uncertain data using linguistic variables and fuzzy sets instead of just numbers. This enables the computing devices to mimic and reason like humans. Fuzzy logic's simplicity and flexibility make it well-suited for problems with incomplete or imprecise data. It uses simple "IF-THEN" rules, making its knowledge representation easy to understand and modify accordingly to build systems that adapt to changing environments and incomplete information. The core concept of fuzzy logic is the membership function, which assigns a numerical value between 0 and 1 to represent how much an element belongs to a fuzzy set [7, 8].

1.2.1.1 Membership function

Membership function can be defined as a function where each element of a fuzzy set is mapped to a membership value ranging from 0 to 1. In simple terms, a membership function is a curve that defines the characteristics of a fuzzy set with a membership value for each member in the set. The membership function defines the fuzziness in a fuzzy set. The degree of membership is essentially a score indicating how well that element fits the characteristics of the fuzzy set. Graphical representations are generally used to represent a membership function. In graphical representations, the x-axis represents the elements of the fuzzy set and the y-axis represents the membership value. The commonly used different membership functions are listed in Table 1.2.

Table 1.2 Types of membership functions

S. No.	Membership Function	Expression
1.	Triangular (x_1, x_2, and x_3 are vertices of triangle)	$y = f(x) = \begin{cases} \frac{x - x_1}{x_2 - x_1}, & x_1 \le x \le x_2 \\ \frac{x - x_2}{x_3 - x_2}, & x_2 \le x \le x_3 \\ 0, & otherwise \end{cases}$
2.	Trapezoidal (x_1, x_2, x_3, and x_4 are vertices of trapezoid)	$y = f(x) = \begin{cases} \frac{x - x_1}{x_2 - x_1}, & x_1 \le x \le x_2 \\ 1, & x_2 \le x \le x_3 \\ \frac{x - x_3}{x_4 - x_3}, & x_3 \le x \le x_4 \\ 0, & otherwise \end{cases}$
3.	Gaussian (c and w are the centre and width of membership function)	$y = f(x) = e^{-0.5\left(\frac{x-c}{w}\right)^2}$
4.	Generalized Bell (c, w, *and* s are the centre, width, and slope of membership function curve)	$f(x) = \frac{1}{1 + \left(\left\lvert\frac{x - c}{w}\right\rvert\right)^{2s}}$
5.	Sigmoid (c and w are the centre and width of membership function)	$f(x) = \frac{1}{1 + e^{[-w(x-c)]}}$

1.2.1.2 Fuzzy inference system (FIS)

FIS is also known by other terms viz., fuzzy-rule-based system, fuzzy logic controller, fuzzy model, fuzzy associative memory, fuzzy expert system or simply fuzzy system due to its wide applications in different domains of discipline. Basically, the whole process of reaching an optimal solution from inputs through a process of fuzzy logic reasoning mimicking human-like decision-making is referred to as an FIS. The main task of FIS is to make decisions based on fuzzy logical reasoning. The decisions are made by using simple "IF-THEN" rules and "OR"/"AND" logical relations. The basic architecture of an FIS consists of a rule base and database combinedly known as a knowledge base, a decision-making block, a fuzzification block and a defuzzification block. The basic block schematic of FIS is shown in Fig. 1.2. Mamdani FIS and Takagi-Sugeno FIS are the main types of FIS. The difference between these two is their approach to output representation and defuzzification. While the Mamdani FIS uses membership functions and a defuzzification process the other depends on linear or constant functions without a defuzzification process to

provide outputs. Compared to the Sugeno FIS, the Mamdani FIS is simpler to implement. There are four stages in the fuzzy inference processing:

Fuzzification: This process involves the conversion of crisp sets of inputs and outputs into fuzzy quantities using the linguistic variables and membership functions to define the fuzziness in the crisp sets.

Fuzzy Inference: In this process, the knowledge base is used to take decisions based on the fuzzy rules devised for specific applications of the system. In simple words, it is a process where the input variables are mapped onto the output variables using the fuzzy logic concept with "IF-THEN" rules.

Aggregation: In this process, all the fuzzy outputs that are obtained after the execution of fuzzy rules are aggregated/combined to form an aggregated fuzzy set.

Defuzzification: The defuzzification process converts the aggregated output fuzzy sets back to crisp quantities. Centroid, max-membership, weighted average, mean-max membership, centre of sums, centre of largest area, and first of maxima and last of maxima are the different types of defuzzification methods.

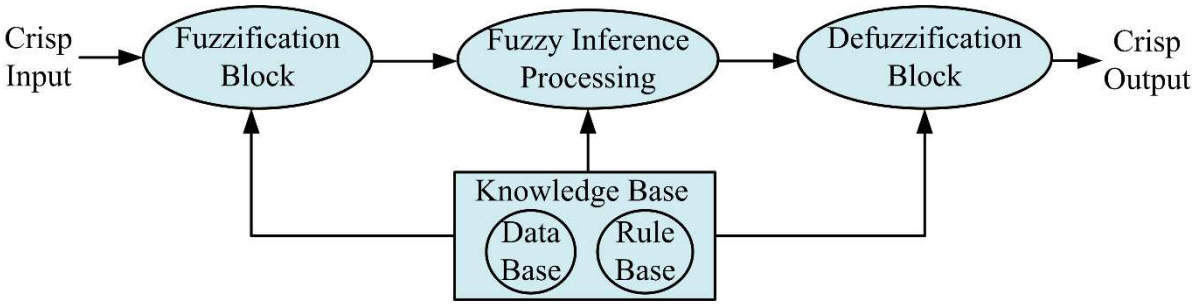

Fig. 1.2 Basic block schematic of FIS

1.2.2 Artificial Neural Networks

The concept of an artificial neuron is an inspiration drawn from the biological neuron. The human brain neuron system design and working mechanism is the base for the artificial neural network (ANN). An ANN acts as a data processing system that mimics the information processing capabilities of the biological nervous system. Brains have billions of interconnected neurons for the exchange, communication, and processing of information. Likewise, an ANN also consists of interconnected artificial neurons. Each typical biological

neuron has three main parts: i) cell body (soma): which contains the nucleus and acts as the central processing unit of the neuron, ii) dendrites: these branch-like structures receive electrical signals from other neurons through junctions called synapses, and iii) axon: this single long fibre transmits the processed electrical signal to other neurons. Fig. 1.3 illustrates the structure of a biological neuron.

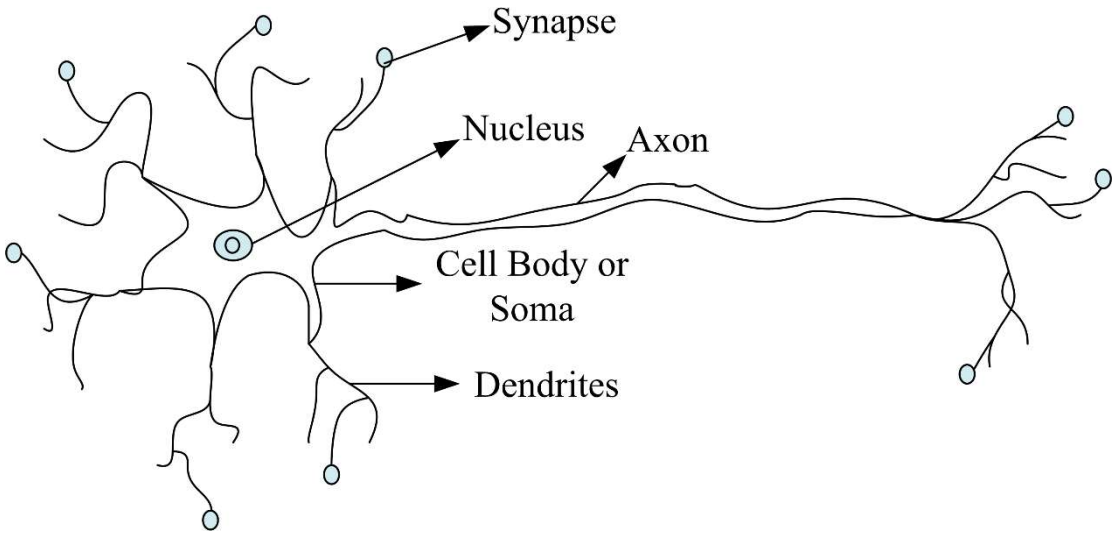

Fig. 1.3 Structure of biological neuron

An artificial neural network (ANN) is essentially a smart computer program (or even specialized hardware) designed to mimic the human brain and tackle specific tasks. It works like a massively parallel processor, distributing information across many interconnected units. ANNs can store and acquire knowledge through a learning process by adjusting their internal connections, allowing them to adapt to new information and excel at tasks like pattern recognition and data classification. A typical artificial neuron has simple components: inputs, summation, an activation function that processes the information, and finally, an output. Fig. 1.4 depicts the structure of an artificial neuron. The working of the neuron can be explained as follows: the net product WX and the input bias are summed up at the summer location, where the net product (WX) is obtained by the multiplication of different inputs ($x_1, x_2, x_3, \ldots, x_n$) with the corresponding weight values ($w_1, w_2, w_3, \ldots, w_n$) respectively. The weights can modify the actual inputs. The activation function (f) processes the net input ($WX+b$) to deliver the output [9]. The output (y) of the neuron is given in Eq. (1.1) and Eq. (1.2) (matrix form), where $W = [w_1, w_2, w_3, \ldots, w_n]$ and $X = [x_1, x_2, x_3, \ldots, x_n]$.

$$y = f(net\ input) = f\left(\sum_{i=1}^{n} w_i x_i + b\right) \tag{1.1}$$

$$y = f(W^T X + b) \tag{1.2}$$

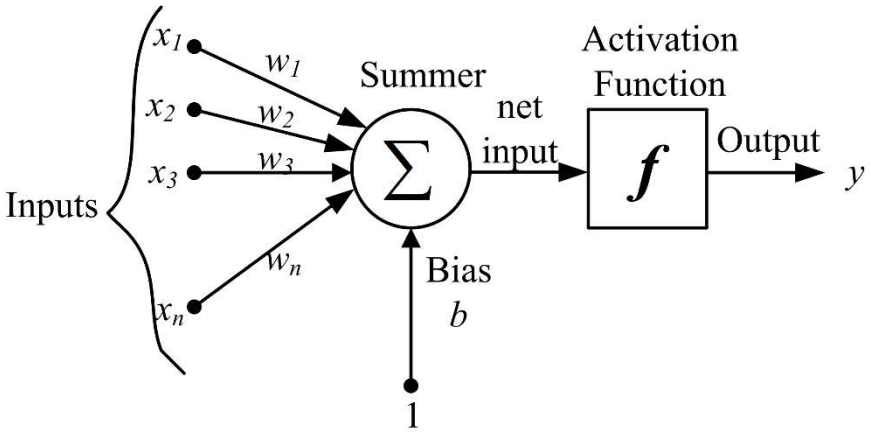

Fig. 1.4 Structure of artificial neuron

The architecture of ANN generally comprises of three layers: input layer, hidden layer, and output layer. The number of neurons in all three layers depends on the application of ANN for a task. The ANNs can be broadly categorized into feedforward neural networks and recurrent neural networks. A feed-forward network is a network which does not have any feedback paths. In this type of network, all three layers are connected in the forward direction by providing the flow of information only in one direction (forward). The input layer sends the information to the hidden layer and the hidden layer transmits the information to the output layer [9, 10]. The recurrent neural network is a network which contains feedback paths from output to input. Recurrent networks are feedback networks with closed-loop paths. Further, feedforward neural networks can be classified as supervised (single-layered/multi-layered) and unsupervised feedforward neural networks.

Activation functions, also known as transfer functions, play a crucial role in extracting meaningful information within artificial neural networks. They filter the net input (a combination of weighted inputs and a bias) and transform it into an output. The choice of activation function depends heavily on the specific task. These functions can be either linear or non-linear, offering different capabilities for processing the information. Some common activation functions used in ANNs are listed in Table 1.3.

Table 1.3 Commonly used activation functions in ANNs

S.No.	Name of Activation Function	Relation between input-output
1.	Hard Limit	$y = f(x) = \begin{cases} 0, & x < 0 \\ 1, & x \geq 0 \end{cases}$
2.	Symmetrical Hard Limit	$y = f(x) = \begin{cases} -1, & x < 0 \\ +1, & x \geq 0 \end{cases}$
3.	Linear	$y = f(x) = x$
4.	Positive Linear	$y = f(x) = \begin{cases} 0, & x < 0 \\ x, & x \geq 0 \end{cases}$
4.	Saturating Linear	$y = f(x) = \begin{cases} 0, & x < 0 \\ x, & 0 \leq x \leq 1 \\ 1, & x > 1 \end{cases}$
5.	Symmetric Saturating Linear	$y = f(x) = \begin{cases} -1, & x < 0 \\ x, & 0 \leq x \leq 1 \\ +1, & x > 1 \end{cases}$
6.	Log-Sigmoid	$y = f(x) = \frac{1}{1 + e^{-x}}$
7.	Hyperbolic Tangent Sigmoid	$y = f(x) = \frac{e^{x} - e^{-x}}{e^{x} + e^{-x}}$

1.2.3 Decision Trees

Decision trees stand as a powerful paradigm of data mining that is the most versatile and effective method in AI. These supervised learning algorithms excel at predicting the relationship between a feature and its target value, making them ideal for various tasks like classification, regression, clustering, and even feature selection. They can handle various data types, including numeric, nominal, and even text, and they can even work with missing or erroneous data. Their ability to analyze large imperfect datasets to deliver accurate predictions with minimal computational effort led to the successful application to solve power system related issues [11].

Decision trees are powerful predictive models used for either classification or regression tasks. They are termed as classification trees when they tackle the classification problem that aims to categorize the data points into specific classes to predict discrete outcomes. They are called as regression trees when used for regression problem that predicts continuous values. While the underlying structure and core working functionality are similar for both trees, the convergence criteria for reaching a terminal node differ based on the specific task. Decision

tree algorithms offer impressive efficiency despite the fact of simplicity. They follow a strategy called “divide and conquer” to grow/construct the trees by recursively splitting the training data until desired patterns emerge within each group, signifying a single class. A decision tree structure comprises three types of nodes: i) root or parent node: the starting point, with only outgoing branches leading to further decision points, ii) test/child/internal node: nodes with both incoming and outgoing branches, representing a specific decision, and iii) leaf/terminal/decision nodes: end points with no outgoing branches, indicating the final predicted class or target value. Fig. 1.5 depicts an illustration of a simple decision tree structure using yes/no questions. Square boxes represent root or test nodes, while circles represent leaf nodes. The features are denoted by f_1, f_2, and f_3, with s_i (i = *1, 2, 3, 4, and 5*) representing optimal split points and C_i (i = *1 to 6*) signifying the predicted classes or target values.

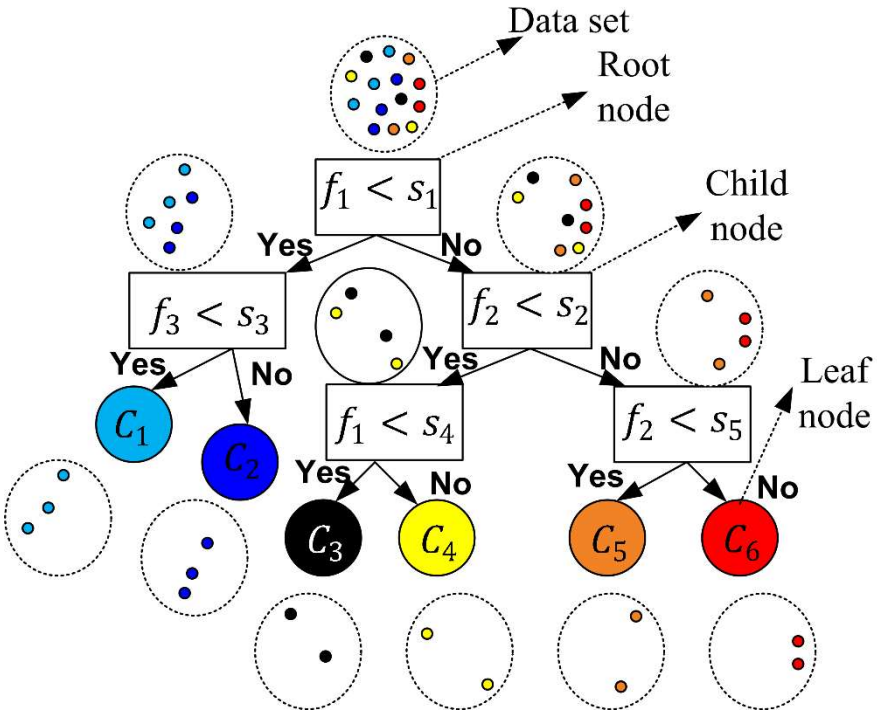

Fig. 1.5 Structure of simple decision tree

There are various kinds of decision tree inducer algorithms viz., CHAID (CHi-squared Automatic Interaction Detector), ID3 (Iterative Dichotomiser 3), CART (Classification and Regression Trees), C 4.5 etc., [11–13]. They automate the process of building optimal predictive models from the given training data by minimizing errors. A decision tree is trained in two stages: (i) the growing stage, which splits the data or grows the tree until a set of

stopping criteria is met; and (ii) the pruning stage, where redundant branches are removed to optimize the tree's depth and prevent overfitting. This creates a more generalizable model with the right level of complexity. The different stopping criteria are listed below:

(i) all the instances in the training set belong to a single class.
(ii) when the maximum depth of the tree has been reached.
(iii) when the number of cases in the terminal nodes is less than the minimum number of cases for parent nodes.
(iv) if the node were split, the number of cases in one or more child nodes would be less than the minimum number of cases for the child nodes.
(v) the best splitting criteria is not greater than a certain threshold.

The decision trees are grown by following optimal splitting criteria that optimize the split to choose the best feature and value for splitting the data based on the impurity measurement of the split. The impurity metrics namely, gain ratio, information gain, Gini index/Gini diversity index, twoing rule, and binary criteria are commonly used for classification purposes while the mean square error reduction of prediction or variance reduction is used for regression purposes. However, a fully grown tree can be complex and prone to overfitting. It is necessary to prune the tree optimally to reduce the unwanted tree size to get a tree with the best minimum size and minimum generalization error striking a balance between complexity and accuracy. The different pruning methods are cost complexity pruning (balancing tree size and prediction error), reduced error pruning (focusing on reducing generalization error), minimum error pruning (selecting the sub-tree with the lowest error), pessimistic error pruning, and critical value pruning [11, 12].

One of the most widely used decision tree algorithms is CART. The CART algorithm uses the Gini index or minimum mean square error of prediction as the splitting criterion and cost complexity pruning method for constructing the tree. The working principle of classification and regression trees is similar, but classification trees predict a class and regression trees predict a real number. A node is pure, if all the instances under it belong to a single class in the classification tree and if the prediction of the mean square error of all instances under the node is minimum in a regression tree [11–14]. For validation of a decision tree, the K-fold cross-validation method is used to choose the tree that gives the least prediction or misclassification error. A flowchart of growing regression trees is shown in Fig. 1.6, where D is the input training dataset with d features $\{f_1, f_2, f_3, \ldots, f_d\}$ and N no. of instances, Y is the

target data, and S is the set of potential splits obtained from D through the exhaustive search method. The best tree is validated using the minimum mean square error of the prediction.

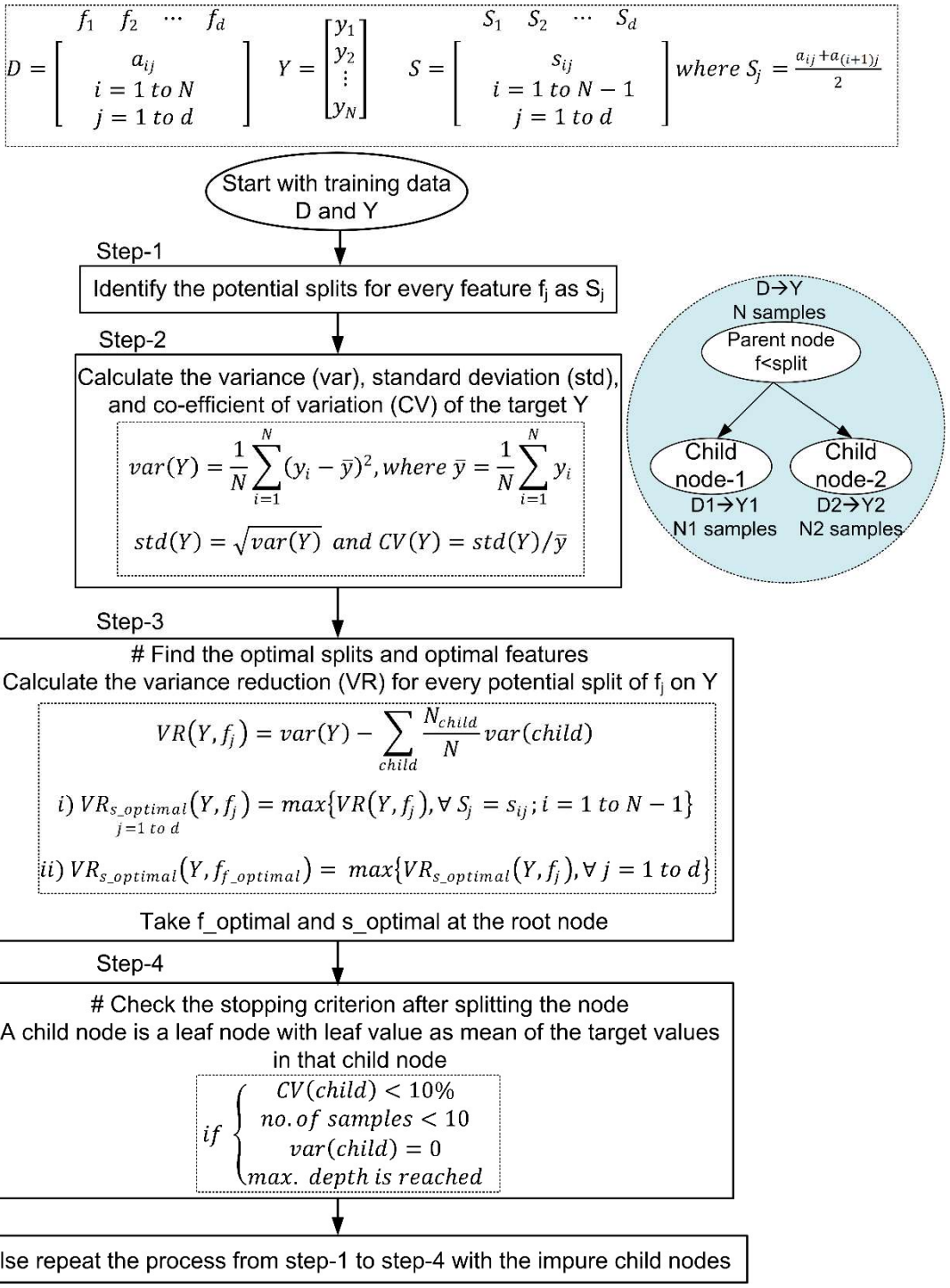

Fig. 1.6 Flowchart of growing regression trees

1.3 Literature Survey

This thesis aims to develop intelligent protection and control schemes for the power system. Several authors have proposed different fault detection and classification (FDC) protection schemes either for three-phase single/double circuit transmission lines, six-phase transmission lines and transmission lines connected to renewable energy sources using threshold-based methods, artificial intelligent methods (fuzzy logic, artificial neural networks (ANNs), support vector machines (SVMs), extreme learning machines (ELMs), decision trees), and hybrid schemes. Similarly, for the frequency control of microgrid, different nature-inspired or evolutionary algorithms are employed to optimize the PI/PID controller parameters. The following subsections describe a brief literature review on transmission line protection schemes and microgrid frequency control strategies implemented by different authors.

1.3.1 Protection Schemes for Three-phase Single/Double Circuit Transmission Lines

Several authors have proposed different fault detection and classification (FDC) protection schemes either for the single circuit or double circuit transmission lines using threshold-based methods [15–19] and artificial intelligent methods [20–27], namely, fuzzy logic, artificial neural networks (ANNs), support vector machines (SVMs), extreme learning machines (ELMs), decision trees, and hybrid schemes [28–31]. The threshold-based methods in [15–19] depend on the voltage and/or current signals transformation. The protection of parallel transmission lines with wavelet transform using two-terminal voltage and current data is proposed in [15]. The FDC protection scheme for the shunt compensated double circuit transmission lines (DCTL) with fast discrete S-transform in [16] and discrete wavelet transform in [17] using the energy of the transformed current signals is proposed. Likewise, the FDC protection scheme for the double circuit transmission lines in [18,19] is proposed with the maximal overlap discrete wavelet transform and three-dimensional triangular fault plane that uses the energy and standard deviation of the wavelets of the current signals. An artificial intelligent FDC protection scheme based on the fuzzy inference system (FIS) is proposed in [20] for the protection of a single-circuit transmission line only. The FDC protection schemes utilizing ANN and discrete Fourier transform (DFT) or discrete wavelet transform (DWT) viz., DFT-ANN in [21], protects the double circuit transmission lines from

the common short circuit faults, and DWT-ANN in [22], protects from cross-country and transforming faults. The DFT-ANN method uses the magnitude of the fundamental component of voltage and current (MFCV and MFCC). The DWT-ANN method uses the standard deviation of the sixth-level detailed coefficients of current signals. The Kalman filtering approach based on the modular SVM using the voltage harmonics for the FDC of faults on the DCTL with non-linear loads has been proposed in [23]. The Kalman filtering technique is computationally expensive and may diverge if the initial estimate or the modelled process is incorrect. In [24], an FDC scheme for a series compensated transmission line based on the modular DWT-ELM has been proposed. Although the ELMs are robust with good generalization ability, their performance is degraded when dealing with huge amounts of training data. The data mining techniques, random forests in [25], decision trees in [26] and [27], protect the FACTS compensated transmission lines, DCTL, and series compensated DCTL, respectively. These methods [25–27] use the instantaneous voltage and current signals (for fault detection only), DFT processed voltage and current data (for identifying the faults during power swing situations), and the two-terminal voltage and current data for deriving the input phase angle of the differential impedance of the lines, respectively. Hybrid protection schemes, namely, a linear discriminant analyzer for the feature extraction in conjunction with the random forest approach tuned by the cuttlefish optimization in [28] and particle swarm optimization (PSO) optimized SVM in [29] or ANN in [30], are proposed for the protection of single-circuit transmission lines only. The accurate performance of the PSO-based protection schemes depends on the optimal values of the algorithm-specific parameters (namely, W, C1, and C2: controls the movement, personal performance, and social performance of the swarms, respectively). A fault classifier based on the supervised relevance vector machine is proposed in [31] for the protection of series compensated transmission lines.

- **Research Gap:** Most of the aforementioned research works reported earlier, particularly for the protection of DCTL are training based artificial intelligent techniques. They require huge sets of training data and proper selection/tuning of training parameters for acquiring accurate FDC. Only a few papers have addressed different fault situations and operating conditions for the performance evaluation of the protection scheme. No work was reported earlier without training the protection module based on artificial intelligence for the protection of DCTL.

1.3.2 Protection Schemes for Six-phase Transmission Line

The acceptance of the six-phase transmission is vaguely encouraged due to the lack of proper protection schemes to tackle the 120 different types of short circuit faults. The existing protection schemes available for single/double circuit three-phase transmission systems are not apt for the six-phase transmission system. The protection schemes developed for the conventional three-phase transmission system either with distance relays or other artificial intelligence-based techniques [32–34] can only utilize the voltage and current information of three phases to detect/classify the fault. But, when these protection schemes are applied to the six-phase line, the relay may or may not operate for all 120 fault combinations. It is reported that a total of twenty-one conventional distance relays (six for phase-ground fault detection and fifteen for phase-phase fault detection) are required for the complete protection of the six-phase line [35]. Only a few works were reported for the protection of six-phase transmission lines. The fault analysis of the six-phase system with sequence components and phase coordinate method is presented in [36, 37] and fault detection based on negative sequence currents is proposed in [38]. A fault detection and classification technique with discrete Fourier transform (DFT) based ANN is proposed in [39, 40] for only six-phases to ground faults and single-phase to ground faults respectively. A fault classification scheme for phase to phase faults (2 – L faults) is implemented using voltage and current signals in [41] with a DWT (Haar wavelet) based ANN approach. The protection for one conductor's open faults in a six-phase transmission system is proposed using ANN in [42]. A complete protection scheme with 22 modular DFT based ANNs (11 – ANNs for FDC and 11 – ANNs for fault location estimation) is presented in [43] which uses voltage and current signals for the protection task. Fault zone identification and fault location estimation with modular ANNs using DWT (db3 wavelet) pre-processed voltage and current signals are proposed [44]. In [45], a hybrid protection scheme is implemented using the harmonic information of voltage signals for FDC with 11 decision tree modules and 11 TLBO tuned ANN modules for fault location estimation. The fuzzy logic-based FDC schemes are presented in [46, 47] using DFT with voltage and current signals.

❖ **Research Gap:** The ANN-based protection schemes reported above have either considered only one type of fault viz. single phase to ground, six-phase to ground, and phase to phase faults or modular ANN methods for fault detection and classification. Only a few works have reported the fault location estimation.

1.3.3 Protection Schemes for Three-phase Transmission Lines Connected to Renewable Energy Sources

Several authors have proposed different protection schemes to identify the faults on transmission lines connected to renewable energy sources which include modified distance protection, differential protection, pilot protection, and training based artificial intelligent schemes. The pilot protection scheme utilizing currents at both ends of the line with a dynamic time-warping algorithm reported in [48] is only for balanced faults and the pilot protection scheme implemented in [49] requires synchronized voltage and current data for fault impedance calculation using short line and distributed line models for wind power integrated transmission lines. Similarly, a modified fast distance relaying scheme utilizing the short line (R-L model) and Bergeron model of transmission line [50] and a modified polygonal distance protection for improved zone-1 performance [51] are proposed for the wind farm connected transmission line. Also, a modified distance protection in [52] utilizing local voltage and current information for calculating line impedance and phase angle of fault impedance, differential protection in [53] utilizing signed correlation and fault index comparison to detect faults with the help of phase currents at both ends of the line, directional protection based on high frequency in [54] with the help of two independent relays processing voltage and current information available at ends of the line locally, and distance protection schemes employing least squares estimation [55] and multiple signal classification algorithm [56] to extract frequency components of voltage and current near to fundamental frequency are proposed by different authors to detect faults on the transmission lines connected to wind farms. Distance protection schemes for transmission lines connected to solar photovoltaic (PV) systems were also reported viz., distance protection based on positive sequence network [57, 58] utilizing either PV side or grid side voltage and current information, and improved/modified distance protection based on fault impedance calculation in [59, 60] either utilizing synchronized/unsynchronized voltage and current data. Artificial intelligence-based protection schemes were also reported for the transmission lines connected to renewable energy sources. An enhanced distance protection with the help of support vector machine-based regression [61] for PV connected lines, ANFIS based fault detection only for wind farm connected lines [62], fault detection/classification technique for wind farm connected lines using transient monitoring index with support vector machine in [63] and in [64] maximal overlap discrete wavelet transform with ANN for symmetrical fault detection only, and the

intelligent protection methods [65, 66] for FACTS compensated line connected to wind farm with deep convolution neural network using variational mode decomposition and random forest classifier using intrinsic time scale decomposition are reported in the literature. Further, PSO optimized thresholds for adaptive differential protection of transmission lines connected to wind power systems are presented in [67, 68].

- **Research Gap:** The protection schemes reported in most of the above-mentioned literature are hectic mathematical analysis-based distance/pilot/differential protection schemes which either require single/double end synchronized/unsynchronized current and/or voltage data for the protection task. On the other hand, the AI based protection methods are reported which require massive datasets towards training the AI protection modules for fault detection/classification considering different operating scenarios of the system. Further, some protection schemes are implemented for the detection of symmetrical or balanced faults only.

1.3.4 Frequency Control of Microgrid

The load frequency control (LFC) problem of an islanded microgrid (MG) is addressed using various artificial intelligent-based PI/PID controllers that are proposed by different authors. The parameters of the PID controller were optimized either by using a single artificial intelligent technique or hybrid techniques. The genetic algorithm in [69], particle swarm optimization (PSO) in [70], social spider optimization in [71], grey wolf optimization (GWO) in [72], firefly algorithm in [73], harmony search optimization in [74], teaching learning based optimization in [75], grasshopper optimization in [76], and cuckoo search optimization in [77] are employed to tune the parameters of PID controller to control the frequency of an islanded microgrid having various renewable energy sources and energy storage devices. Similarly, an artificial neural network based PID controller in [78], an adaptive fuzzy PI controller in [79], PSO optimized adaptive fuzzy PI controller in [80], a combination of GWO and PSO optimized adaptive fuzzy PI controller in [81], and a hybrid of firefly and PSO algorithm based PID controller in [82] are designed for the frequency control of an islanded microgrid.

In the control studies, the AI-optimized PID controllers are well suited for MG frequency control applications. However, for certain operating scenarios, it has been observed that these PID controllers have underperformed due to the difficulty in finding an optimal operating state. This underperformance is mostly caused by an improper offset between the derivative

and integral gain components. A PI controller can minimize the system's error during the steady state. If the operator has increased the integral gain component the steady state error is minimized. However, the system exhibits undesirable behaviour during the transient state. The system's stability and speed are reduced by the dominant integral component. Similarly, the dominant PD component improves the system's transient response. But, the system's steady-state response is disturbed.

Recently, the concept of multi-stage controllers has been implemented by several authors due to their robust performance in regulating the frequency of an islanded MG or multi-MG with renewable energy sources and energy storage systems. The multi-stage PID (MPID) control structures were proposed by different authors to tackle the frequency control problem. A hybrid of whale and pattern search algorithms in [83], fuzzy tuned multi-stage PID and fractional order multi-stage PID controllers optimized with grasshopper optimization [84] and future search algorithms [85], chaotic crow search algorithm for fuzzy PD-TID controller in [86], and salp swarm optimization for PI-PD controller in [87] are proposed by different authors to control the frequency of microgrid.

❖ **Research Gap:** From the above literature, it is understood that the regulation of frequency of MG either having RES or ESS (energy storage systems) in islanded mode is achieved with different controller structures whose parameters are optimized with a variety of swarm intelligent techniques. The performance of these techniques mainly depends on the choice of specific parameters of the algorithm and the improper choice may roll the solution towards local optimum values. Although the controller's approach based on fuzzy logic or fractional order calculus is exhibiting better performance but at the cost of optimizing the structure of the fuzzy inference system or the fractional order system parameters along with controller gain constants. Also, from the literature, it was observed that controlling the frequency of an islanded MG having RES and PHEVs with an MPID controller is rarely investigated.

1.4 Research Gaps and Motivation

1.4.1 Research Gaps

The research gaps mentioned at the end of each subsection are summarized below:

- From the literature of Section 1.3.1, it is observed that, protection schemes reported for the three-phase single or double circuit transmission lines have implemented the

training based artificial intelligent techniques that require extensive training datasets with at least two protection modules for the complete protection of the line. Also, proper tuning and selection of algorithm specific training parameters play a vital role in achieving accurate performance of the protection jobs.

- From the literature of Section 1.3.2, it is observed that, ANNs were successfully implemented for the protection of six-phase transmission lines. But either the protection schemes developed were only for one type of fault (6-LG or 1-LG or 2-L faults) or the modular ANN concept was implemented for FDC of all types of faults.
- From the literature of Section 1.3.3, it is observed that, the training based artificial intelligent protection schemes or modified distance protection schemes involving hectic mathematical analysis are majorly reported for the fault detection on the transmission line connected with the renewable energy sources.
- From the literature of Section 1.3.4, it is observed that, for controlling the frequency of an islanded microgrid having RES and PHEVs with a multi-stage PID controller is rarely investigated. Further, the selection of appropriate optimal techniques for modifying the control parameters is crucial to improvise the MG's dynamic response.

1.4.2 Motivation

Following the research gaps, the motivations for this thesis are listed below:

- To develop an artificial intelligent protection scheme i.e. free from training of the module for the protection of three phase double circuit transmission lines and also suitable for single circuit operation.
- To develop an artificial intelligent protection scheme of a single module for six phase transmission line that can detect and classify all 120 types of short circuit faults. Also, a fault location estimation approach for the six phase lines.
- To develop an artificial intelligent protection scheme i.e. free from the training of the module for the protection of three phase transmission lines connected to renewable energy resources viz. wind and solar power plants. To propose a fault location estimation approach for such transmission lines.
- To control the frequency of an islanded microgrid having renewable energy resources and plug-in hybrid electric vehicles (PHEVs) using a multi-stage PID controller whose parameters are optimized with the help of nature inspired optimization algorithm. The

NFL (No Free Lunch) theorem states that no single metaheuristic approach can solve all engineering optimization issues and that there is always an opportunity for improvement.

1.5 Contributions of the Thesis

Following the motivations of the thesis to develop artificial intelligent protection and control schemes/strategies towards the fine operation of the power system, four contributions are presented in this thesis under the titles given below:

Contribution-1: Single Fuzzy Inference Based Fault Detection and Classification Protection Scheme for Different Types of Short Circuit Faults on Double Circuit Transmission Lines.

Contribution-2: Mono ANN Module Protection Scheme and Multi ANN Modules for Fault Location Estimation for a Six Phase Transmission Line Using Discrete Wavelet Transform.

Contribution-3: A Novel Protection Scheme for Transmission Lines Connected to Solar Photovoltaic and Wind Turbine Farms Using Fuzzy Logic Systems and Bagged Ensemble Learning.

Contribution-4: Frequency Control of an Islanded Microgrid with Multi-stage PID Control Approach Using Moth Flame Optimization Algorithm.

1.6 Organization of the Thesis

The thesis is organized into six chapters. A brief discussion of each chapter is given below to provide an overview of the thesis:

Chapter 1 outlines the growing demand for electrical energy globally and the crucial role of transmission lines. It emphasizes the importance of protecting these lines and maintaining grid frequency, especially in microgrids. This chapter introduces a brief about AI techniques like fuzzy logic, neural networks, and decision trees and reviews their application in transmission line protection for various line configurations and renewable energy integration. It also covers AI-optimized PI/PID controllers for microgrid frequency control. Following the discussion on research gaps and motivations, an overview of the thesis structure is presented at the end of this chapter.

Chapter 2 proposes an AI-based fault detection and classification system for double circuit transmission lines using a single fuzzy inference module. It addresses the limitations of conventional relays in protecting double circuit transmission lines, then details: i) feature extraction using discrete Fourier transform, ii) proposed scheme methodology, iii) performance evaluation under various fault types, operating scenarios, and varying parameters, and iv) comparison with other AI techniques and summary of the chapter.

Chapter 3 proposes an AI-based fault detection and classification scheme for six-phase transmission lines using a single ANN module. It also proposes multiple ANN modules for estimating the fault location in each phase. This chapter highlights the advantages of six-phase lines and the complexity of their protection compared to three-phase systems. It considers a six-phase line i.e. between the buses Springdale and McCalmont of Allegheny power system and discusses the proposed method using discrete wavelet transform and neural networks. The performance for various fault scenarios for 120 types of faults with varying fault parameters is evaluated. The comparison results and summary are presented at the end.

Chapter 4 proposes a hybrid AI scheme (fuzzy system and bagged ensemble learner) for protecting transmission lines connected to renewable energy sources (50 MW solar power and 50 MW wind power). It addresses the limitations of traditional transmission line distance protection methods and describes the simulated power system. The proposed scheme combines: i) feature extraction with discrete Fourier transform, ii) a fuzzy logic system for fault detection and classification, and bagged ensemble decision trees for fault location estimation. The proposed scheme's performance is evaluated for various fault types under different solar irradiations and wind speeds. The reliability of fault detection/classification and location estimation modules is validated through the simulations with the help of the confusion matrix and Chi-square statistical analysis test. Finally, this chapter presents comparison results and concludes with a summary of the method.

Chapter 5 proposes a multi-stage PID (MPID) controller optimized by a moth flame optimization (MFO) algorithm for frequency control in an islanded microgrid (Bella Coola microgrid) with renewables and plug-in hybrid electric vehicles. It addresses the limitations of conventional PID controller structure and discusses the mathematical models for microgrid and MFO algorithm. The performance of the MFO algorithm is appraised with other meta-heuristic techniques (PSO, GOA, and TLBO) in optimizing PID parameters. Later, the

performance MFO-PID and MFO-MPID controllers is evaluated and compared under different operating conditions of the microgrid. The impact of electric vehicles on frequency control and microgrid stability through eigenvalue and root locus analysis is assessed. This chapter concludes with a comparison and summary of the proposed controller.

Chapter 6 presents the overall conclusions of the proposed methods towards the protection and control of power systems from the preceding chapters. This chapter also includes the future scope of the research in the direction of protection of transmission lines and frequency control of a microgrid or multi microgrids using further sophisticated artificial intelligent techniques.

*****

Chapter 2

Single Fuzzy Inference Based Fault Detection and Classification Protection Scheme for Different Types of Short Circuit Faults on Double Circuit Transmission Lines

2.1 Introduction

The vast extent of non-insulated transmission lines experience different weather conditions that make them easily prone to stochastic fault conditions. The protection of double circuit transmission lines (DCTL) with conventional distance relays is difficult due to the mutual inductive coupling between the phases of the two circuits. Whenever a fault occurs on one of the circuits, the fault current is also induced into the healthy phase(s) of the other circuit of DCTL besides the faulty phase(s). So, the distance relay operation i.e., based on the voltage and current measurements, may issue a false trip to the healthy phase(s) of the line(s). The zero-sequence mutual impedance of the lines, fault path resistance, various faults, pre-fault system conditions, and the effects due to infeed currents and shunt capacitances pose problems to the distance relaying schemes [88–90]. The main aim of the transmission line protection scheme is to identify and isolate the fault as quickly as possible to maintain the stability of the system. The quick detection and classification of faults help the repairs/maintenance crew to improve the service restoration time. A reliable protection scheme ensures the safe and secure operation of the transmission network with minimal interruption and early restoration of the quality power supply.

The present chapter proposes an artificial intelligence-based protection scheme with a single FIS module for the FDC of faults on the DCTL. The proposed FIS based FDC protection scheme is based on the simple fuzzy logic concept. It uses only the magnitude of the fundamental frequency component of three-phase currents and zero sequence currents of both the lines of the sending end bus that are pre-processed with DFT. The proposed FDC protection scheme is implemented in the MATLAB/Simulink environment on 400 kV, 50 Hz, 300 km DCTL; it correctly detects and identifies the different fault types within one cycle time (20 ms). The key advantages of the proposed protection scheme are:

- Require no training of the FIS module.
- No communication link (hence no communication delay as single-end data is used).
- Single FIS module suitable for single and double circuit operation.
- Reduced complexity of protection task as the simple fuzzy logic concept is involved.

2.2 Details of Double Circuit Power System Model

Fig. 2.1 shows the one-line diagram of the considered power system model. The considered power system network is modelled and simulated in the MATLAB/Simulink

environment. It consists of a three-phase double circuit transmission line of 400 kV, 50 Hz, 300 km long line that is fed from the three phase sources at both ends of the line [21]. The transmission line is divided into three sections (section-1, section-2, and section-3) each 100 km in length. The two three-phase sources of 400 kV, 50 Hz having a short circuit capacity of 1.25 GVA and X/R ratio of 10 are connected at the bus B1 (sending end bus) and bus B4 (receiving end bus). The three-phase source connected at the bus B4 represents Thevenin's equivalent source of the interconnected grid. A load of 100 kW and 100 kVar is connected at bus B1. At bus B4, a load of 250 kW is connected. The distributed parameter model block from MATLAB is used to implement the double circuit transmission line to address the effect of the distributed shunt capacitance and mutual coupling of impedance between the lines of the two circuits. The three-phase fault breakers are used to simulate the different types of short circuit faults (symmetrical and unsymmetrical faults) with a particular fault inception time and fault resistance. The system parameters and operating conditions are detailed in Appendix – I.

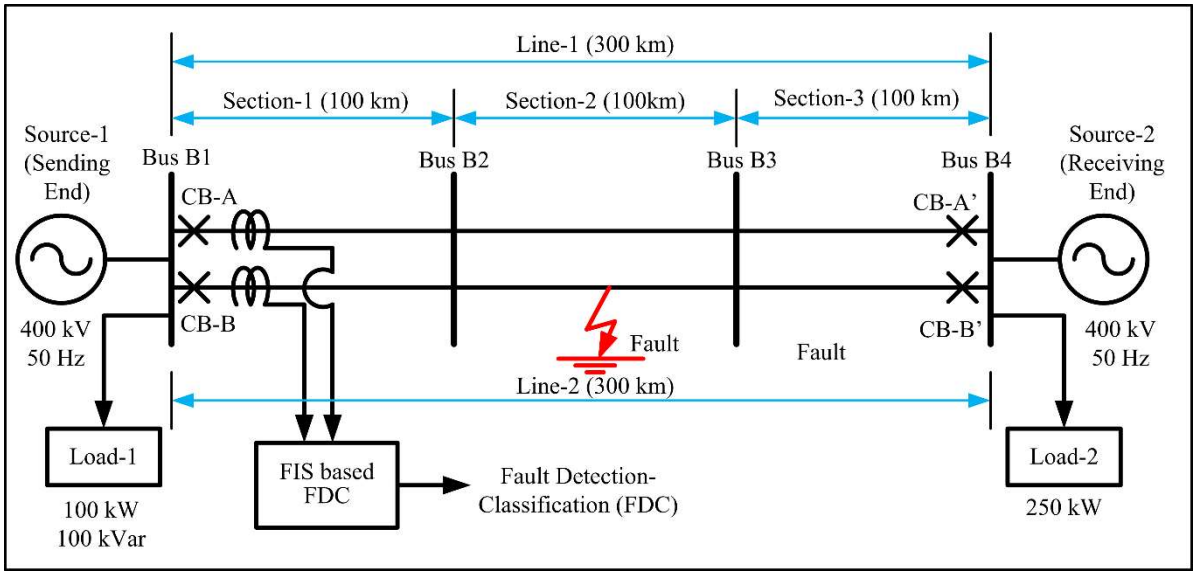

Fig. 2.1 One-line diagram of the considered double circuit power system model

2.3 Development of Proposed Protection Scheme with FIS for FDC

In general, any protection scheme has broadly two stages: i) feature extraction and ii) the actual method of the protection scheme. In the present work, the DFT is used for the feature extraction process and the fuzzy inference system is used for the protection scheme.

2.3.1 Feature Extraction Process with DFT

The raw fault data of instantaneous voltage/current signals available at the relaying point cannot better represent the fault signatures useful for the protection task as it is highly oscillatory and transient in nature. Therefore, they should be discretized and pre-processed for digital protection applications. The time-domain raw signal has to be transformed into a frequency-domain signal to extract the useful features for relaying purposes using the signal processing technique (DFT).

The three-phase instantaneous current signals of line-1 and line-2 available at the relaying point (Bus B1 in Fig. 2.1) are used for the proposed protection scheme. To filter out the higher-order harmonics in the recorded instantaneous current signals of line-1 and line-2, the second-order low-pass Butterworth filter with a cut-off frequency of 480 Hz is used. The filtered current signals are sampled at a 1 kHz sampling frequency according to the Nyquist sampling theorem. The full cycle DFT is applied to the discrete current samples of line-1 and line-2 to extract the magnitude of the fundamental frequency component of current signals. The DFT *X(k)* of a discrete-time signal *x(n)* is given in Eq. (2.1)[91].

$$X[k] = \frac{1}{N}\sum_{n=0}^{N-1} x(n)e^{-j2\pi nk/N} \tag{2.1}$$

where *x(n)* is the discrete-time signal, *k = 0, 1, 2, 3, ..., N-1, n = 0, 1, 2, 3, ..., N-1,* and *N* is the no. of samples per cycle.

The zero-sequence currents (ZSCs) are available only when the ground is involved in the fault loop. So, the zero-sequence analyser from MATLAB is used to extract the ZSCs of both the lines at bus B1 for ground faults detection/classification purpose. Therefore, the required seven input features for the proposed FIS based FDC scheme are the magnitudes of fundamental frequency components of the six phase currents (|*Ia1*|, |*Ib1*|, |*Ic1*| of line-1 and |*Ia2*|, |*Ib2*|, |*Ic2*| of line-2) and the sum of ZSCs of line-1 and line-2 (|*I0*| = |*I01*|+|*I02*|).

2.3.2 Proposed FIS Based FDC Protection Scheme

The proposed protection scheme uses the fuzzy logic concept [8]. The fuzzy logic systems are simple in structure, flexible, and easy to implement. The fuzzy logic system accepts any type of data (vague or imprecise) and provides a precise solution with human-like reasoning. They are independent of the mathematical model of the system and can solve non-linear

models/problems without rigorous computational effort. The fuzzy logic concept is based on the fuzzy set theory. It introduces the idea of partial true or partial false values. The operation of the fuzzy logic system is based on the fuzzy rules framed using the simple *"IF-THEN"* conditional arguments that maps the input and output fuzzy sets using the fuzzy linguistic variables (i.e., represented with the membership functions). The functional operation of a fuzzy inference system consists of three stages: i) fuzzification, ii) fuzzy inference processing, and iii) defuzzification.

In the present work, a single fuzzy inference system module is implemented using the Fuzzy Logic Toolbox of MATLAB for the FDC of short circuit faults to protect the three-phase DCTL. Fig. 2.2 and Fig. 2.3 depict the schematic diagram and the flowchart of the proposed FIS based FDC protection scheme. It has seven inputs (*+Y|Ia1|, +Y|Ib1|, +Y|Ic1|, -Y|Ia2|, -Y|Ib2|, -Y|Ic2|, and |I0|*) and seven outputs (*'A1', 'B1', 'C1', 'A2', 'B2', 'C2' and 'G'*). The input features required for the protection task are obtained from the feature extraction process i.e., detailed in Section 2.3.1. The FIS based FDC module outputs *'A1', 'B1', 'C1'* for line-1 and *'A2', 'B2', 'C2'* for line-2 are used to represent the healthy/faulty phase(s) for the FDC task. The output *'G'* is used to detect the ground faults. The output labels *"0"* (to indicate the healthy condition) and *"1"* (to indicate the faulty condition) are used for all the outputs (*Ai, Bi, Ci, and G; i=1, 2*).

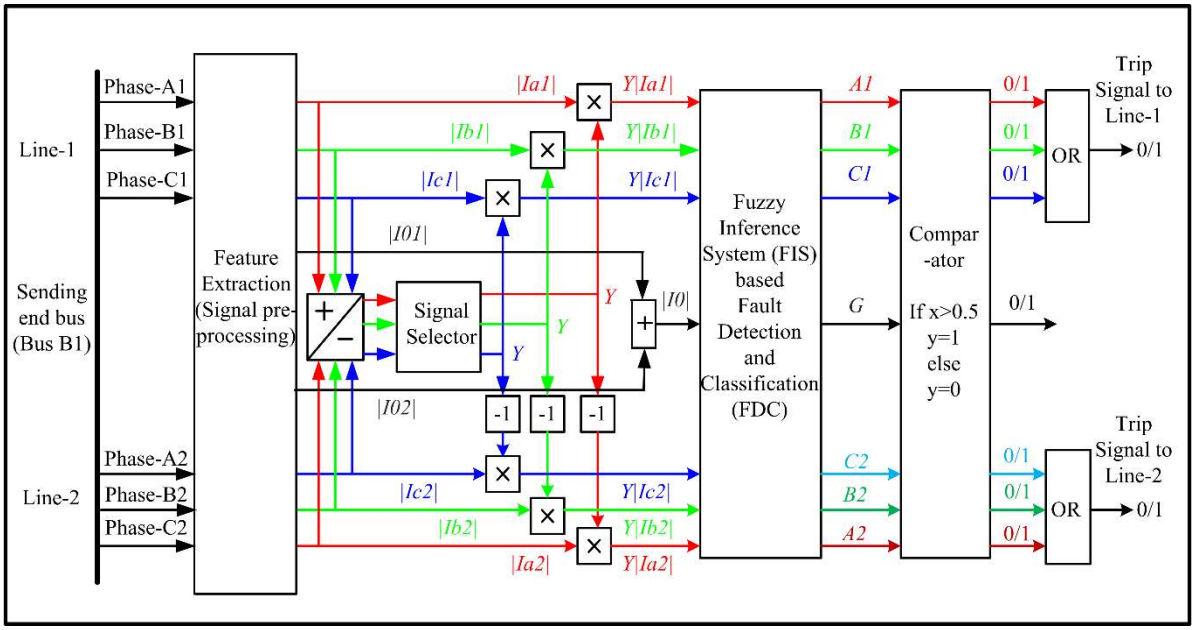

Fig. 2.2 Block diagram of the proposed FIS based FDC protection scheme

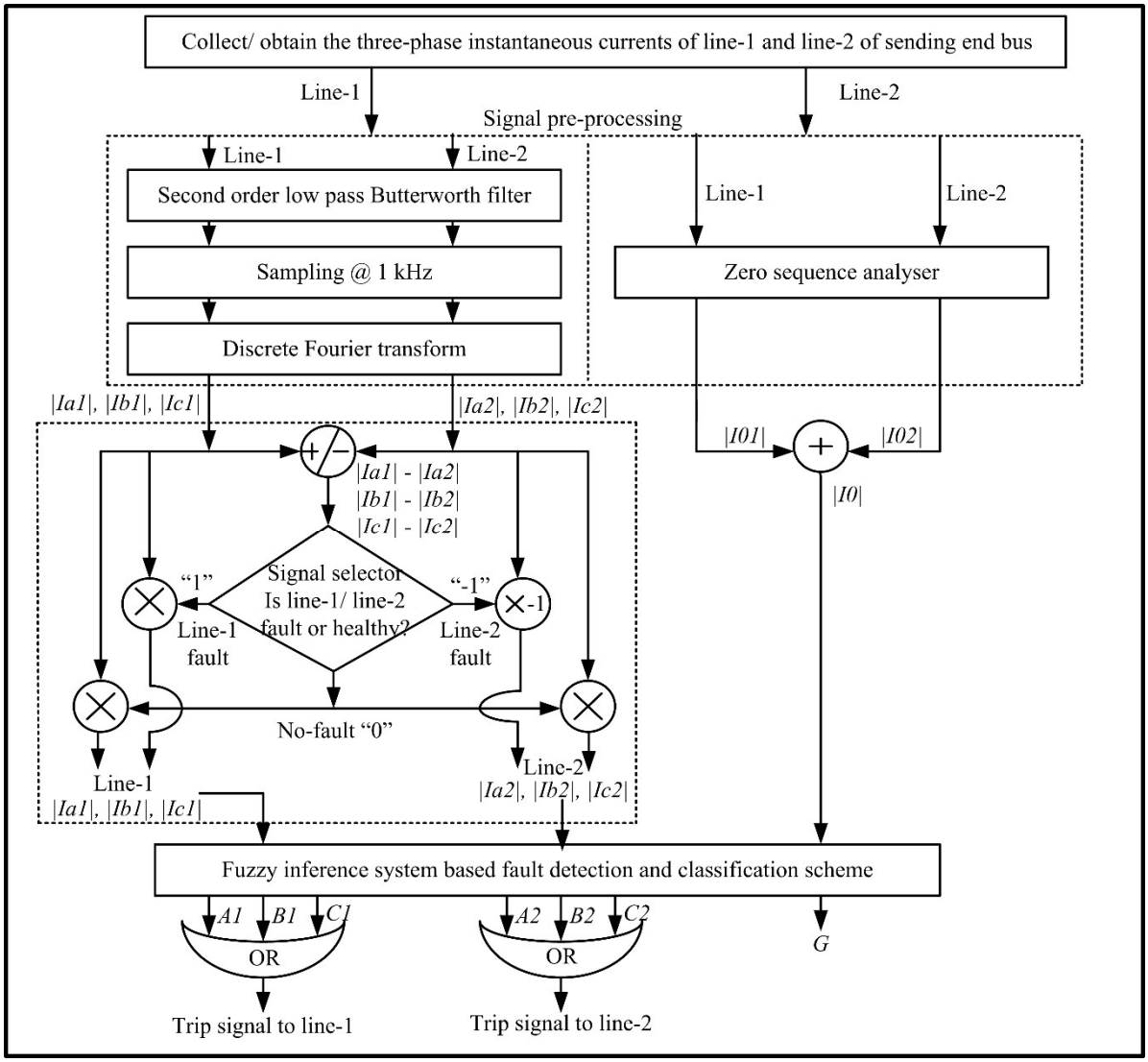

Fig. 2.3 Flowchart of the proposed FIS based FDC protection scheme

The input features obtained after the feature extraction process have been modified by using the signal selector output to have a better understandability of the input features. Eq. (2.2) specifies the signal selector output (Y) based on the threshold condition. A wide range of simulation studies have been performed on the power system network shown in Fig. 2.1 by simulating different types of faults with varying fault resistances and fault inception angles at different fault locations for determining the threshold.

$$Y = \begin{Bmatrix} -1; & |Ip1| - |Ip2| < -3\ A \\ 0; -3\ A \leq |Ip1| - |Ip2| \leq 3\ A \\ 1; & |Ip1| - |Ip2| > 3\ A; \end{Bmatrix} where\ p = a, b, c\ phases \quad (2.2)$$

The signal selector output is *"1"* or *"-1"* if the fault is in line-1 or line-2. The signal selector output is *"0"* if the system is healthy. The input features of line-1 are multiplied with the signal selector output and the input features of line-2 are multiplied with the negative value of the signal selector output. Thus, the product of signal selector output and input features yields a positive magnitude for the actual faulty phases and a negative magnitude for the healthy phases. The modified vector of input features in Eq. (2.3) is given as input to the FIS based FDC protection module.

$$Modified\ vector\ of\ input\ features = [+Y|Ia1| \quad +Y|Ib1| \quad +Y|Ic1| \quad -Y|Ia2| \quad -Y|Ib2| \quad -Y|Ic2| \quad |I0|]^T \qquad (2.3)$$

where $|I0| = |I01| + |I02|$.

The inputs and outputs of the proposed FIS based FDC protection module are fuzzified using triangular membership functions. It is generally represented by the three vertices of the triangle. Although the triangular membership functions are chosen based on the trial-and-error basis method by conducting a series of simulations with varying extreme fault conditions, it can easily detect even the smallest changes in the input and output. Table 2.1 presents the information on input and output membership functions. Each of the input and output variable space is grouped under two fuzzy linguistic variables (two membership functions) using the triangular membership functions. The input linguistic variables *'Fault (F)'* and *'No-Fault (NF)'* are used for the input variable $\pm Y|Ipi|$. The *'+'* sign is for line-1 input features and the *'-'* sign is for line-2 input features. The input linguistic variable *'Absent (A)'* and *'Present (P)*' are used for the input variable $|I0|$. Similarly, the output linguistic variables *'LOW (L)'* and *'HIGH (H)'* are used for the output variables *Ai, Bi, Ci,* and *G (i = 1, 2)*.

Table 2.1 Input and output membership functions

Input Variable	Input Linguistic Variable [Triangular Membership Function]	Output Variable	Output Linguistic Variable [Triangular Membership Function]
$\pm Y\|Ipi\|$	No-Fault *(NF)*	*Pi*	LOW *(L)*
	Fault *(F)*		HIGH *(H)*
$\|I0\|$	Absent *(A)*	*G*	LOW *(L)*
	Present *(P)*		HIGH *(H)*
where *p=a, b, c and i=1, 2*		where *P=A, B, C and i=1, 2*	

Table 2.2 presents the rule base or framed rules for the proposed FIS based FDC protection scheme. A total of 22 fuzzy rules are framed for the proposed protection scheme. The first row and column in Table 2.2 represent the input linguistic variables and all other rows and columns represent the output linguistic variables. For example, the rule corresponding to the second row and column with $i = 1$ is "*If Y|Ia1| is 'No-Fault' and Y|Ib1| is 'Fault' and Y|Ic1| is 'No-Fault' and |I0| is 'Present' then A1 is 'LOW' B1 is 'HIGH' C1 is 'LOW' G is 'HIGH'*". Similarly, all other rules are framed. Depending on the fault current the input is directly mapped to the output based on the fired fuzzy rules. The FIS provides the degree of fault severity as a crisp value after the defuzzification process. The centroid method of defuzzification is used. The seven outputs of the FIS based FDC module are given to the comparator block to have the binary outputs in each phase (*"0"* and *"1"*). The trip signal to the circuit breakers of line-1/line-2 is generated by the *"OR"* operation of the FIS based FDC module binary outputs of line-1/line-2. When any short circuit fault occurs on the line, the outputs of FIS based FDC protection module shows *"HIGH"* with "1" for faulty phase(s) and the healthy phases shows *"LOW"* with *"0",* indicating the FDC.

Table 2.2 Rule base for the FIS based FDC

Input Linguistic Variables *(±Y|Ici|, |I0|) → (±Y|Iai|, ±Y|Ibi|), i=1,2* ↓	*[NF, A]*	*[NF, P]*	*[F, A]*	*[F, P]*
[NF, NF]	*[L, L, L, L]*	-	-	*[L, L, H, H]*
[NF, F]	-	*[L, H, L, H]*	*[L, H, H, L]*	*[H, L, H, H]*
[F, NF]	-	*[H, L, L, H]*	*[H, L, H, L]*	*[H, L, H, H]*
[F, F]	*[H, H, L, L]*	*[H, H, L, H]*	*[H, H, H, L]*	-
where *NF* = No-Fault, *F* = Fault, *A* = Absent, *P* = Present, *L* = LOW, *H* = HIGH				

2.4 Results and Discussion

The performance/response of the proposed FIS based FDC protection scheme is tested for all the ten types of short circuit faults on the transmission lines and different operating conditions of the system shown in Fig. 2.1 with varying fault parameters viz., fault location (L_f) (1 km to 299 km), fault inception angle (Φ) (0º to 360º), and fault resistance (R_f) (0 Ω to

200 Ω). The proposed FDC scheme response is also evaluated for cross-country faults, evolving faults, and high impedance faults (HIF). Further, the performance has been evaluated under current transformer (CT) saturation, noisy environment, and fault during power swing conditions. The following subsections discuss the simulation test results and comparison results of the proposed FDC protection scheme.

2.4.1 Test Results for Variation in the Fault Parameters

The faults on the transmission lines are random in nature, i.e., they can occur at any point on the transmission lines at any instant with any fault resistance. The performance of the proposed FDC scheme is evaluated for the fault parameter variations. Fig. 2.4 (a) and (b) represents the three phase instantaneous currents of line-1 and line-2 of the sending end bus (Bus B1) for a single line to ground (LG) fault in line-1 (AG-1) simulated at a fault location (L_f) of 250 km from the bus B1 with fault resistance (R_f) of 50 Ω and fault inception angle (Φ) of 0º (fault inception time, T_f = 60 ms). Fig. 2.4 (c) depicts the input features (magnitude of fundamental component and zero sequence currents) extracted using the feature extraction process. From Fig. 2.4 (c), it can be observed that there is also a rise in the current magnitude of the healthy phase along with the faulty one due to the zero sequence mutual impedance of the lines. Fig. 2.4 (d) and (e) depicts the response of the proposed FIS based FDC protection scheme that correctly detects and classifies the fault, and issues a trip signal in 4 ms after the occurrence of the fault.

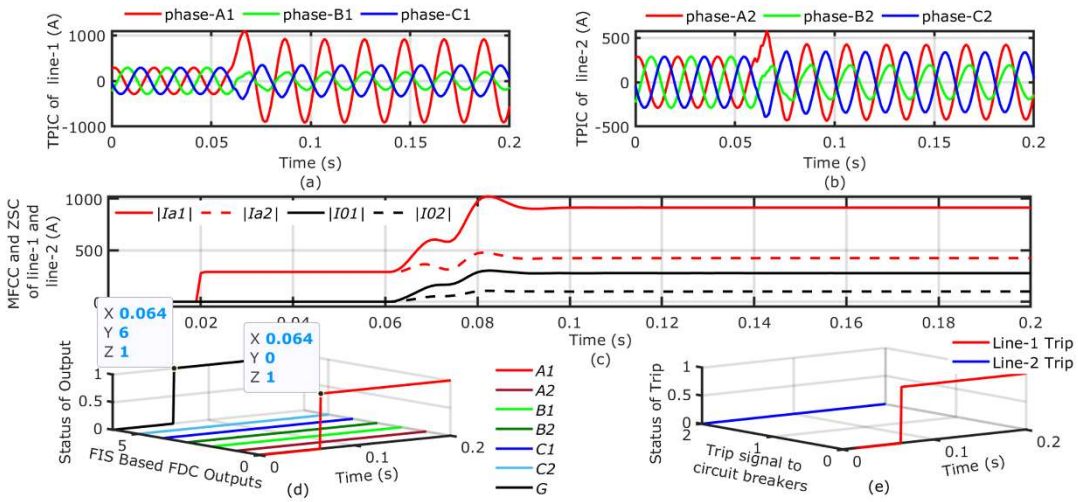

Fig. 2.4 (a) and **(b)** Current waveforms of line-1 and line-2 during the LG fault in line-1 (AG-1), **(c)** MFCCs and ZSCs of line-1 and line-2, **(d)** FIS based FDC outputs, and **(e)** Trip signal to circuit breakers

Table 2.3 gives the test results of the proposed FIS based FDC protection scheme with variations in the fault parameters.

Table 2.3 Test results for variations in the fault parameters

S. No	Fault Parameters	Fuzzy Inference System Based Fault Detection and Classification Outputs							Instant of Fault Detection and Classification Time (ms)						
	Fault Type-Line no., Fault Location (km), Fault Resistance (Ω), Fault Inception Angle (Time of fault (ms))	A 1	B 1	C 1	A 2	B 2	C 2	G	A 1	B 1	C 1	A 2	B 2	C 2	G
1	AG-1, 80, 50, 0º (60)	1	0	0	0	0	0	1	63	-	-	-	-	-	63
2	BCG-1, 30, 120, 90º (65)	0	1	1	0	0	0	1	-	68	70	-	-	-	68
3	AC-1, 170, 10, 45º (62.5)	1	0	1	0	0	0	0	67	-	67	-	-	-	-
4	ABC-1, 280, 20, 180º (70)	1	1	1	0	0	0	0	75	75	82	-	-	-	-
5	BG-2, 210, 200, 150º (68.33)	0	0	0	0	1	0	1	-	-	-	-	73	-	73
6	ABG-2, 299, 200, 0º (60)	0	0	0	1	1	0	1	-	-	-	77	77	-	79
7	BCG-2, 165, 150, 300º (76.67)	0	0	0	0	1	1	1	-	-	-	-	80	82	80

2.4.2 Test Results for Remote End Fault with High Fault Resistance and Close-in Faults

Unlike the conventional distance relay which depends on the voltage and current measurements at the relay point, the proposed protection scheme is dependent only on the current signals at the relaying point. Fig. 2.5 (f) depicts the response of the proposed FIS based FDC protection scheme for the remote end fault (LLG fault in the line-2 (ABG-2)) simulated at L_f = 299 km from the bus B1 with R_f = 200 Ω and Φ = 0º (T_f = 60 ms). The proposed FDC protection scheme can detect and classify the fault within one cycle time of fundamental frequency.

The performance of the proposed protection scheme is evaluated for remote end and close-in faults and the test results are depicted in Table 2.4. In Table 2.4, the fault parameter column gives the details of the simulated fault type in line-1/line-2 with different fault locations, fault resistances, and fault inception angles. The proposed protection scheme detects remote end faults and close-in faults effectively.

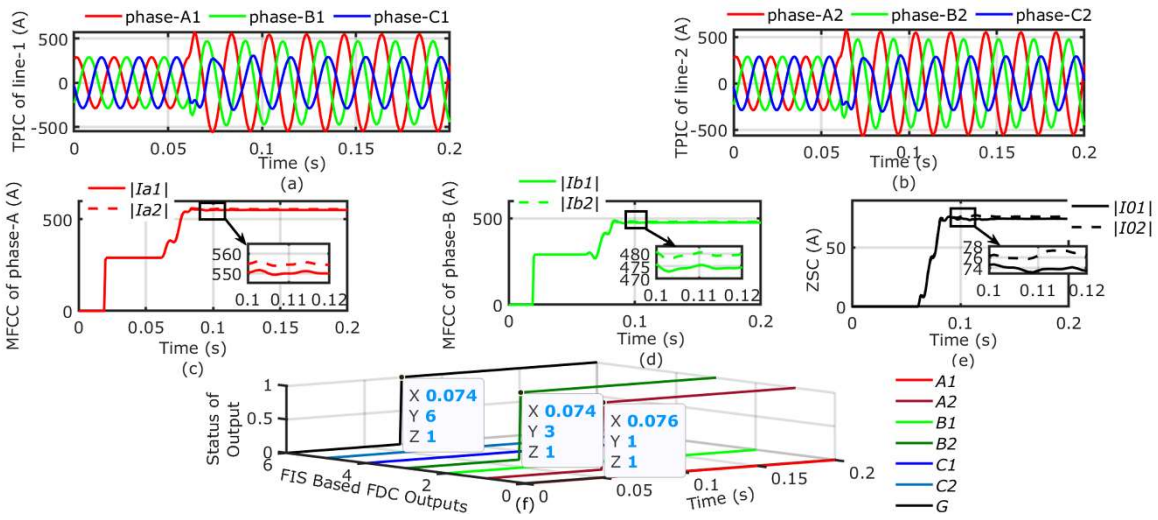

Fig. 2.5 (a) and **(b)** Current waveforms of line-1 and line-2 respectively for the remote end fault, ABG-2 fault (L_f = 299 km, R_f = 200 Ω and Φ = 0º (T_f = 60 ms)), **(c)**, **(d)**, and **(e)** MFCCs for phase-A and phase-B, and ZSCs respectively for line-1 and line-2, and **(f)** FIS based FDC outputs

Table 2.4 Test results for remote end and close-in faults

S.No	Fault Parameter	Fuzzy Inference System Based Fault Detection and Classification Outputs							Instant of Fault Detection and Classification Time (ms)				
	Fault Type-Line no., Fault Location (km), Fault Resistance (Ω), Fault Inception Angle (Time of fault (ms))	A1	B1	C1	A2	B2	C2	G	A1	B1	C1	G	
1	AG-1, 1, 5, 0º (60)	1	0	0	0	0	0	1	62	-	-	62	Close-in Faults
2	ABG-1, 5, 15, 45º (62.5)	1	1	0	0	0	0	1	64	66	-	64	
3	ABC-1, 15, 20, 90º (65)	1	1	1	0	0	0	0	66	67	66	-	
4	AC-1, 20, 10, 270º (75)	1	0	1	0	0	0	0	77	-	77	-	
5	AG-1, 299, 180, 0º (60)	1	0	0	0	0	0	1	75	-	-	75	Remote End Faults
6	ABG-1, 295, 190, 45º (62.5)	1	1	0	0	0	0	1	74	82	-	74	
7	AB-1, 298, 25, 90º (65)	1	1	0	0	0	0	0	79	79	-	-	
8	ABC-1, 293, 20, 270º (75)	1	1	1	0	0	0	0	87	82	82	-	

2.4.3 Test Results for Cross-country and Evolving Faults

The cross-country fault (CCF) is defined as the earth faults occurring on different phases at different locations of the same circuit or different circuits at different instants or the same instant of time. The fault which incepts in one phase and spreads/creeps to the other phases of the same circuit after a few cycles at the same location is called an evolving fault (EF) [18]. The proposed FDC protection scheme can detect and classify the cross-country and evolving faults as LG, LLG, LL, and LLL faults. As per the proposed FDC scheme, if the difference in

the FDC time of any two phases is greater than the half-cycle time (10 ms), then the detected fault is an evolving fault. Otherwise, it is a common short circuit fault. Fig. 2.6 (b) depicts the test result for a cross-country fault with fault-1 (AG-1 in line-1) and fault-2 (CG-2 in line-2) simulated at L_f = 30 km from bus B1, with R_f = 100 Ω, and Φ = 0º (T_f = 60 ms). The FDC time for the cross-country fault is within half-cycle time (10 ms), as depicted in Fig. 2.6 (b). Fig. 2.7 (b) depicts the test result for the evolving fault with fault-1: LG fault in the line-1 (AG-1) at L_f = 150 km with R_f = 50 Ω and Φ = 0º (T_f = 60 ms) and fault-2: LG in the line-1 (BG-1) at L_f = 150 km with R_f = 50 Ω and Φ = 0º (T_f = 80 ms). The FDC time for the evolving fault is within 5 ms time after the fault inceptions and the difference in FDC time of the faulty phases is greater than 10 ms time, as shown in Fig. 2.7 (b).

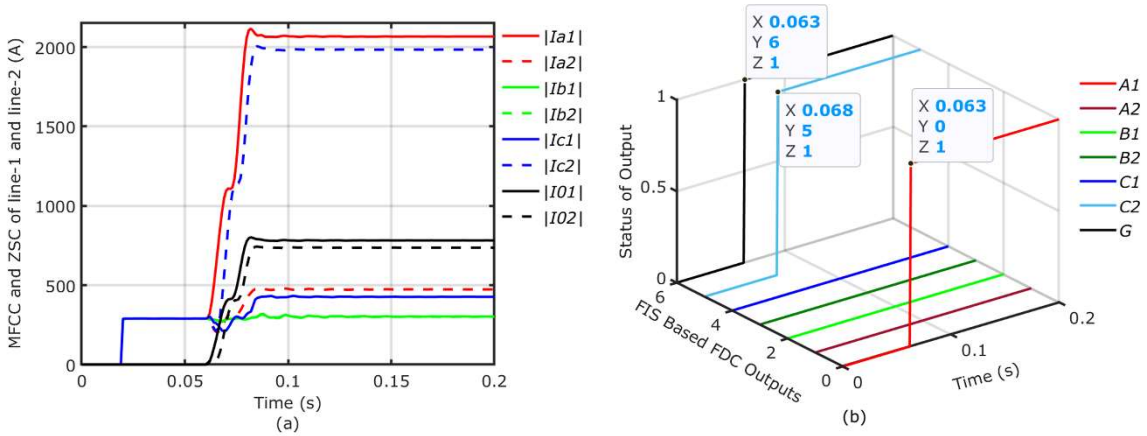

Fig. 2.6 (a) MFCCs and ZSCs of line-1 and line-2 for the cross-country fault and **(b)** FIS based FDC outputs

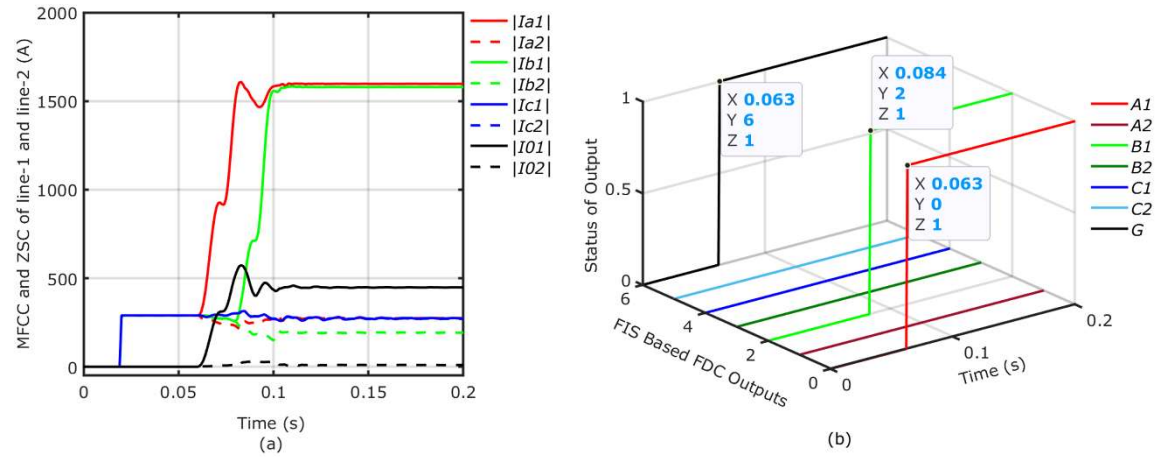

Fig. 2.7 (a) MFCCs and ZSCs of line-1 and line-2 for the evolving fault and **(b)** FIS based FDC outputs

The performance of the proposed protection scheme is evaluated for the cross-country and evolving faults. The test results are depicted in Table 2.5 and Table 2.6 with fault parameters of fault-1 and fault-2 in the first two columns and the FIS based FDC outputs along with the instant of the FDC time in the third column.

Table 2.5 Test results of the proposed protection scheme for cross-country faults

S. No.	Cross-Country Faults		Fuzzy Inference System Based Fault Detection and Classification Outputs (Instant of Fault Detection and Classification Time (ms))						
	Fault-1	Fault-2							
	Fault Type-Line no., Fault Location (km), Fault Resistance (Ω), Fault Inception Angle (Time of fault (ms))	Fault Type-Line no., Fault Location (km), Fault Resistance (Ω), Fault Inception Angle (Time of fault (ms))	A1	B1	C1	A2	B2	C2	G
1	AG-1, 7, 50, 0° (60)	BG-1, 55, 50, 0º (60)	1 (63)	1 (62)	0 (-)	0 (-)	0 (-)	0 (-)	1 (62)
2	BCG-1, 50, 150, 0º (60)	AG-1, 250, 10, 0º (60)	1 (66)	1 (63)	1 (69)	0 (-)	0 (-)	0 (-)	1 (64)
3	AG-1, 98, 90, 45º (62.5)	CG-1, 205, 60, 45º (62.5)	1 (65)	0 (-)	1 (70)	0 (-)	0 (-)	0 (-)	1 (65)
4	CG-1, 170, 75, 45º (62.5)	AG-1, 258, 200, 45º (62.5)	1 (76)	0 (-)	1 (68)	0 (-)	0 (-)	0 (-)	1 (67)
5	AG-1, 1, 200, 90º (65)	CG-1, 299, 5, 90º (65)	1 (75)	0 (-)	1 (70)	0 (-)	0 (-)	0 (-)	1 (70)
6	AG-1, 1, 200, 90º (65)	CG-1, 299, 200, 90º (65)	1 (74)	0 (-)	1 (81)	0 (-)	0 (-)	0 (-)	1 (73)
7	CG-1, 65, 15, 180º (70)	BG-1, 165, 15, 180º (70)	0 (-)	1 (73)	1 (79)	0 (-)	0 (-)	0 (-)	1 (74)
8	AG-1, 190, 40, 270º (75)	CG-1, 260, 50, 270º (75)	1 (81)	0 (-)	1 (79)	0 (-)	0 (-)	0 (-)	1 (79)
9	AG-1, 80, 30, 0º (60)	BG-2, 110, 30, 0º (60)	1 (63)	0 (-)	0 (-)	0 (-)	1 (63)	0 (-)	1 (63)
10	BG-1, 10, 100, 0º (60)	CG-2, 290, 100, 0º (60)	0 (-)	1 (63)	0 (-)	0 (-)	0 (-)	1 (71)	1 (63)

Table 2.6 Test results of the proposed protection scheme for evolving faults

S. No.	Evolving Faults		Fuzzy Inference System Based Fault Detection and Classification Outputs (Instant of Fault Detection and Classification Time (ms))						
	Fault-1	Fault-2							
	Fault Type-Line no., Fault Location (km), Fault Resistance (Ω), Fault Inception Angle (Time of fault (ms))	Fault Type-Line no., Fault Location (km), Fault Resistance (Ω), Fault Inception Angle (Time of fault (ms))	A1	B1	C1	A2	B2	C2	G
1	AG-1, 20, 50, 0º (60)	CG-1, 20, 50, 0º (80)	1 (63)	0 (-)	1 (88)	0 (-)	0 (-)	0 (-)	1 (64)
2	BG-1, 90, 100, 0º (60)	CG-1, 90, 100, 0º (80)	0 (-)	1 (63)	1 (89)	0 (-)	0 (-)	0 (-)	1 (63)
3	ABG-1, 150, 40, 90º (65)	CG-1, 150, 40, 90º (85)	1 (75)	1 (71)	1 (89)	0 (-)	0 (-)	0 (-)	1 (71)
4	AC-1, 190, 10, 90º (65)	BG-1, 190, 10, 90º (85)	1 (70)	1 (91)	1 (70)	0 (-)	0 (-)	0 (-)	1 (90)
5	BG-1, 245, 150, 180º (70)	AG-1, 245, 150, 180º (90)	1 (94)	1 (82)	0 (-)	0 (-)	0 (-)	0 (-)	1 (82)
6	CG-1, 280, 200, 270º (75)	BG-1, 280, 200, 270º (95)	0 (-)	1 (102)	1 (88)	0 (-)	0 (-)	0 (-)	1 (88)
7	AG-1, 110, 200, 300º (76.67)	BG-1, 110, 200, 300º (96.67)	1 (85)	1 (102)	0 (-)	0 (-)	0 (-)	0 (-)	1 (85)
8	BC-1, 135, 15, 0º (60)	AG-1, 135, 15, 0º (80)	1 (85)	1 (70)	1 (70)	0 (-)	0 (-)	0 (-)	1 (82)
9	AG-1, 50, 25, 0º (60)	BC-1, 50, 25, 0º (80)	1 (63)	1 (83)	1 (88)	0 (-)	0 (-)	0 (-)	1 (63)

2.4.4 Test Results for Power Swing (PS) Conditions and Fault During Power Swing (FPS) Conditions

One of the reasons for the stressed conditions of the power system is the power swing. The variations or oscillations in the power flow angle is called power swing. The power swings are due to the sudden switching on/off of heavy loads, loss of lines or generators, loss of frequency synchronism, and the clearance of short circuit faults. The power swing blocking (PSB) unit provided with the distance relays avoids unnecessary tripping of the lines and blocks the conventional distance relay operation during the power swings [19, 92, 93]. When a fault occurs during the power swing, the relay may not detect the fault. A protection scheme should be good enough to block the trip signal during a power swing condition and issue the trip signal for a fault during the power swing condition. The proposed protection scheme

performance has been evaluated for the power swing condition and fault during a power swing condition. For this case, the generator model from MATLAB is used along with the transformer with the parameters available in [92]. Fig. 2.8 (a) depicts the current waveform during power swing conditions due to the switching of heavy load (500 MW) at bus B4 at 0.6 s. Fig. 2.8 (b) presents the FIS based FDC outputs with *'LOW'* or *'0'* status for the power swing condition.

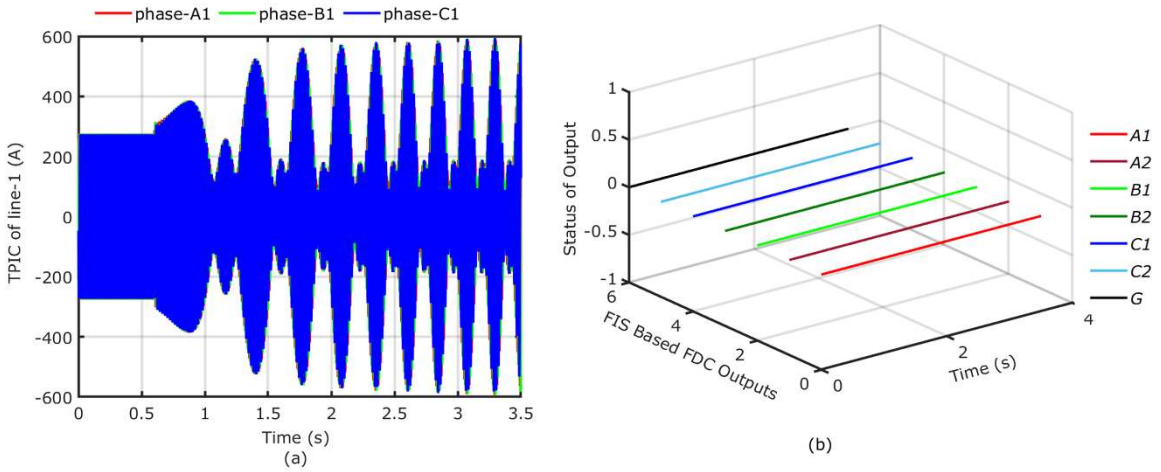

Fig. 2.8 (a) Current waveforms of line-1 during power swing condition due to the switching of heavy load at 0.6 s and (b) FIS based FDC outputs

The proposed FDC protection scheme performance is also evaluated for the fault during the power swing condition. The current waveform for fault during power swing condition is depicted in Fig. 2.9 (a). The power swing is because of the loss of line-2 at an instant of 0.7 s due to the clearance of ABG-2 fault (L_f = 150 km, R_f = 50 Ω, and T_f = 0.6 s) and the fault is LG fault in the line-1 (AG-1) at L_f = 50 km, R_f = 0.01 Ω, and T_f = 2 s. During the single circuit operation, line-1 carries the total power of the system due to the loss of line-2. So, the line-1 inputs applied to the FIS based FDC module are reduced to half to avoid tripping during power swing conditions. Fig. 2.9 (b) presents the FIS based FDC outputs for fault during power swing conditions. It is clear from Fig. 2.9 (b) that the proposed FDC protection scheme can detect/classify the fault correctly for fault during power swing conditions. All the FIS based FDC outputs are *"LOW"* with *"0"* during power swing mode and *"HIGH"* with *"1"* for the fault during the power swing mode for faulty phases.

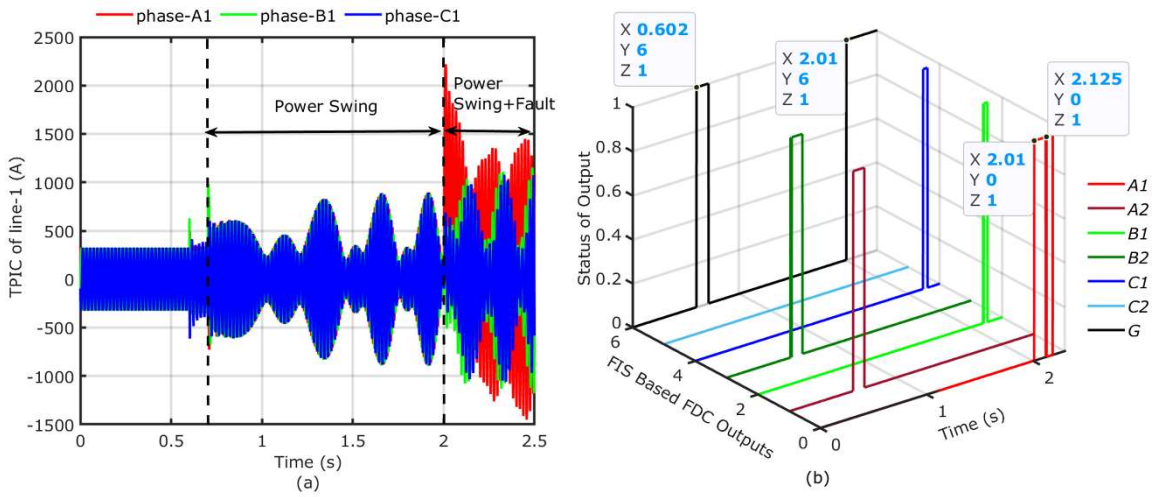

Fig. 2.9 (a) Current waveforms of line-1 for a fault during the power swing case at 2 s and **(b)** FIS based FDC outputs

2.4.5 Test Results in the Presence of Noisy Environment

The recorded current signals at the relaying point may be contaminated with noise due to the integrated circuits in the data acquisition devices and other data pre-processing devices in the power system network. To evaluate the performance of the proposed FDC protection scheme in a noisy environment, the white Gaussian noise with different signal to noise ratios (SNR in dB) 20, 30, 40, 50, and 60 dB is added in current signals. Fig. 2.10 depicts the proposed protection scheme response for the LLG fault in the line-1 (ABG-1, L_f = 50 km, R_f = 100 Ω, and Φ = 0º (at 60 ms)) with the SNR of 30 dB.

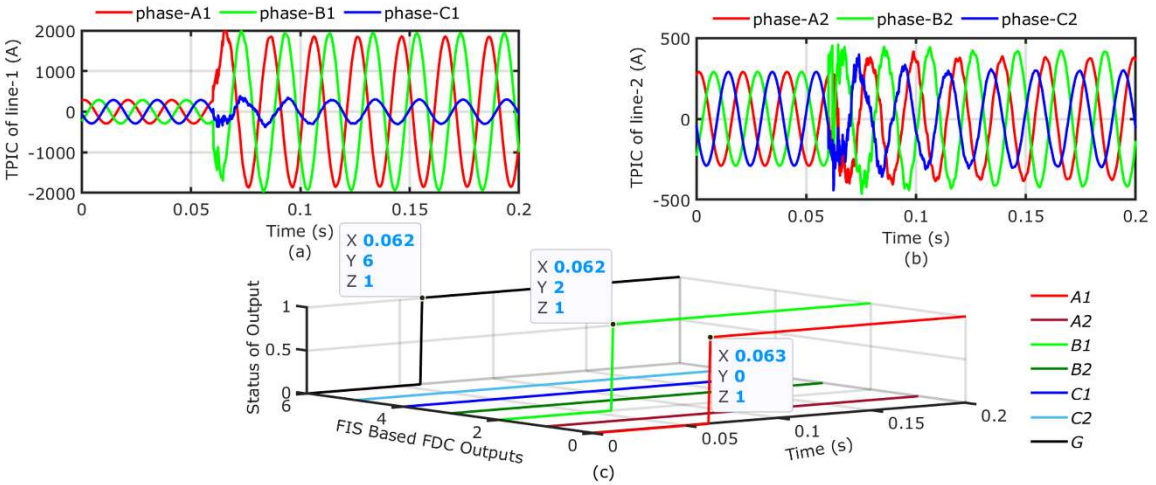

Fig. 2.10 (a) and **(b)** Current waveforms of line-1 and line-2 respectively during the LLG fault in the line-1 (ABG-1) with the SNR of 30 dB, and **(c)** FIS based FDC outputs

Table 2.7 depicts the tabulated test results of the proposed protection scheme response for different fault types in line-1 at L_f = 50 km from the bus B1 with R_f = 100 Ω and Φ = 0º (at 60 ms) in the presence of a noisy environment. As seen in Table 2.7, the proposed FIS based FDC protection scheme can detect and classify the faults within a half-cycle time of fundamental frequency.

Table 2.7 Test results of the proposed FDC protection scheme in the presence of noise

S. No.	Signal to Noise Ratio (SNR in dB)	Fault Type	Fuzzy Inference System Based Fault Detection and Classification Outputs							Instant of Fault Detection and Classification Time (ms)						
			A1	B1	C1	A2	B2	C2	G	A1	B1	C1	A2	B2	C2	G
1	20	AG-1	1	0	0	0	0	0	1	63	-	-	-	-	-	63
2		ABC-1	1	1	1	0	0	0	0	63	63	68	-	-	-	-
3	30	ABG-1	1	1	0	0	0	0	1	63	62	-	-	-	-	62
4		AB-1	1	1	0	0	0	0	0	63	63	-	-	-	-	-
5	40	AG-1	1	0	0	0	0	0	1	63	-	-	-	-	-	63
6		ABG-1	1	1	0	0	0	0	1	63	63	-	-	-	-	63
7	50	BG-1	0	1	0	0	0	0	1	-	63	-	-	-	-	63
8		ABC-1	1	1	1	0	0	0	0	63	63	68	-	-	-	-
9	60	BCG-1	0	1	1	0	0	0	1	-	63	69	-	-	-	63
10		CG-1	0	0	1	0	0	0	1	-	-	68	-	-	-	68

2.4.6 Test Results for High Impedance Faults (HIF)

The high impedance faults are concerned with the problems like arcing, fire, and electrocution. The HIF occurs when the live power conductor touches the tree branches or comes in contact with surfaces like asphalt, rocks, sandy soils, and concrete structures like buildings. A simplified Emanuel's HIF model [94–96] shown in Fig. 2.11 (c) is implemented to simulate the HIF. It consists of two anti-parallel diodes (D_p – positive half cycle diode and D_n – negative half cycle diode) with fault resistances R_p, R_n and the DC voltage sources V_p, V_n to represent the inception of the arcing voltages of air in the soil and/or between trees and the line. During the HIF simulation, the unequal values of R_p, R_n and V_p, V_n are varied randomly in the range of 200 Ω to 1000 Ω and 100 kV to 200 kV respectively [97]. Fig. 2.11 (d) depicts the test result of the proposed FDC protection scheme for the high impedance fault on the phase-A1 of the line-1 (HIF-A1) at L_f = 90 km from the bus B1 (T_f = 60 ms). The FDC

time by the proposed FDC protection scheme is 13 ms for the HIF-A1 as depicted in Fig. 2.11 (d).

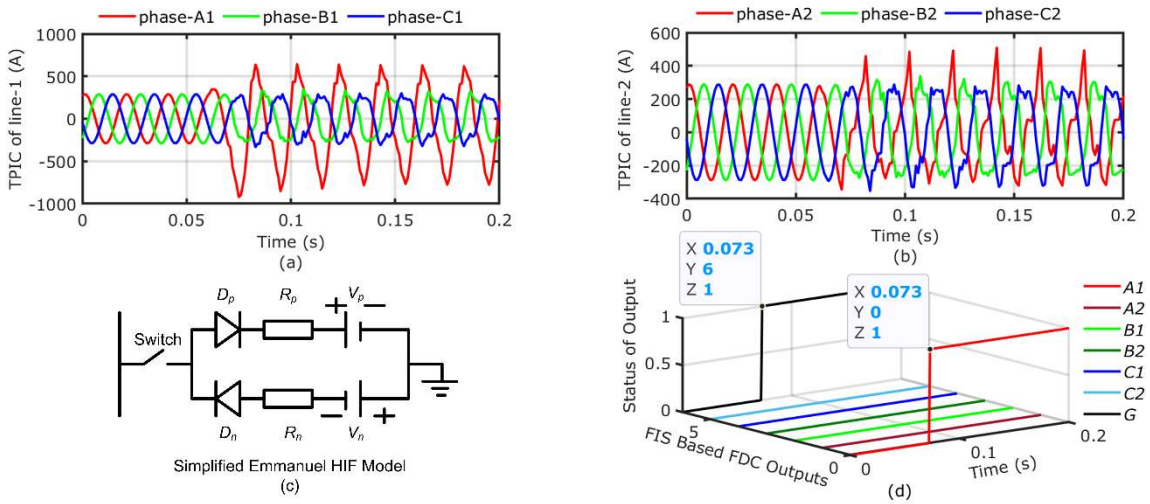

Fig. 2.11 (a) and **(b)** Currents waveforms of line-1 and line-2 for HIF-A1 respectively, **(c)** Simplified Emanuel's HIF model, and **(d)** FIS based FDC outputs

Table 2.8 presents the test results of the proposed FDC protection scheme for the HIF at different locations.

Table 2.8 Test results of the proposed protection scheme against high impedance faults

S. No	High Impedance Fault at $T_f = 60$ ms	Fault Location (km)	Fuzzy Inference System Based Fault Detection and Classification Outputs							Instant of Fault Detection and Classification Time (ms)						
			A1	B1	C1	A2	B2	C2	G	A1	B1	C1	A2	B2	C2	G
1	HIF-A1	1	1	0	0	0	0	0	1	64	-	-	-	-	-	64
2	HIF-A1	10	1	0	0	0	0	0	1	64	-	-	-	-	-	64
3	HIF-C1	70	0	0	1	0	0	0	1	-	-	76	-	-	-	76
4	HIF-A1	90	1	0	0	0	0	0	1	73	-	-	-	-	-	73
5	HIF-B1	150	0	1	0	0	0	0	1	-	72	-	-	-	-	72
6	HIF-A1	250	1	0	0	0	0	0	1	74	-	-	-	-	-	74
7	HIF-B1	275	0	1	0	0	0	0	1	-	77	-	-	-	-	77
8	HIF-A1	290	1	0	0	0	0	0	1	76	-	-	-	-	-	76
9	HIF-C1	295	0	0	1	0	0	0	1	-	-	80	-	-	-	80
10	HIF-A1	298	1	0	0	0	0	0	1	79	-	-	-	-	-	79

2.4.7 Test Results Under the Effect of Current Transformer Saturation

The high amount of dc offset current in the fault current is responsible for the CT saturation. The contribution of dc offset current is maximum in the fault current when the fault occurs at the zero fault inception angle. The reduced amount of the measured CT secondary current is due to the CT saturation. It is erroneous because it is not the facsimile of all the primary current. The distance relays may underreach/overreach due to the blinding of the relay caused by the CT saturation [21, 98, 99]. To consider the CT saturation effect on the proposed protection scheme performance, the saturated current transformers from MATLAB are used for the three-phase current measurements with the ratings of 25 VA and a CT ratio of 2000 A/5 A which are assumed to saturate at 2 pu. Fig. 2.12 (a) depicts the three-phase instantaneous currents of line-1 under CT saturation for the LG fault in the line-1 (AG-1) (L_f = 1 km, R_f = 5 Ω, and Φ = 0º (T_f = 60 ms)). Fig. 2.12 (b) depicts the FIS based FDC outputs detecting the fault in 2 ms time after the fault inception. It is evident from Fig. 2.12 (b) that CT saturation does not affect the proposed FDC protection scheme.

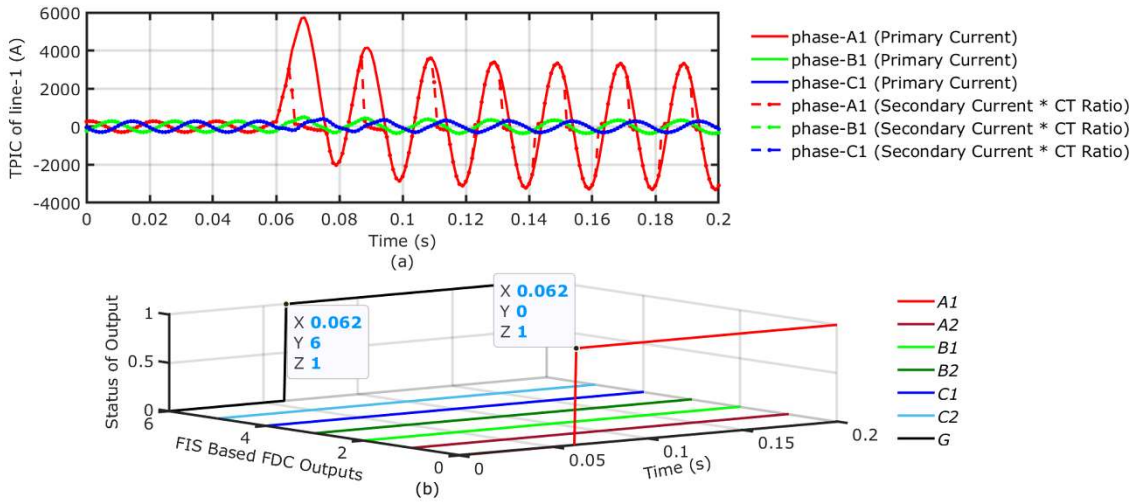

Fig. 2.12 (a) Currents waveforms of lines-1 for the LG fault in the line-1 (AG-1) under CT saturation and **(b)** FIS based FDC outputs under CT saturation

The FIS based FDC scheme response for different faults with CT saturation is tabulated in Table 2.9.

Table 2.9 Test results of the proposed protection scheme under current transformer saturation

S. No.	Fault Parameter	Fuzzy Inference System Based Fault Detection and Classification Outputs							Instant of Fault Detection and Classification Time (ms)						
	Fault Type-Line no., Fault Location (km), Fault Resistance (Ω) and [Fault Inception Angle = 0º (Time of fault = 60 ms)]	A1	B1	C1	A2	B2	C2	G	A1	B1	C1	A2	B2	C2	G
1	AG-1, 1, 5	1	0	0	0	0	0	1	62	-	-	-	-	-	62
2	CG-1, 5, 100	0	0	1	0	0	0	1	-	-	68	-	-	-	68
3	BC-1, 10, 10	0	1	1	0	0	0	0	-	65	65	-	-	-	-
4	BG-1, 15, 15	0	1	0	0	0	0	1	-	62	-	-	-	-	62
5	AG-2, 150, 0.01	0	0	0	1	0	0	1	-	-	-	63	-	-	63
6	BCG-2, 150, 0.01	0	0	0	0	1	1	1	-	-	-	-	63	71	63
7	AB-2, 150, 0.01	0	0	0	1	1	0	0	-	-	-	63	63	-	-
8	ABG-1, 297, 0.01	1	1	0	0	0	0	1	64	67	-	-	-	-	67
9	BG-1, 299, 0.01	0	1	0	0	0	0	1	-	73	-	-	-	-	73
10	ABC-1, 299, 0.01	1	1	1	0	0	0	0	66	66	71	-	-	-	-

2.4.8 Test Results for the Overall Performance

The overall efficacy of the performance of the proposed FIS based FDC protection scheme for all the ten types of short circuit faults is evaluated. The fault parameters tabulated in Table 2.10 are considered for the common short circuit fault simulation studies.

Table 2.10 Variation in the fault parameters considered

S. No.	Fault Parameter	Variation of Fault Parameter
1	Fault location (km)	1-299 km with an increment of 4 km (1, 4, 8, …, 99, 101, 104, 108, …, 199, 201, 204, 208, …, 299 km, a total of 156 locations with 78 locations in each line)
2	Fault resistance (Ω)	0.01, 50, 100, 150, and 200 Ω (5-Fault resistances)
3	Fault inception angle (Φ)	0º, 45º, and 270º (3-Fault inception angles)
4	Fault type	All ten common short circuit faults (10-Fault types) Line to ground: AG, BG, and CG Line to line: AB, BC, and CA Line to line to ground: ABG, BCG, and CAG Line to line to line: ABC
Therefore, a total of 23,400 different fault cases are simulated and tested (156 * 5 * 3* 10 = 23, 400)		

The FDC accuracy is defined as the ratio of the total number of correct fault detections to the total number of correct and false detections. The average accuracy for FDC of the short circuit faults by the proposed FDC protection scheme is 99.7535%. The individual FDC accuracies for the LG, LL, LLG and LLL are 99.9145%, 95.7264%, 99.4586%, and 99.9145% respectively.

Fig. 2.13 (a), (b), and (c) depicts the individual response times of the FDC outputs *'A1', 'B1',* and *'C1'* for triple line fault cases shown in Table 2.10 for the section-1, section-2, and section-3 of the line-1. Fig. 2.13 (d), (e), and (f) represent the difference in the response time of any two FDC outputs and the 'AND' operation response time of the FDC outputs. It is observed from Fig. 2.13 that the FDC response time is less than 12 ms for most of the faults and the difference in the response time of any two FDC outputs is less than half-cycle time (10 ms). For all the simulated fault cases shown in Table 2.10, the FDC response time results are similar to those shown in Fig. 2.13. However, the difference in response time of any two FDC outputs is zero for the line to line faults. The FDC response time for all the common short circuit fault types is less than one cycle time by the proposed protection scheme.

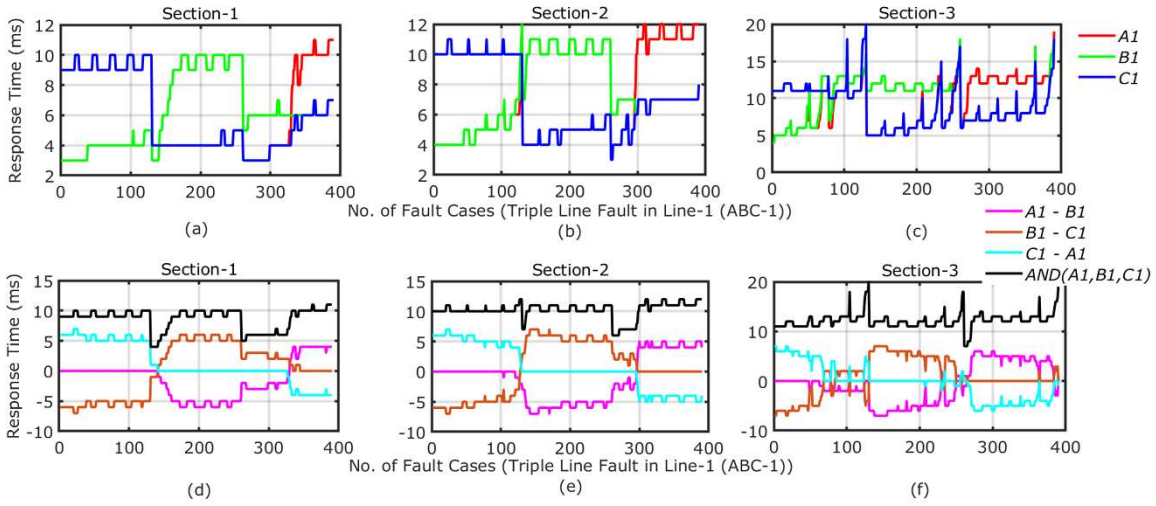

Fig. 2.13 (a), (b), and **(c)** Individual response times of the FDC outputs for triple line fault cases in the section-1, section-2, and section-3 of the line-1, **(d), (e),** and **(f)** Difference in the response time of any two FDC outputs and also the AND operation of the responses for the triple line faults cases of the line-1

2.4.9 Test Results Under Various Operating Conditions of the System

The operating conditions of a real power system network are not ideal all the time because of its complex structure and nature. The operating voltage, frequency, power flow angles, and

transmission line parameters (resistance, inductance, and capacitance) are not constant all the time. They vary depending on the system conditions or other external factors. The reasons for the variations in the ideal operating conditions of the power system are: i) the switching of the generators or loads causes the variations in the ideal operating voltage, ii) to match the load demand and power generation the power flow angles are varied, and iii) the variations of the transmission line parameters are due to the ageing effect, corrosion, and degradation of the conductor because of the weather and environmental conditions. The performance of the proposed FDC protection scheme has been evaluated for various operating conditions and the results are depicted in Table 2.11. The operating voltage and frequency are varied in the range of ±5% of the nominal values, the power flow angle ($\Delta\delta$) is varied between 5º and 40º, the short circuit capacity (SCC) and X/R ratio of the sending end source are varied ±250 MVA and 10 to 60 respectively, and the transmission line parameters are varied in the range of ±10% of the actual values.

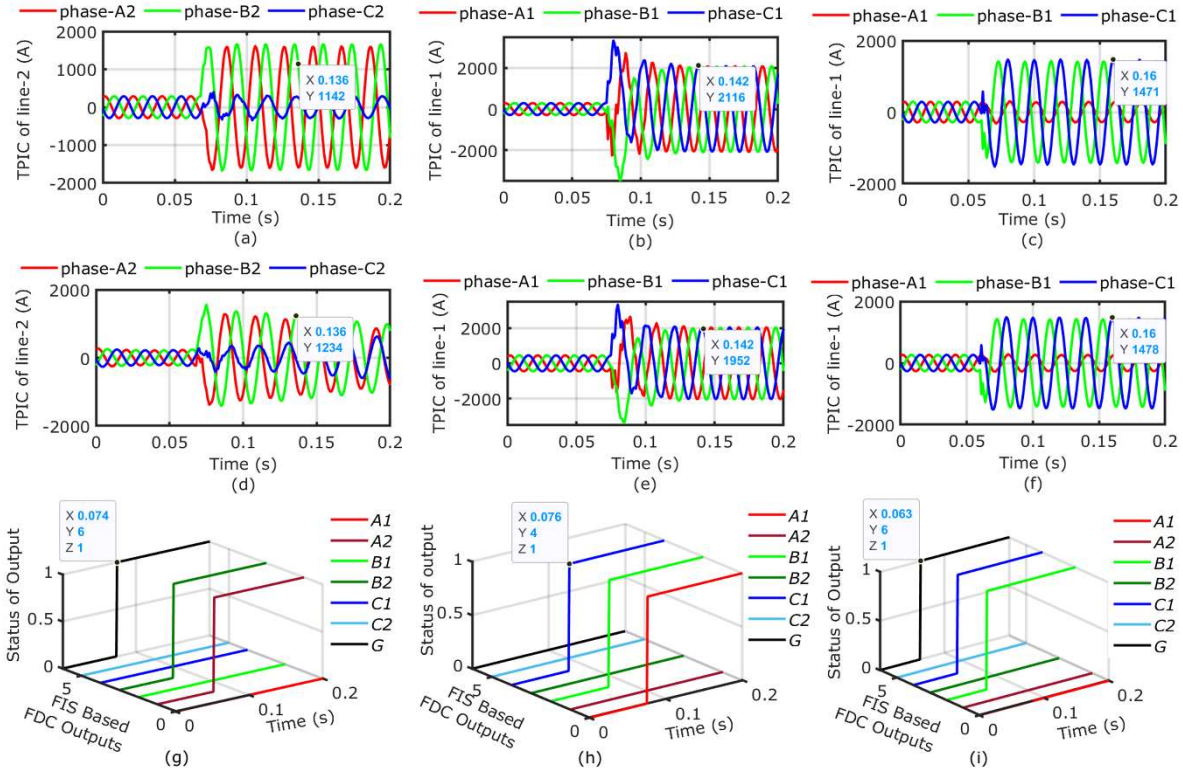

Fig. 2.14 (a) and **(d)** Current waveforms of line-2 for the LLG fault in the line-2 (ABG-2) without and with frequency variation of -2.5%, **(b)** and **(e)** Current waveforms of line-1 for a triple line fault in the line-1 (ABC-1) without and with power angle variation ($\Delta\delta$) of 40º, **(c)** and **(f)** Current waveforms of line-1 for the LLG fault in the line-1 (BCG-1) without and with

transmission line parameters variation of -10%, **(g), (h),** and **(i)** FIS based FDC outputs for the cases in **(d), (e),** and **(f)** respectively

Table 2.11 Test results of the proposed FDC protection scheme under various operating conditions

S. No.	Variation in Operating Conditions	Fault Type-Line no., Fault Location (km), Fault Resistance (Ω), Fault Inception Angle (Time of fault (ms))	Fuzzy Inference System Based Fault Detection and Classification Outputs (Instant of Fault Detection and Classification Time (ms))						
			A1	B1	C1	A2	B2	C2	G
	Voltage Variation (*%ΔV*)								
1	+5 %	AG-1, 50, 100, 0º (60)	1 (63)	0 (-)	0 (-)	0 (-)	0 (-)	0 (-)	1 (63)
2	+2.5 %	BCG-1, 50, 100, 90º (65)	0 (-)	1 (70)	1 (67)	0 (-)	0 (-)	0 (-)	1 (67)
3	-2.5 %	AC-1, 50, 30, 270º (75)	1 (77)	0 (-)	1 (77)	0 (-)	0 (-)	0 (-)	0 (-)
4	-5 %	ABC-1, 50, 20, 180º (70)	1 (72)	1 (72)	1 (78)	0 (-)	0 (-)	0 (-)	0 (-)
	Frequency Variation (*%Δf*)								
5	+5%	CG-2, 90, 150, 0º (60)	0 (-)	0 (-)	0 (-)	0 (-)	0 (-)	1 (65)	1 (65)
6	+2.5%	BC-2, 90, 25, 45º (62.5)	0 (-)	0 (-)	0 (-)	0 (-)	1 (66)	1 (66)	0 (-)
7	-2.5%	ABG-2, 90, 100, 150º (68.33)	0 (-)	0 (-)	0 (-)	1 (79)	1 (74)	0 (-)	1 (74)
8	-5%	ABC-2, 90, 25, 270º (75)	0 (-)	0 (-)	0 (-)	1 (85)	1 (88)	1 (85)	0 (-)
	Power Flow Angle Variation (*Δδ*)								
9	5º	BG-1, 50, 60, 0º (60)	0 (-)	1 (63)	0 (-)	0 (-)	0 (-)	0 (-)	1 (63)
10	10º	ABC-1, 60, 15, 90º (65)	1 (68)	1 (71)	1 (68)	0 (-)	0 (-)	0 (-)	0 (-)
11	15º	AC-1, 70, 10, 270º (75)	1 (77)	0 (-)	1 (77)	0 (-)	0 (-)	0 (-)	0 (-)
12	20º	ACG-1, 80, 60, 180º (70)	1 (73)	0 (-)	1 (78)	0 (-)	0 (-)	0 (-)	1 (73)
13	25º	ABG-2, 90, 80, 180º (70)	0 (-)	0 (-)	0 (-)	1 (72)	1 (72)	0 (-)	1 (72)
14	30º	AB-2, 95, 5, 0º (60)	0 (-)	0 (-)	0 (-)	1 (61)	1 (61)	0 (-)	0 (-)
15	35º	BG-2, 105, 100, 90º (65)	0 (-)	0 (-)	0 (-)	0 (-)	1 (69)	0 (-)	1 (69)
16	40º	ABC-2, 120, 10, 270º (75)	0 (-)	0 (-)	0 (-)	1 (760	1 (77)	1 (76)	0 (-)
	SCC Variation (MVA)								
17	+250	AG-2, 150, 50, 0º (60)	0 (-)	0 (-)	0 (-)	1 (63)	0 (-)	0 (-)	1 (63)
18	+250	BCG-1, 150, 50, 90º (65)	0 (-)	1 (70)	1 (67)	0 (-)	0 (-)	0 (-)	1 (67)
19	-250	AC-1, 150, 15, 0º (60)	1 (67)	0 (-)	1 (67)	0 (-)	0 (-)	0 (-)	0 (-)
20	-250	ABC-1, 150, 15, 90º (65)	1 (70)	1 (71)	1 (70)	0 (-)	0 (-)	0 (-)	0 (-)
	Variation of X/R Ratio								
21	10	ABG-1, 225, 200, 0º (60)	1 (65)	1 (720	0 (-)	0 (-)	0 (-)	0 (-)	1 (65)
22	20	CG-1, 240, 50, 90º (65)	0 (-)	0 (-)	1 (69)	0 (-)	0 (-)	0 (-)	1 (69)
23	30	BC-1, 250, 30, 180º (70)	0 (-)	1 (83)	1 (83)	0 (-)	0 (-)	0 (-)	0 (-)
24	40	AG-2, 260, 150, 180º (70)	0 (-)	0 (-)	0 (-)	1 (75)	0 (-)	0 (-)	1 (75)
25	50	ABC-2, 270, 30, 270º (75)	0 (-)	0 (-)	0 (-)	1 (87)	1 (81)	1 (81)	0 (-)
26	60	BCG-2, 280, 170, 0º (60)	0 (-0	0 (-)	0 (-)	0 (-)	1 (71)	1 (78)	1 (71)
	Variation of Transmission Line Parameters (*%ΔZ*)								
27	+ 10%	AG-1, 125, 100, 0º (60)	1 (63)	0 (-)	0 (-)	0 (-)	0 (-)	0 (-)	1 (63)
28	+ 5%	ACG-1, 125, 50, 90º (65)	1 (68)	0 (-)	1 (68)	0 (-)	0 (-)	0 (-)	1 (70)
29	- 5%	AC-2, 125, 20, 180º (70)	0 (-)	0 (-)	0 (-)	1 (76)	0 (-)	1 (76)	0 (-)
30	- 10%	ABC-2, 125, 25, 270º (75)	0 (-)	0 (-)	0 (-)	1 (79)	1 (81)	1 (79)	0 (-)
31	- 10 %	BCG-1, 125, 100, 0º (60)	0 (-)	1 (63)	1 (69)	0 (-)	0 (-)	0 (-)	1 (63)

Fig. 2.14 (a) and (d) depict the three-phase instantaneous currents of line-2 for the LLG fault in the line-2 (ABG-2) (L_f = 90 km, R_f = 100 Ω, and Φ = 150º (T_f = 68.33 ms)) without and with frequency variation of -2.5% respectively. Fig. 2.14 (b) and (e) depict the three-phase instantaneous currents of line-1 for the triple line fault in the line-1 (ABC-1) (L_f = 120 km, R_f = 25 Ω, and Φ = 270º (T_f = 75 ms)) without and with the variation of the power flow angle ($\Delta\delta$) of 40º respectively. Fig. 2.14 (c) and (f) represent the three-phase instantaneous currents of line-1 for the LLG fault in the line-1 (BCG-1) (L_f = 125 km, R_f = 100 Ω, and Φ = 0º (Tf = 60 ms)) without and with -10% variation in the transmission line parameters respectively. Fig. 2.14 (g), (h), and (i) shows the FIS based FDC outputs for the fault with frequency variation, power flow angle variation, and transmission line parameters' variations respectively. The proposed scheme is able to detect the faults even with different operating conditions.

2.4.10 Comparison of the Proposed Protection Scheme with Other Protection Techniques

A comparison of the proposed FDC protection scheme with the other earlier reported artificial intelligent protection techniques is shown in Table 2.12 concerning the method employed, performance, fault parameter considerations, and other operating conditions**.** In Table 2.12, all the protection schemes were employed on the 400 kV, 50 Hz transmission system. In Table 2.12, all the intelligent protection schemes for single or double circuit transmission lines require the training of the modules for protection purposes except the FIS based protection schemes. The FIS based protection scheme implemented in column-1 is only for the single circuit lines. However, the proposed FDC protection scheme is for the double circuit lines with a single FIS module and works for the single circuit operation also. The comparison results shows the equal performance and effectiveness of the proposed non-training-based FDC protection scheme even with the fault parameters variations and for different fault scenarios that are not considered by the training-based protection schemes reported in Table 2.12.

Table 2.12 Comparison of the proposed FDC scheme with other artificial intelligent protection schemes

S. No.	Comparison Parameter	Reference						
		[22]	[23]	[100]	[101]	[102]	[103]	Proposed
1	Transmission line length	198 km, double circuit	200 km, double circuit	200 km, double circuit	150 km, single circuit	100 km, single circuit	300 km, single circuit	300 km, double circuit
2	Method and feature extraction technique (sampling frequency)	ANN and DWT (1 kHz, 1.2 kHz, 10 kHz)	SVM and Kalman filtering technique (1 kHz)	Ensemble of decision trees and least square & Adaline algorithms (1 kHz)	Decision tree and mathematical morphology (1.2 kHz)	Deep learning and DWT (20 kHz)	Chebyshev neural network and DWT (5 kHz)	FIS and DFT (1 kHz)
3	Input type (no. of inputs)	The standard deviation of 6^{th} level detailed coefficients of line currents; neutral current (7)	Fundamental, 3^{rd}, 5^{th}, and 7^{th} harmonic components of voltage signal (3)	DC offset and fundamental component of currents (7)	Sequence components of voltage and current (8)	The energy of 5^{th} level detailed coefficients of voltage and current (6)	The energy of 4^{th} level detailed coefficients of current (6)	MFCC, ZSC (7)
4	No. of modules	2	5	11	1	1	4	1
5	Protected line length	1-197 km	99.5% of the line (200 km)	1-200 km	1-150 km	1-99 km	30-270 km	1-299 km
6	Relay operation time (ms)	< 10 ms	< 10 ms	< 20 ms	< 5 ms	< 20 ms	< 10 ms	< 12 ms (section-1 & 2) < 20 ms (section-3)
7	L_f (km)	1-197 km (54 locations)	1-200 km	-	1-150 km in steps of 20 km	1-99 km	30-270 km in steps of 30 km (10 locations)	1-299 km with an increment of 4 km (156 locations)
8	R_f (Ω)	0-100 Ω	0-100 Ω	-	0-20 Ω	0.1-100 Ω	0-150 Ω	0.01-200 Ω
9	Φ	0º-270º	0º-360º	-	0º-90º	0º-180º	0º-115º	0º-360º
10	No. of fault cases	500	-	-	77000	10400	23400	23400
11	FDC accuracy	99.70%	-	99.64 %	99.98%	99.55%	98.33%	99.754%
12	CCF & EF	Yes	No	No	No	No	No	Yes
13	PS & FPS	Yes	Yes	Yes	No	No	No	Yes
14	CT saturation	Yes	No	No	No	No	No	Yes
15	HIF	No	No	No	No	Yes	No	Yes
16	Noisy context	Yes	No	Yes	No	Yes	No	Yes

2.5 Summary

In this chapter, an artificial intelligence-based protection scheme with a single FIS for FDC of the short circuit faults on the DCTL has been proposed. The proposed FIS based FDC scheme uses the MFCCs extracted by DFT and the ZSCs of the sending end bus only for the protection task. It can detect and classify all ten types of short circuit faults within one cycle time and with an average FDC accuracy of 99.7535%. Also, it correctly detects and classifies the different fault types with varying fault parameters for HIF, cross-country faults, evolving faults, CT saturation, noisy conditions, PS and FPS conditions, and variations in operating conditions. Furthermore, the proposed FDC scheme is passive to the variations in the fault parameters and varying operating conditions. It can work for the single circuit operation also. The comparison results justify the aptness and effectiveness of the proposed protection scheme rather than the training-based protection schemes. The main advantage of the proposed protection scheme is the non-requirement of module training and communication link. It is simple and efficient with reduced complexity.

*****

Chapter 3

Mono ANN Module Protection Scheme and Multi ANN Modules for Fault Location Estimation for a Six Phase Transmission Line Using Discrete Wavelet Transform

3.1 Introduction

Nations across the world have aimed to reduce carbon emissions by encouraging renewable energy sources to generate clean energy. Despite the global economic crisis in 2020, there is a record rise in the global renewable energy generation capacity i.e., 260 GW during COVID 2019 pandemic. Solar (127 GW) and wind (111 GW) dominated this capacity expansion by 91% [2]. The resulting intermittent generation and centralized demand require increased transmission capacities. In many countries, obtaining a new right of way to build an overhead line is very difficult. Building new transmission line corridors is quite an expensive and time-consuming process. Also encounters the land availability problem and opposition from the environmentalists for ecological reasons. In the pursuit of meeting the increasing power demands, the generation or power transfer capabilities of the transmission network have to be increased. The environmental, economic, and land availability concerns for building the new transmission infrastructure to have enhanced power transfer capabilities, led the power system engineers to search for alternate methods. The extra high voltage (EHV) transmission lines can serve the purpose but the EHV lines produce strong electric fields at the ground surface, possible biological effects, visual pollution, and audible noise. HVDC transmission is another alternative but the demerit is, it requires huge capital for installation and operation. In 1972, H. C. Barnes and L.D. Barthold had proposed the high phase order transmission systems for maximizing the power density by employing the existing transmission corridors efficiently. The high phase order transmission is a viable solution. The six-phase transmission with the existing three-phase double circuit transmission line without major alterations paved the way with 73% more power transfer capability. The other benefits of six-phase transmission over three-phase transmission are i) reduced phase to phase voltages, ii) current imbalances are minimum – so single-pole switching is possible, iii) reduced radio and audible noise and corona losses are minimum, iv) high compatibility and stability, v) reduced conductor surface gradients, and vi) improved thermal loading capability, surge impedance loading, voltage regulation and better efficiency of lines [4, 5, 104, 105]. Now, the countries viz. China and the United Kingdom have again started research investigations on upgrading the three-phase double circuit transmission lines to six-phase lines for future needs [106, 107]. The acceptance of the six-phase transmission is vaguely encouraged due to the lack of proper protection schemes to tackle the 120 different types of short circuit faults. The segregation of 120 types of faults is detailed in Fig. 1.1 of Chapter 1.

The maximum number of phases of a transmission line apart from six-phase can be nine, twelve or even twenty-four phases i.e., multiples of the conventional three-phase system to provide interfacing with the existing three-phase system through transformers. Different tower structures are analysed to have simple and compact spacing of lines with minimum insulation cost. The fact that the adjacent phase to phase voltages are less in high-phase order systems compared to the conventional three-phase system made it possible for the compaction of the lines [108]. For six and twelve phase configurations, the hexagonal placement is preferred. Generally, the phase conductors are placed sequentially on the vertices and/or on the edges of the hexagon. Fig. 3.1 (a) and 3.1 (d) shows an example of the schematic of the phases on the tower of a six-phase and twelve-phase transmission line. However, due to the transposition of phases, each position is occupied by every phase in the order of phase sequence.

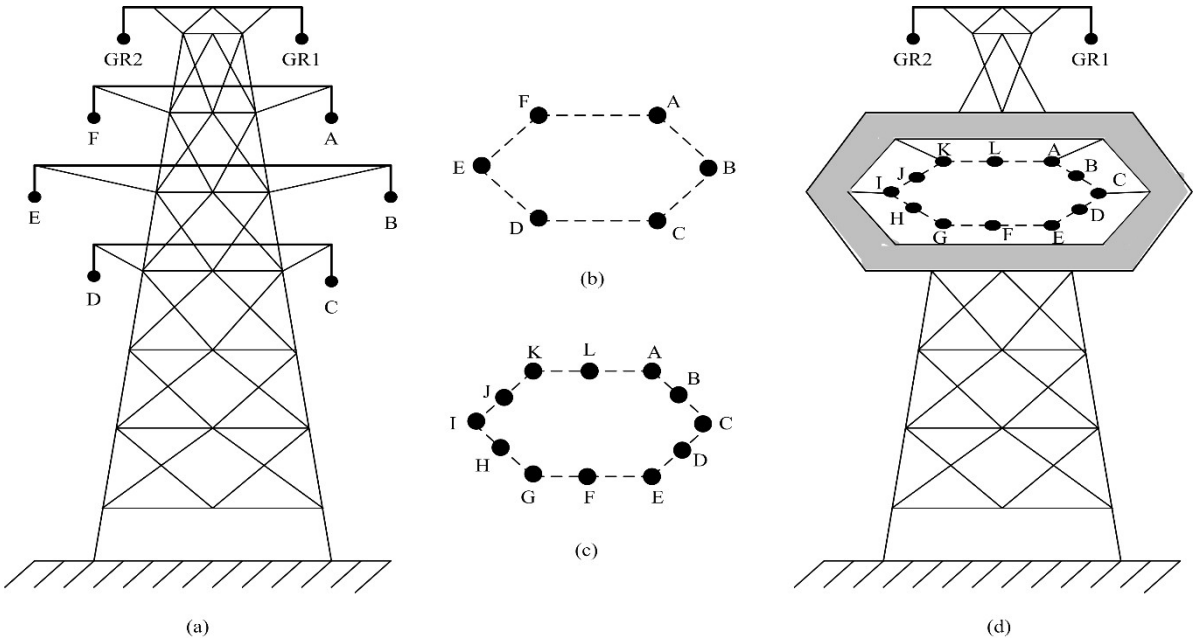

Fig. 3.1 Schematic of tower structures **(a)** and **(b)** Six-phase line, **(c)** and **(d)** Twelve-phase line

In the present chapter, a complete protection scheme (fault detection/classification and fault location estimation (FLE)) is proposed using only the phase current information of the sending end bus with discrete wavelet transform (DWT) and artificial neural networks. Unlike the earlier works, the proposed scheme implemented only a single module of ANN for fault detection and classification. For fault location estimation, the modular ANN method is implemented where each ANN module gives the fault location estimation in all six phases.

3.2 Details of Six-phase Transmission System

The six-phase Allegheny's power transmission system is considered for the present work referring to the line between the buses Springdale and McCalmont [4]. It consists of a 138 kV, 60 Hz single circuit six-phase transmission line of 68 km length fed from the sources at both the ends (sending and receiving ends) of the line. The sending end (source-1) and receiving end (source-2) source impedances are 2.03 + j9.04 Ω and 4 + j17.94 Ω with short circuit capacities of 1.25 GVA respectively. Two loads (load-1, 80 MW and load-2, 60 MVar) are connected at the receiving end bus, B2. Fig. 3.2 shows the one-line diagram of the considered six-phase power system network along with a block diagram of the proposed protection scheme. The DWT-ANN based relay is installed at the sending end bus, B1. The six-phase transmission line parameters are given in Appendix – II.

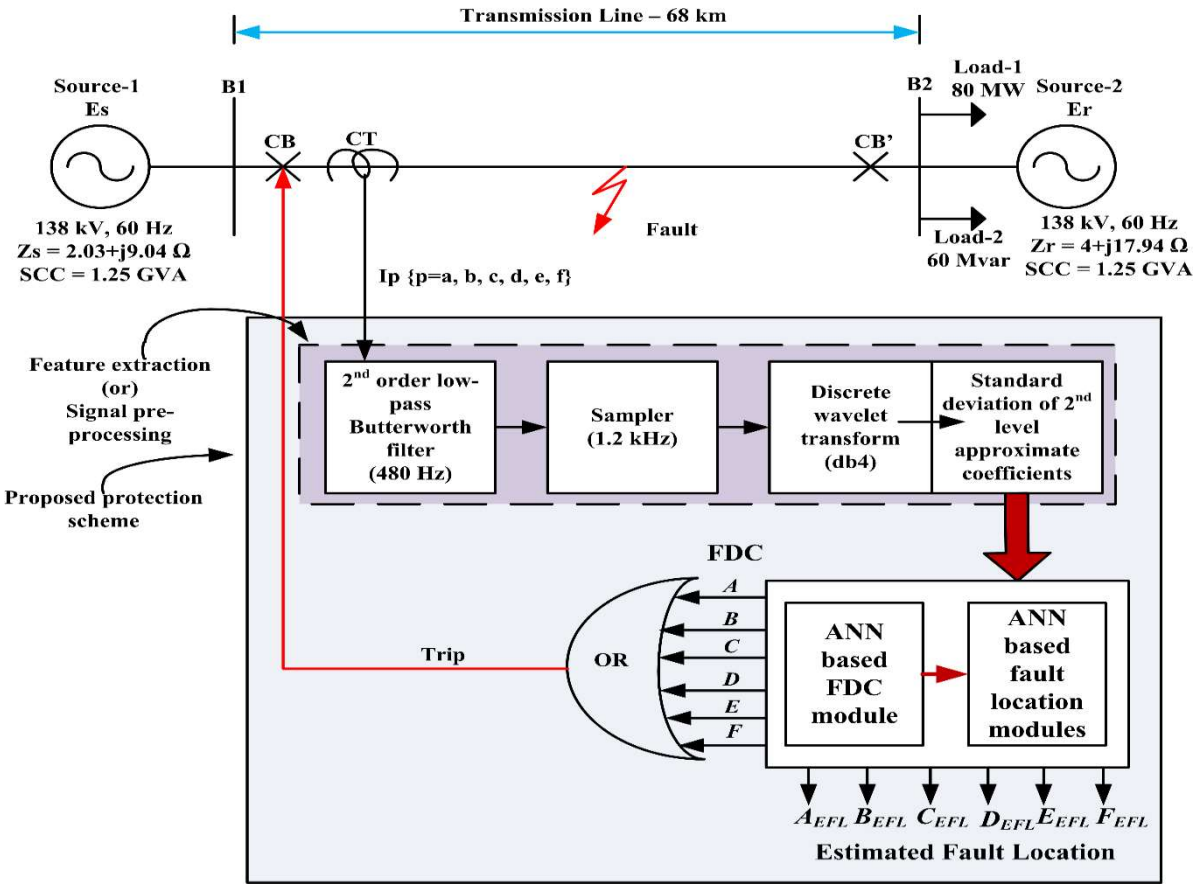

Fig. 3.2 One-line diagram of the considered six-phase transmission system along with a block diagram of the proposed protection scheme

Tables 3.1 and 3.2 depict the basic system description and the line configuration data of the six-phase system considered in the present work. The model used in the work takes into account the distributive nature of the transmission line by considering the uniform distribution of resistance, inductance, and capacitance along the line length. The six-phase transmission line model is implemented and simulation studies are carried out using the software MATLAB®/Simulink platform.

Table 3.1 Basic system description data

System Voltage	138 kV
No. of phases	6
No. of circuits	1
No. of sub-conductors per phase	1
Total no. of ground wires	2
Earth resistivity	100 Ω-m
Frequency	60 Hz
Base voltage	138 kV
Base power	100 MVA
Line length	68 km

Table 3.2 Line configuration data

Phase no.	Conductor designation	Horizontal spacing X (ft)	Height at tower Y (ft)	Mid-span clearance (ft)
1	*a*	-11	68	56
2	*b*	-14	55	43
3	*c*	-11	42	30
4	*d*	11	42	30
5	*e*	14	55	43
6	*f*	11	68	56
0	*GR1*	-6	77.5	67.1
0	*GR2*	6	77.5	67.1

3.3 Development of Proposed Protection Scheme with DWT & ANN

From the protection point of view, any short circuit fault has to be detected and isolated as early as possible to mitigate the effect of the fault on the system and to estimate the fault

location accurately to send the repairmen's crew. In the present work, a protection scheme is proposed for the six-phase transmission system shown in Fig. 3.2 using the discrete wavelet transform and artificial neural network. With the proposed protection scheme, two protection tasks are accomplished. The first task is to identify and classify the fault and the second task is to estimate the fault location. There are two stages in the proposed protection scheme, i) feature extraction process and ii) actual protection scheme implemented using the ANNs.

3.3.1 Feature Extraction Process with DWT

To implement any digital protection scheme, a proper feature of the system (either voltage/current) has to be used to accomplish the protection task. The recorded time-domain raw data of instantaneous voltage/current signals available at the relaying point may not be used as such, so to extract the useful features from the raw data, a transform has to be used to convert the signal to the frequency domain or time-frequency domain. Discrete wavelet transform (DWT) is one of the most widely used signal processing techniques in engineering domains which analyses the signal both in time and frequency domains. This transform has gained a lot of popularity in power system protection because it efficiently analyses the non-stationary signals and localizes the signal in time and frequency domains. In DWT, the signal is decomposed into a number of levels and each level corresponds to a particular frequency band. This transform provides the degree of similarity between the signal to be analysed and the analysing signal in terms of detail coefficients (higher frequency components) and approximate coefficients (lower frequency components). The proper selection of the mother wavelet plays an important role in analysing the signal [44, 109–111]. A schematic diagram of the signal decomposition by DWT is shown in Fig. 3.3. In the present work, the instantaneous current signals in each phase of the sending end bus (B1) are employed for the protection task. The instantaneous current signals of bus B1 are pre-processed with the second-order low-pass Butterworth filter (anti-aliasing filter) with a cut-off frequency of 480 Hz to eliminate the higher-order harmonics in the signal. Butterworth filters are used because they provide maximum flat characteristics in the passband region. Eq. (3.1) gives the general expression for the n^{th} order low-pass Butterworth filter. These filtered signals are sampled at a 1.2 kHz sampling frequency (20 samples per one cycle data of 60 Hz frequency) according to the Nyquist sampling criteria. The expression for the second-order low-pass Butterworth filter with a cut-off frequency of 480 Hz and Nyquist sampling frequency of 1.2 kHz is given in Eq. (3.2). The DWT is implemented on the sampled current signals with the Daubechies

wavelet, db4 is used as the mother wavelet. The standard deviation *(std)* of the second level approximate coefficients of current signals in each phase are used as the features for the protection scheme. The basic expression for the DWT of a signal *S(t)* is given in Eq. (3.3), where *S(k)* is the sampled signal, b_0^m is the scaling parameter, kb_0^m is the translation parameter, and Ψ is the mother wavelet [112].

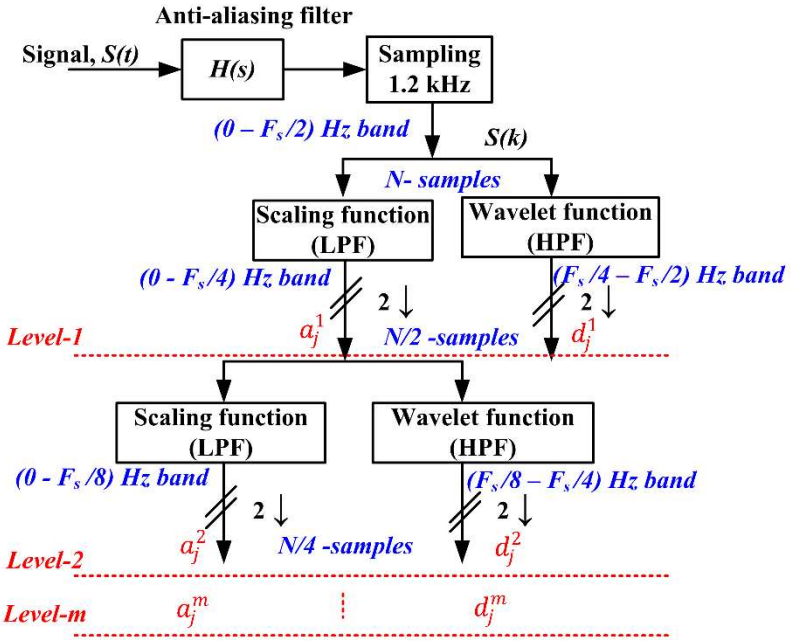

Fig. 3.3 Signal pre-processing and DWT decomposition

$$H(s) = \frac{y(1)s^n + y(2)s^{n-1} + \cdots + y(n+1)}{x(1)s^n + x(2)s^{n-1} + \cdots + x(n+1)} \tag{3.1}$$

$$H(s) = \frac{0.6389s^2 + 1.2779s + 0.6389}{s^2 + 1.143s + 0.4128} \tag{3.2}$$

$$DWT(S, m, n) = \frac{1}{\sqrt{b_0^m}} \sum_k S(k) \Psi^* \left(\frac{n - kb_0^m}{b_0^m} \right) \tag{3.3}$$

If d_j^m and a_j^m represent the detail and approximate coefficients of m^{th} level of decomposition, then the standard deviation of approximate coefficients is given by Eq. (3.4).

$$Standard\ deviation\ (std) = \sqrt{\frac{1}{N-1} \sum_{j=1}^{N} \left(a_j^m - \frac{1}{N} \sum_{j=1}^{N} a_j^m \right)^2} \tag{3.4}$$

Where N is the no. of coefficients. The process of calculating the standard deviation of second-level approximate coefficients of current signals is carried out consecutively for each cycle window of 20 instantaneous current samples, viz. window-1 of 1-20 samples, window-2 of 2-21 samples, and so on. Therefore, the required features obtained after the feature extraction process are std_a, std_b, std_c, std_d, std_e, and std_f for each of the six phases.

3.3.2 Proposed ANN Based Protection Scheme for FDC and FLE

ANNs have gained a lot of importance in the engineering domains, especially for the protection of three-phase single-circuit and double circuit transmission lines for their ability of self-adaptability to varying operating conditions, non-linear function approximation, pattern recognition, and learning capabilities. The main advantage of ANN is the high-speed online computation. The feedforward neural networks with the Levenberg-Marquardt training algorithm are implemented using MATLAB for fault detection/classification (FDC) and fault location estimation (FLE). The flowchart for the Levenberg-Marquardt algorithm (LMA) is given the Fig. 3.4. The Levenberg-Marquardt algorithm is the fastest algorithm and takes less execution time to train the ANN [113]. This optimization algorithm is an iterative method used to solve the non-linear least square problems. It is a combination of the Gauss-Newton method and the gradient descent method [114, 115]. For training the ANN, LMA is used to learn the weights and biases of the neural network. The advantage of the Levenberg-Marquardt algorithm is, that it attains second-order training speed without the requirement to calculate the Hessian matrix.

There is no hard and proven rule to achieve the optimal architecture (no. of hidden layers and no. of neurons) of the artificial neural network (ANN). A series of pilot runs based on the hit-and-trail basis method is the general process for selecting the architecture of ANN. The features that should be taken care of while training the ANN are architecture, neural network parameters (weights and biases), type of activation function, and training/learning algorithm.

Unlike the modular ANNs reported earlier for fault detection and classification of 120 types of faults, the present work proposed a single ANN_FDC module with the standard deviation of second-level approximate coefficients of six-phase currents of sending end bus as inputs and six outputs (*A, B, C, D, E,* and *F*) one for each phase for faulty phase detection and classification of faults. The most important tasks in training the ANN are the generation

of training samples, preparation of input training and target data sets, selection of the optimum no. of hidden layers, and choosing the activation functions for the proper pattern recognition. The training and the testing data samples are generated by simulating the different types of faults with varying fault locations, fault inception angles, and fault resistances on the six-phase transmission system shown in Fig. 3.2 on the MATLAB®/ Simulink platform.

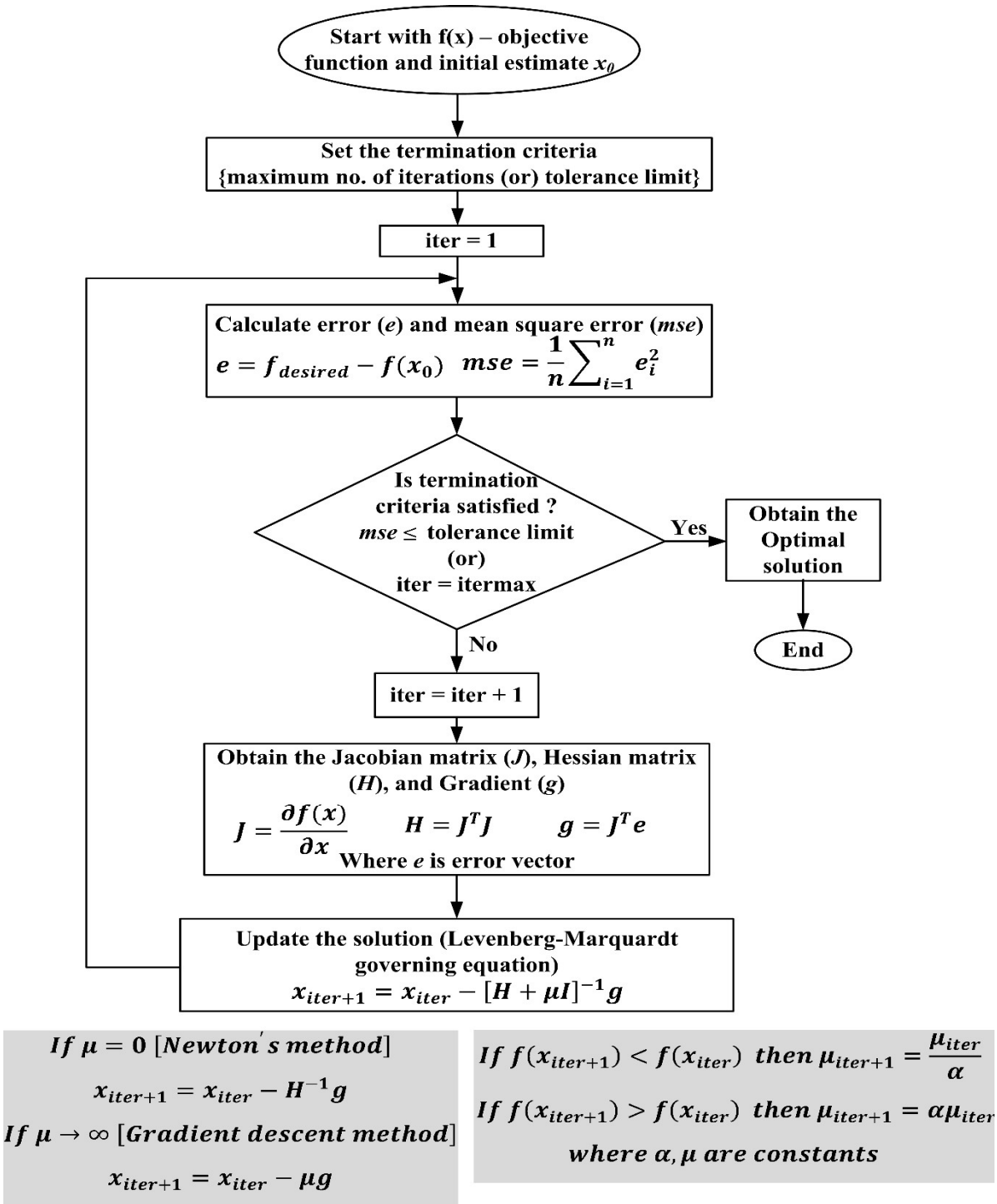

Fig. 3.4 Flow chart of Levenberg-Marquardt algorithm

Table 3.3 presents the different fault parameter variations considered for generating the training and testing data samples. Ten post-fault data samples of the standard deviation of second-level approximate coefficients of sending end bus phase currents are collected for each of the simulated faults and hence the training data set is created. Table 3.4 presents the number of samples collected for each type of fault for the training and testing data sets. For the fault detection in each phase and classification purpose, the ANN_FDC module outputs are labelled as *'+1'* and *'-1'*. The output *'+1'* is used to indicate the fault condition and *'-1'* is used to indicate the healthy/no-fault (NF) condition in the particular phase.

Table 3.3 Fault parameter variations considered in the training and testing data samples

S. No.	Fault Parameter	Variations considered	
		In the training data	In the testing data
1.	Fault resistance (Ω)	0.01 Ω, 50 Ω, and 100 Ω	30 Ω and 70 Ω
2.	Fault inception angle (º)	0º and 90º	0º and 45º
3.	Fault location (km)	1 km, 4 km, 8 km, …, 64 km, and 67 km (18-locations)	1 km, 6 km, 12 km, …, 60 km, and 66 km (12 - locations)
4.	No. of fault types	120	120
5.	Total no. of fault cases considered	3*2*18*120=12960; 1-no fault case	2*2*12*120=5760; 1-no fault case

Table 3.4 Number of training and testing data samples collected for each type of fault

S. No.	Fault type	Training		Testing	
		No. of cases	No. of samples	No. of cases	No. of samples
1.	1-LG and No fault	(6*3*2*18)+1 = 649	649*10 = 6490	(6*2*2*12)+1 = 289	289*20 = 5780
2.	2-LG and 2-L	2*(15*3*2*18) = 3240	3240*10 = 32400	2*(15*2*2*12) = 1440	1440*20 = 28800
3.	3-LG and 3-L	2*(20*3*2*18) = 4320	4320*10 = 43200	2*(20*2*2*12) = 1920	1920*20 = 38400
4.	4-LG and 4-L	2*(15*3*2*18) = 3240	3240*10 = 32400	2*(15*2*2*12) = 1440	1440*20 = 28800
5.	5-LG and 5-L	2*(6*3*2*18) = 1296	1296*10 = 12960	2*(6*2*2*12) = 576	576*20 = 11520
6.	6-LG and 6-L	2*(1*3*2*18) = 216	216*10 = 2160	2*(1*2*2*12) = 96	96*20 = 1920
7.	Total	12961	129610	5761	115220

In order to select the optimal architecture of the ANN for fault detection and classification, a no. of pilot runs were carried out with the generated training data with different no. of hidden layers and neurons, and with different activation functions on a trial-and-error basis method. The optimal architecture of ANN_FDC, type of activation functions, training input and output data sizes, and mean square error achieved during training are presented in Table 3.5 for the fault detection and classification module. Fig. 3.5 presents the architecture 6-18-18-6 of the ANN_FDC module with 6 – input neurons, 18 – neurons each in the two hidden layers, and 6 – output layer neurons with tansig activation function in all the layers. Fig. 3.6 presents the mean squared error (*mse*) achieved during the training process of the ANN_FDC module.

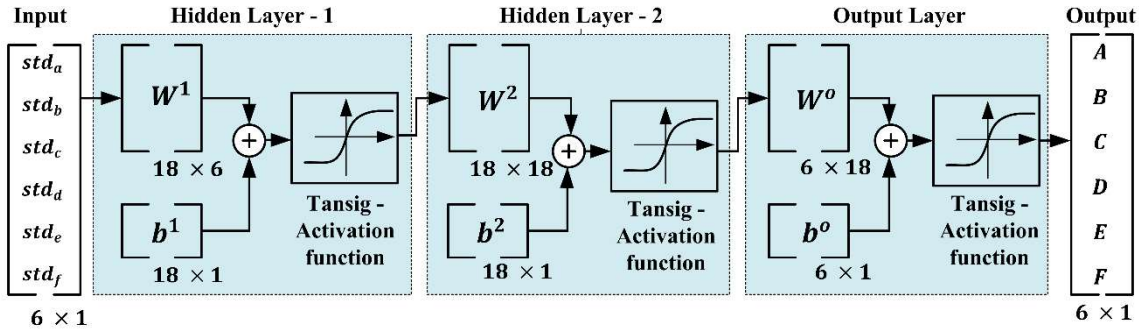

Fig. 3.5 Architecture of ANN_FDC module

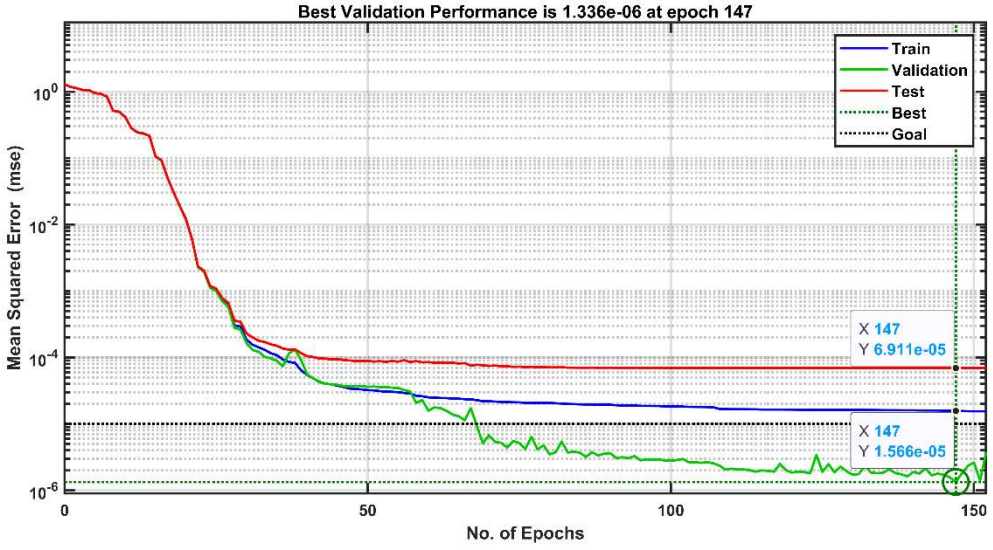

Fig. 3.6 Mean squared error achieved during the training of the ANN_FDC module

For identifying the involvement of ground in the grounded faults, in 1998, M. Akke and J. T. Thorp [116] proposed a current index that separates the faults with zero-sequence

currents from the faults without zero-sequence currents for a three-phase system. The fault index expression that is used to identify the grounded faults is given in Eq. (3.5) for an '*n*' phase system.

$$Current\ index\ or\ Fault\ index\ (FI) = \frac{\sum|I_p|}{median(|I_1|, |I_2|, \dots, |I_p|)} \quad (3.5)$$

$$where\ p = 1, 2, \dots, n\ phases$$

$$If\ FI > 0.05, then\ ground\ is\ present.$$

$$If\ FI \leq 0.05, then\ ground\ is\ absent.$$

In the present study, the above current index has been extended up to the six-phase system (*n = 6 phases i.e., p = a, b, c, d, e, and f phases*) and instead of fault index, the standard deviation of fault index is used to detect the ground involvement in the fault given in Eq. (3.6) and Eq. (3.7).

$$Standard\ deviation\ (std_{FI}) = \sqrt{\frac{1}{M-1}\sum_{j=1}^{M}\left(FI_j - \frac{1}{M}\sum_{j=1}^{M} FI_j\right)^2} \quad (3.6)$$

$$where\ M = no.of\ current\ samples\ per\ 60\ Hz\ cycle.$$

$$Ground\ (G) = \begin{cases} +1, if\ std_{FI} > 0.05, then\ ground\ is\ present \\ -1, if\ std_{FI} \leq 0.05, then\ ground\ is\ absent \end{cases} \quad (3.7)$$

Where std_{FI} is the standard deviation of fault index, I_a, I_b, I_c, I_d, I_e, and I_f are the six-phase instantaneous currents of the bus B1. The involvement of ground is detected with *'+1'* when the std_{FI} is greater than the threshold and *'-1'* is used to identify that no involvement of ground in the fault. In the present work, there are eleven ANN modules for fault location estimation (FLE), one for each type of fault. In all the ANN fault location estimation modules, there are six inputs and six outputs one for each phase. The input training data set to the ANN_FLE modules is the standard deviation of second-level approximate coefficients of the currents of bus B1 with the fault parameters shown in Table 3.3. For training the ANN_FLE modules, the target data set is created with the actual fault locations for the faulty phases and healthy phases are labelled with 140 km. A series of trials are run with the training data to select the best ANN_FLE modules. The architecture, type of activation function, input and output data size, and mean square error (*mse*) achieved during training of the best ANN_FLE modules

are shown in Table 3.5. The tansig activation function is used for the hidden layers and the purelin activation function is used for the output layers of ANN fault location estimation modules.

Table 3.5 Details of ANN architecture for FDC and fault location estimation

S. No.	ANN for	Architecture	Activation function	Input & output data size	MSE achieved during training
1.	ANN_FDC	6-18-18-6	Tansig	6 x 129610	1.336e-06
2.	ANN_FLE_1-LG	6-25-25-6	Tansig & purelin	6 x 6490	9.97e-07
3.	ANN_FLE_2-L	6-25-25-25-6	Tansig & purelin	6 x 16210	1.70e-05
4.	ANN_FLE_2-LG	6-25-25-25-6	Tansig & purelin	6 x 16210	1.22e-05
5.	ANN_FLE_3-L	6-25-25-25-25-6	Tansig & purelin	6 x 21610	1.59e-04
6.	ANN_FLE_3-LG	6-30-30-30-6	Tansig & purelin	6 x 21610	9.03e-05
7.	ANN_FLE_4-L	6-25-25-25-25-6	Tansig & purelin	6 x 16210	3.68e-05
8.	ANN_FLE_4-LG	6-25-25-25-25-6	Tansig & purelin	6 x 16210	3.22e-05
9.	ANN_FLE_5-L	6-25-25-25-6	Tansig & purelin	6 x 6490	3.84e-06
10.	ANN_FLE_5-LG	6-30-30-30-6	Tansig & purelin	6 x 6490	5.52e-06
11.	ANN_FLE_6-L	6-15-15-6	Tansig & purelin	6 x 1090	9.97e-07
12.	ANN_FLE_6-LG	6-15-15-6	Tansig & purelin	6 x 1090	1.00e-06

The flowchart of the proposed protection scheme is shown in Fig. 3.7. In the proposed protection scheme, the single-end pre-processed current data is fed to all 12 ANN modules simultaneously. The ANN_FDC module output and FI output information are used for fault detection/classification purposes. Based on fault type information the particular fault type of the ANN_FLE module is selected to have the estimated fault location in each phase. The '*OR*' operation on the ANN_FDC module outputs is used to generate the trip signal to the circuit breakers.

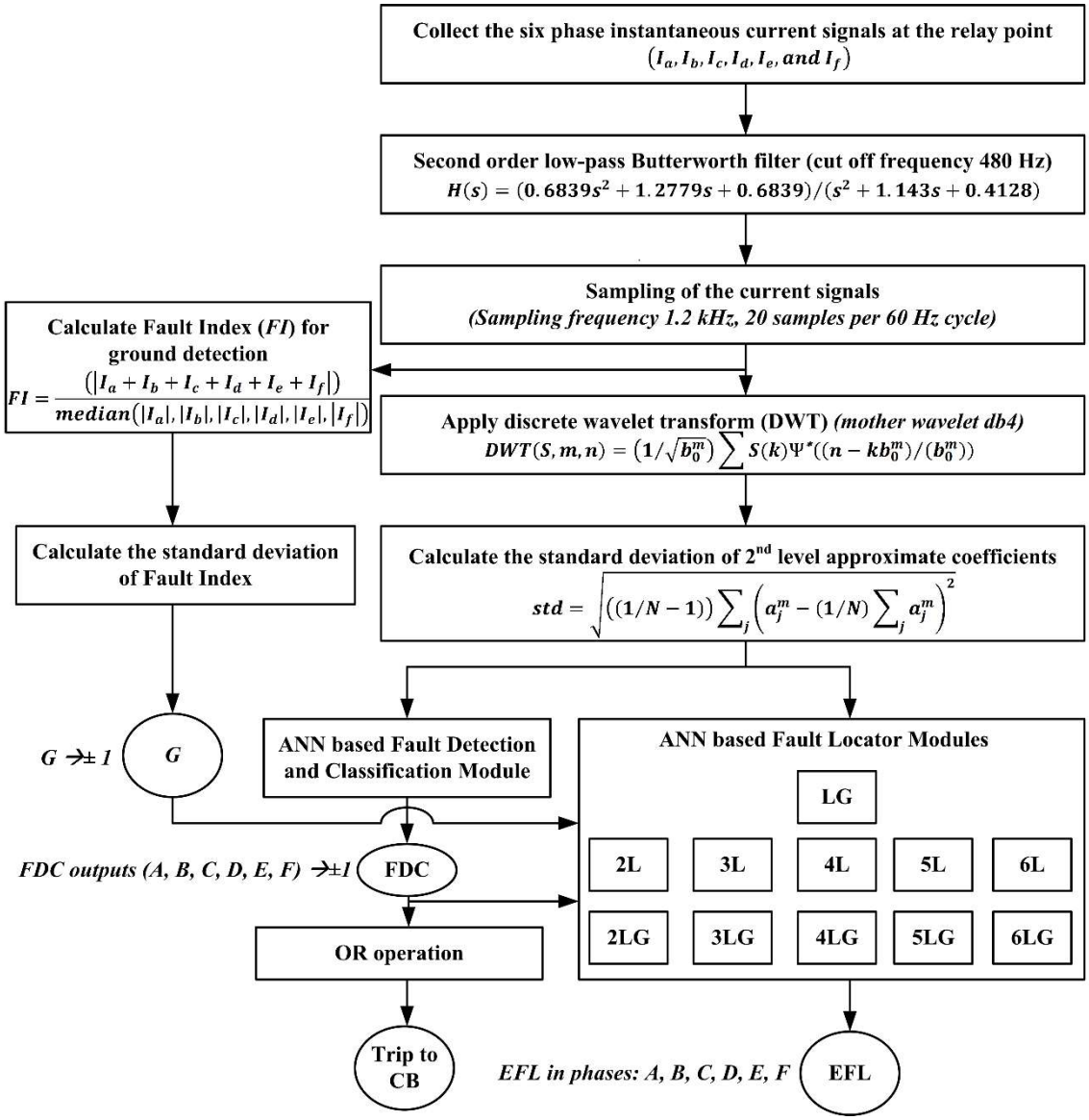

Fig. 3.7 Flowchart of the proposed protection scheme with DWT and ANN

3.4 Results and Discussion

The performance of the proposed protection scheme has been evaluated by conducting a series of simulations by varying the fault parameters viz. fault resistance (R_f) (0 – 100) Ω, fault inception angle (Φ) (0º - 360º), and fault location (L_f) (1 – 68) km. Further, to validate the proposed protection scheme, testing data that is different from the training data is generated using the fault parameters shown in Table 3.3 and the no. of fault cases (5761) and samples considered (115220) is shown in Table 3.4. The accuracy and the dependability of the proposed protection scheme for fault detection and classification are assessed w.r.t

training and testing data using the confusion matrices. The accuracy and dependability are evaluated as [45]

$$Accuracy = \frac{total\ no.of\ fault\ cases\ predicted\ correctly}{total\ no.of\ actual\ fault\ cases\ and\ no\ fault\ cases} \times 100 \quad (3.8)$$

$$Dependability = \frac{total\ no.of\ fault\ cases\ predicted\ correctly}{total\ no.of\ actual\ fault\ cases} \times 100 \quad (3.9)$$

The performance of the protection scheme for the fault location estimation for all the fault location modules is evaluated in terms of percentage error in the estimated fault location for all the phases as [44]

$$\%\ Error\ in\ the\ estimated\ fault\ location\ (\%E) = \frac{E_{fl} - L_a}{total\ length\ of\ the\ line} \times 100 \quad (3.10)$$

Where E_{fl} and L_a are the estimated fault location and actual fault location.

3.4.1 Performance Evaluation of the ANN_FDC Module for Varying Fault Parameters

The fault detection/classification of the proposed protection scheme is effective and efficient even with the variation of fault parameters. A four-phase to ground fault (4-LG, (ABCDG)) is simulated at fault location (L_a) of 10 km from bus B1 with fault resistance (R_f) 30 Ω and fault inception angle (Φ) of 0° (fault inception time (T_f) 0.05 s) and the six-phase instantaneous currents at bus B1 are shown in Fig. 3.8 (a). Fig. 3.8 (b) presents the standard deviation of the second level approximate coefficients of the current signals i.e., pre-processed input features by DWT to ANN modules. Fig. 3.8 (c) presents the standard deviation of the fault index i.e., used for the ground detection. Fig. 3.8 (d) shows the fault detection and classification outputs for the ANN_FDC module where the faulty phases are detected as a fault with the level of output *'+1'* after the inception of fault while the healthy phases are shown with *'-1'* level of output. Hence the ANN_FDC module clearly identifies and classifies the fault as ABCDG fault with maximum and minimum FDC time as 2.5 ms (0.0525 ms – 0.05 ms = 2.5 ms) and 3.33 ms (0.0533 ms – 0.05 ms = 3.33 ms) which is much less than one cycle time (16.67 ms). The performance of the ANN_FDC module for varying fault resistance is evaluated and the results are tabulated in Table 3.6. The fault location and the fault inception angle (fault inception time) are kept constant at 34 km and 0º (0.05 s) and

the different faults are simulated with different resistances. It can be observed from Table 3.6 that the proposed ANN_FDC module correctly identifies the faults within 7 ms time (less than one cycle time).

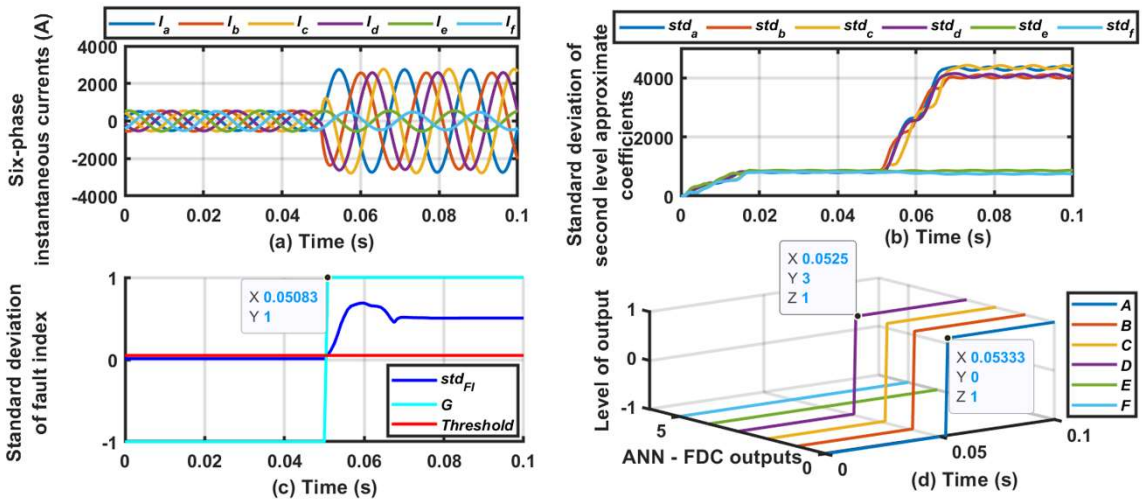

Fig. 3.8 (a) Six phase instantaneous currents, **(b)** Input patterns for the ANN_FDC module, **(c)** Fault index for ground detection, and **(d)** ANN-based fault detection and classification module outputs

Table 3.6 Results of the ANN_FDC module for the varying fault resistance

S. No.	Fault type with varying R_f (Ω) L_a = 34 km, FIA (Φ^o) = 0º (FIT = 0.05 s)	ANN_FDC module outputs							FDC time (ms)	
		A	*B*	*C*	*D*	*E*	*F*	*G*	Min.	Max.
1.	CG with 70 Ω	-1	-1	1	-1	-1	-1	1	5.83	5.83
2.	BDE with 5 Ω	-1	1	-1	1	1	-1	-1	1.67	5.0
3.	CDFG with 25 Ω	-1	-1	1	1	-1	1	1	2.5	6.67
4.	ACDE with 10 Ω	1	-1	1	1	1	-1	-1	2.5	5.83
5.	ABCDFG with 85 Ω	1	1	1	1	-1	1	1	2.5	5.5
6.	ABCDEF with 30 Ω	1	1	1	1	1	1	-1	2.5	5.83

The performance of the ANN_FDC module for varying fault locations is evaluated and the results are tabulated in Table 3.7. The fault resistance and the fault inception angle (fault inception time) are kept constant at 75 Ω and 0º (0.05 s) and the different faults are simulated at different fault locations. It can be observed from Table 3.7 that the proposed ANN_FDC module correctly identifies the faults within 9 ms time (less than one cycle time). The performance of the ANN_FDC module for varying fault inception angles is evaluated and the results are tabulated in Table 3.8. The fault resistance and the fault location are kept constant

at 90 Ω and 50 km, and the different faults are simulated at different fault inception angles. It can be observed from Table 3.8 that the proposed ANN_FDC module correctly identifies the faults within 8 ms time (less than one cycle time).

Table 3.7 Results of the ANN_FDC module for the varying fault location

S. No.	Fault type with varying L_a (km) R_f = 75 Ω, FIA (Φ^o) = 0º (FIT = 0.05 s)	ANN_FDC module outputs							FDC time (ms)	
		A	*B*	*C*	*D*	*E*	*F*	*G*	Min.	Max.
1.	AG at 3 km	1	-1	-1	-1	-1	-1	1	3.33	3.33
2.	ACG at 20 km	1	-1	1	-1	-1	-1	1	3.33	7.5
3.	BEFG at 40 km	-1	1	-1	-1	1	1	1	2.5	7.5
4.	BCDE at 55 km	-1	1	1	1	1	-1	-1	3.33	8.3
5.	ABCDE at 65 km	1	1	1	1	1	-1	-1	2.5	5.0
6.	ABCDEF at 67 km	1	1	1	1	1	1	-1	2.5	5.83

Table 3.8 Results of the ANN_FDC module for the varying fault inception angles

S. No.	Fault type with varying FIA (Φ^o), (FIT (s)), L_a = 50 km, R_f = 90 Ω	ANN_FDC module outputs							FDC time (ms)	
		A	*B*	*C*	*D*	*E*	*F*	*G*	Min.	Max.
1.	FG at 0º (0.05 s)	-1	-1	-1	-1	-1	1	1	6.67	6.67
2.	DF at 45º (0.05208 s)	-1	-1	-1	1	-1	1	-1	2.92	4.59
3.	ACDG at 60º (0.05278 s)	1	-1	1	1	-1	-1	1	3.05	3.89
4.	BCEF at 120º (0.0556 s)	-1	1	1	-1	1	1	-1	3.57	5.23
5.	ACDEF at 180º (0.0583 s)	1	-1	1	1	1	1	-1	2.53	6.7
6.	ABCDEF at 270º (0.0625 s)	1	1	1	1	1	1	-1	2.5	7.5

Table 3.9 Confusion matrix w.r.t training data

		Predicted faults												
		1-LG	**2-L**	**2-LG**	**3-L**	**3-LG**	**4-L**	**4-LG**	**5-L**	**5-LG**	**6-L**	**6-LG**	**NF**	**Total**
	1-LG	638	-	10	-	-	-	-	-	-	-	-	-	648
	2-L	-	1620	-	-	-	-	-	-	-	-	-	-	1620
	2-LG	-	13	1606	-	1	-	-	-	-	-	-	-	1620
	3-L	-	-	-	2160	-	-	-	-	-	-	-	-	2160
True	**3-LG**	-	-	-	-	2152	-	8	-	-	-	-	-	2160
faults	**4-L**	-	-	-	-	-	1620	-	-	-	-	-	-	1620
	4-LG	-	-	-	-	-	13	1607	-	-	-	-	-	1620
	5-L	-	-	-	-	-	-	-	648	-	-	-	-	648
	5-LG	-	-	-	-	-	-	-	-	648	-	-	-	648
	6-L	-	-	-	-	-	-	-	-	-	108	-	-	108
	6-LG	-	-	-	-	-	-	-	-	-	-	108	-	108
	NF	-	-	-	-	-	-	-	-	-	-	-	1	1

Table 3.10 Confusion matrix w.r.t testing data

		Predicted faults												
		1-LG	**2-L**	**2-LG**	**3-L**	**3-LG**	**4-L**	**4-LG**	**5-L**	**5-LG**	**6-L**	**6-LG**	**NF**	**Total**
True faults	**1-LG**	288	-	-	-	-	-	-	-	-	-	-	-	288
	2-L	-	720	-	-	-	-	-	-	-	-	-	-	720
	2-LG	-	7	713	-	-	-	-	-	-	-	-	-	720
	3-L	-	-	-	960	-	-	-	-	-	-	-	-	960
	3-LG	-	-	-	-	960	-	-	-	-	-	-	-	960
	4-L	-	-	-	-	-	720	-	-	-	-	-	-	720
	4-LG	-	-	-	-	-	7	713	-	-	-	-	-	720
	5-L	-	-	-	-	-	-	-	288	-	-	-	-	288
	5-LG	-	-	-	-	-	-	-	-	288	-	-	-	288
	6-L	-	-	-	-	-	-	-	-	-	48	-	-	48
	6-LG	-	-	-	-	-	-	-	-	-	-	48	-	48
	NF	-	-	-	-	-	-	-	-	-	-	-	1	1

To obtain the overall assessment of the proposed fault detection and classification of the ANN_FDC module, confusion matrices w.r.t to training and testing data are presented in Table 3.9 and Table 3.10. The true and predicted fault types are represented on the left and top of the tables. The accuracy and the dependability of the proposed protection scheme w.r.t fault detection and classification are given in Table 3.11. From the table, it can be understood that the proposed method's performance is efficient and accurate in the FDC task.

Table 3.11 Performance index of ANN_FDC module for FDC

S. No.	Performance index	w.r.t Training data	w.r.t Testing data
1.	Accuracy	$\frac{12916}{12961} \times 100 = 99.65\%$	$\frac{5747}{5761} \times 100 = 99.76\%$
2.	Dependability	$\frac{12915}{12960} \times 100 = 99.645\%$	$\frac{5746}{5760} \times 100 = 99.76\%$

3.4.2 Performance Evaluation of the ANN_FLE Modules for Varying Fault Parameters

The performance of the proposed protection scheme's ANN_FLE fault location estimation modules detailed in Table 3.5 is evaluated for the different faults simulated i.e., with varying fault parameters. A single line to ground fault (AG) is simulated at a fault location of 65 km from bus B1 at 0.05 s with a fault resistance of 80 Ω and a double line to ground fault (ABG) is simulated at a fault location of 1 km from bus B1 at 0.05 s with fault

resistance of 60 Ω. The response of the ANN_FLE_1-LG module for the AG fault and the ANN_FLE_2-LG module for the ABG fault is shown in Fig. 3.9 and Fig. 3.10. It can be observed from Fig. 3.9 that the proposed ANN_FLE_1-LG module approximately estimates the actual fault location for the faulty phase (A-phase) as 65.3 km while the healthy phases as 140 km. Similarly, the estimated fault location is obtained as 0.8737 km and 0.9271 km as depicted in Fig. 3.10 for the faulty phases. Some of the test results of the proposed ANN_FLE modules are depicted in Table 3.12, Table 3.13, and Table 3.14 for different faults. It is evident from the test results in Fig. 3.9, Fig. 3.10, and Tables 3.12, 3.13, and 3.14 that the proposed method provides approximately near-fault location estimation results.

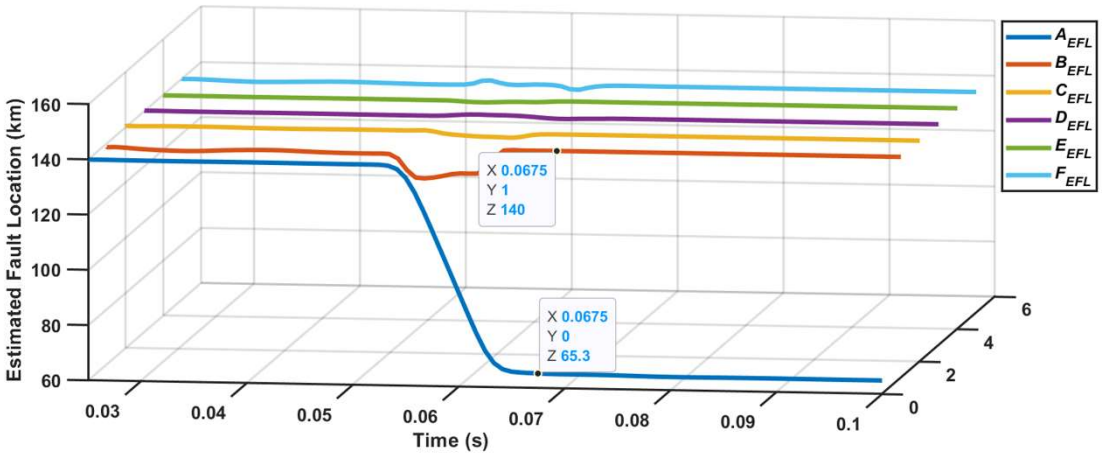

Fig. 3.9 Estimated fault location by the ANN_FLE_1-LG module for AG fault at 65 km, fault resistance of 80 Ω and fault inception angle of 0° (fault inception time 0.05 s)

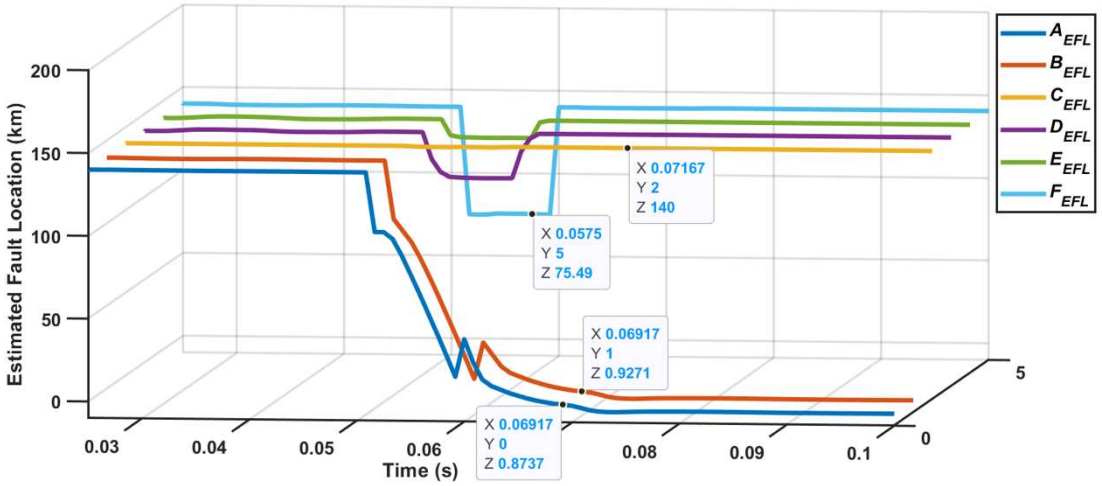

Fig. 3.10 Estimated fault location by the ANN_FLE_2-LG module for ABG fault at 1 km, fault resistance of 60 Ω and fault inception angle of 0° (fault inception time 0.05 s)

Table 3.12 Estimated fault location by the ANN_FLE modules with R_f = 0.01 Ω, Φ^o =0º, and L_a = 5 km

Estimated fault location for different faults with R_f = 0.01 Ω, FIA (Φ^o) = 0º, and L_a = 5 km								
		Estimated fault location (E_{fl}) in each phase (km)						
S. No.	Fault Type	A_{EFL}	B_{EFL}	C_{EFL}	D_{EFL}	E_{EFL}	F_{EFL}	Max. % E
1.	AG	5.043	140	140	140	140	140	0.063%
2.	ABG	5.235	5.259	140	140	140	140	0.38%
3.	ABCG	5.37	5.588	5.437	140	140	140	0.865%
4.	ABCDG	5.452	5.349	5.463	5.525	140	140	0.772%
5.	ABCDEG	4.788	4.822	4.831	4.802	4.831	140	-0.311%
6.	ABCDEFG	4.927	4.927	4.927	4.927	4.927	4.927	-0.107%
7.	ABCDEF	4.977	4.979	4.977	4.977	4.977	4.98	-0.034%
8.	ABCDE	5.052	5.053	5.05	5.053	5.032	140	0.078%
9.	ABCD	5.014	5.215	4.962	5.004	140	140	0.316%
10.	ABC	5.593	6.035	5.431	139.6	140.2	139.3	1.522%
11.	AB	4.719	4.932	139.8	140.4	140.1	140.2	-0.413%

Table 3.13 Estimated fault location by the ANN_FLE modules with R_f = 90 Ω, Φ^o = 270º, and L_a = 66 km

Estimated fault location for different faults with R_f = 90 Ω, FIA (Φ^o) = 270º, and L_a = 66 km								
		Estimated fault location (E_{fl}) in each phase (km)						
S. No.	Fault Type	A_{EFL}	B_{EFL}	C_{EFL}	D_{EFL}	E_{EFL}	F_{EFL}	Max. % E
1.	AG	66.1	140	140	139.9	140	140	0.147%
2.	ABG	66.12	66.26	139.8	140	140	140	0.382%
3.	ABCG	63.23	63.43	65.25	140.6	140.5	140.2	-4.074%
4.	ABCDG	66.01	66.21	66.18	66.29	139.9	140	0.426%
5.	ABCDEG	66.5	66.75	66.72	67.08	140	139.7	2.647%
6.	ABCDEFG	66.22	66.22	66.22	66.22	66.22	66.22	0.324%
7.	ABCDEF	66.18	66.18	66.63	66.18	66.18	66.18	0.926%
8.	ABCDE	66.04	66.17	66.16	66.14	65.3	140	-1.029%
9.	ABCD	66.32	66.14	66.32	66.38	141.6	138.4	0.559%
10.	ABC	65.03	67.19	67.28	140.7	140.7	139.4	1.882%
11.	AB	65.84	65.6	140.9	141.2	140.1	139.5	-0.588%

Table 3.14 Estimated fault location by the ANN_FLE modules with varying fault parameters

		Estimated fault location (E_{fl}) in each phase (km)						
S. No.	Fault type with R_f (Ω), FIA (Φ^o), and L_a (km)	A_{EFL}	B_{EFL}	C_{EFL}	D_{EFL}	E_{EFL}	F_{EFL}	Max. % E
1.	AG with 40 Ω, 0º, and 15 km	14.9	140	140	140	140	140	-0.147%
2.	ABG with 75 Ω, 30º, and 35 km	35.64	35.83	140	140	140	139.5	1.221%
3.	ABC with 5Ω, 60º, and 50 km	49.83	48.95	49.87	140.3	141.1	140.3	-1.544%
4.	ABCDG with 60 Ω, 90º, and 30 km	29.59	29.55	29.59	29.59	140.1	139.9	-0.662%
5.	ABCDE with 15 Ω, 120º, and 45 km	43.25	43.24	43.25	43.24	43.24	140	-2.588%
6.	ABCDEF with 20 Ω, 150º, and 55 km	53.82	53.82	53.82	53.82	53.82	53.82	-1.735%

Further to analyse the overall performance of the ANN_FLE modules, the training and testing data samples that are given in Table 3.3 and Table 3.4 are used to estimate the fault location. The percentage error in the estimated fault location in all the faulty phases is calculated using Eq. (3.10). Table 3.15 presents the no. of fault cases for all the phases under each range of percentage error in the estimated fault location for the ANN_FLE_1-LG fault location estimation module w.r.t training data and the same has been depicted in Fig. 3.11 with the percentage proportion of 1-LG fault cases under each error range. It can be observed that about 99% of the 1-LG fault cases are within the ±1% error range.

Table 3.15 No. of 1-LG fault cases under each range of percentage error in the estimated fault location (w.r.t training data)

		No. of fault cases					
Fault Location Module	Phase	% E1: -1% to +1%	% E2: -2% to -1% and +1% to +2%	% E3: -3% to -2% and +2% to +3%	% E4: -4% to -3% and +3% to +4%	% E5: -5% to -4% and +4% to +5%	% E6: -10% to -5% and +5% to +10%
ANN_FLE _1-LG module (108 fault cases for each phase)	A	108	0	0	0	0	0
	B	108	0	0	0	0	0
	C	108	0	0	0	0	0
	D	108	0	0	0	0	0
	E	107	1	0	0	0	0
	F	106	2	0	0	0	0
6 x 108 = 648	1-LG	645	3	0	0	0	0

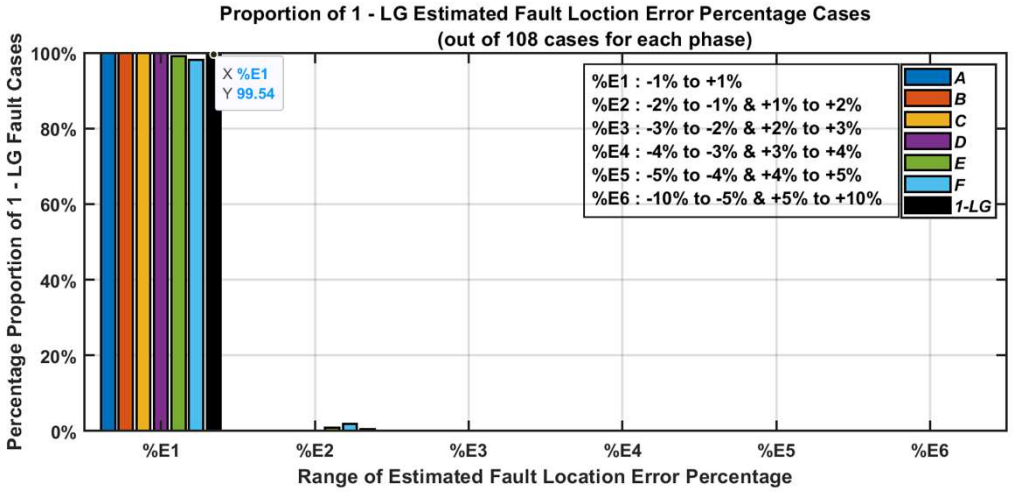

Fig. 3.11 Proportion of 1-LG estimated fault location error percentage fault cases in different error percentage ranges (w.r.t training data)

Similarly, Table 3.16 presents the no. of fault cases for all the phases under each range of percentage error in the estimated fault location for all the fault location estimation modules w.r.t training data and Fig. 3.12 portrays the same with the percentage proportion of fault cases under each error range that is shown in Table 3.16. It can be observed that about 81% of all the fault cases are within the ±1% error range.

Table 3.16 No. of fault cases under each range of percentage error in the estimated fault location (w.r.t training data)

		No. of fault cases					
Fault Location Module	Phase	% E1: -1% to +1%	% E2: -2% to -1% and +1% to +2%	% E3: -3% to -2% and +2% to +3%	% E4: -4% to -3% and +3% to +4%	% E5: -5% to -4% and +4% to +5%	% E6: -10% to -5% and +5% to +10%
All fault location estimation modules. (6804 fault cases per phase)	A	5403	989	260	79	26	47
	B	5488	954	237	60	29	36
	C	5634	832	210	64	25	39
	D	5443	964	272	73	26	26
	E	5471	968	257	68	21	19
	F	5740	765	198	55	14	32
6 x 6804 = 40824	All faults	33179	5472	1434	399	141	199

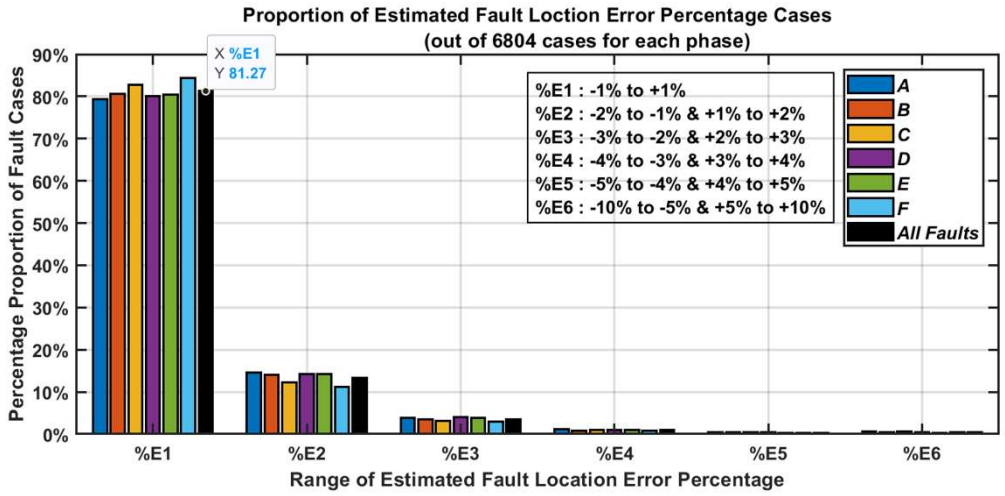

Fig. 3.12 Proportion of all the estimated fault location error percentage fault cases in different error percentage ranges (w.r.t training data)

Similarly, Table 3.17 and Table 3.18 present the no. of fault cases for each phase in each of the percentage error ranges for the ANN_FLE_1-LG module and all the fault location estimation modules w.r.t testing data. Fig. 3.13 and Fig. 3.14 present the proportion percentage of fault cases for each phase under different error ranges for the data shown in Table 3.17 and Table 3.18. It is observed from Fig. 3.13 and Fig. 3.14 that about 98% and 53% proportion of fault cases are within the ±5% error range in the estimated fault location.

Table 3.17 No. of 1-LG fault cases under each range of percentage error in the estimated fault location (w.r.t testing data)

		No. of fault cases					
Fault Location Module	Phase	% E1: -1% to +1%	% E2: -2% to -1% and +1% to +2%	% E3: -3% to -2% and +2% to +3%	% E4: -4% to -3% and +3% to +4%	% E5: -5% to -4% and +4% to +5%	% E6: -10% to -5% and +5% to +10%
ANN_FLE _1-LG module (48 fault cases for each phase)	A	41	7	0	0	0	0
	B	30	4	5	5	1	3
	C	34	8	2	3	1	0
	D	38	6	2	1	1	0
	E	27	10	4	6	0	1
	F	29	14	3	2	0	0
6 x 48 = 288	1-LG	199	49	16	17	3	4

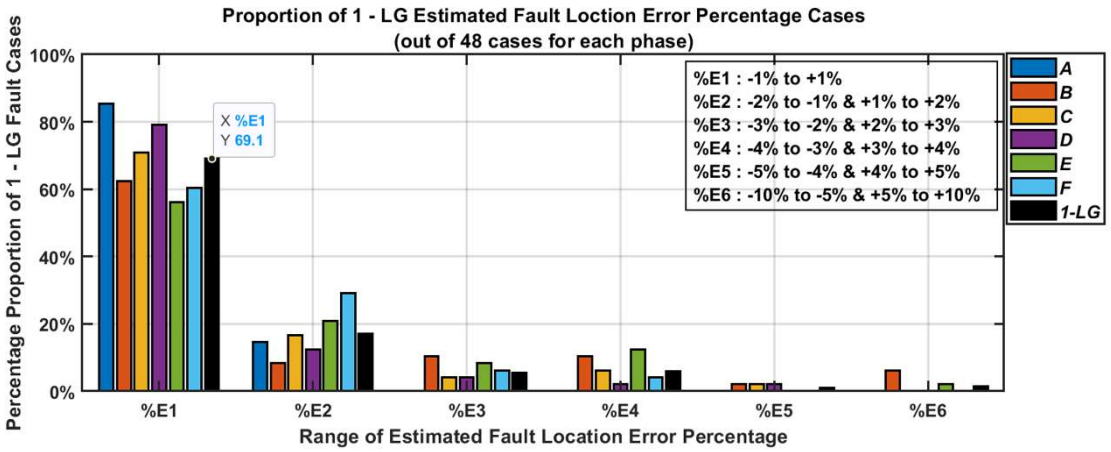

Fig. 3.13 Proportion of 1-LG estimated fault location error percentage fault cases in different error percentage ranges (w.r.t testing data)

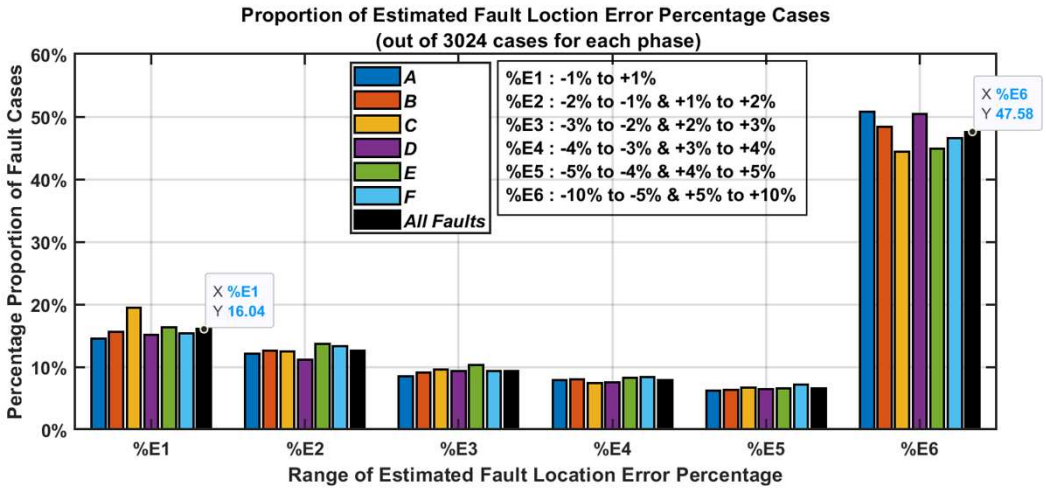

Fig. 3.14 Proportion of all the estimated fault location error percentage fault cases in different error percentage ranges (w.r.t testing data)

Table 3.18 No. of fault cases under each range of percentage error in the estimated fault location (w.r.t testing data)

		No. of fault cases					
Fault Location Module	Phase	% E1: -1% to +1%	% E2: -2% to -1% and +1% to +2%	% E3: -3% to -2% and +2% to +3%	% E4: -4% to -3% and +3% to +4%	% E5: -5% to -4% and +4% to +5%	% E6: -10% to -5% and +5% to +10%
All fault location estimation modules. (3024 fault cases per phase)	A	439	365	258	238	189	1535
	B	470	381	275	244	190	1464
	C	589	376	291	224	202	1344
	D	456	338	283	228	195	1524
	E	493	412	313	249	199	1358
	F	463	402	281	254	216	1408
6 x 3024 = 18144	All faults	2910	2274	1701	1437	1191	8633

Table 3.19 Comparison of the proposed scheme with other existing schemes

S. No.	Comparison Term	Reference					
		[43]	[45]	[46]	[117]	[118]	Proposed
1.	Protection technique	ANN	Fuzzy inference system	Decision tree and TLBO tuned ANN	Adaptive PSO tuned ANN	Bat algorithm tuned deep neural network	ANN
2.	Signal pre-processing technique	DFT	DFT	Least square Adaline algorithm	DWT	Stacked encoder-grayscale images	DWT
3.	Voltage or current information requirement	Voltage and current	Voltage and current	Voltage	Voltage and current	Voltage and current	Current
4.	No. of FDC modules	11	7	11	11	11	1
5.	No. of fault cases	4930	-	28830	21600	4836	5761
6.	FDC accuracy	100%	98.02%	99.64%	100%	99.45%	99.76%
7.	FDC time	16.67 ms	16.67 ms	12.4 ms	14 ms	16.67 ms	16.67 ms
8.	No. of FLE modules	11	-	11	11	-	11

3.4.3 Comparison of Proposed Scheme with Other Existing Schemes

A comparison of the proposed protection scheme with the existing protection schemes is presented in Table 3.19. Since the proposed protection technique uses only phase current information for the protection task, it requires only a current transformer. The cost of the potential transformer can be saved as the voltage information is not required for the protection task. The sending end bus data is utilized, therefore there is no requirement for a communication link and hence no communication latency. As a smaller sampling frequency (1.2 kHz) is used the cost of the digital fault recorder, computational complexity, and data storage/handling problem can be minimized. Unlike the other multi-ANN modules technique for fault detection and classification, the proposed technique uses only a single ANN module that greatly reduces the computational burden and a good deal of time for training and selection of the optimal architecture of multi-ANN modules.

3.5 Summary

In this chapter, a protection scheme based on DWT and ANN is proposed for the complete protection of the six-phase transmission line. A single ANN_FDC module is proposed to identify and classify all the 120 types of faults. The performance of this module is evaluated with training and testing data in terms of accuracy and dependability. The performance indices show that the proposed FDC module is efficient and effective with 99.76% accuracy. Moreover, the proposed technique is resistant to fault parameter variations and detects all types of faults within one cycle time (16.67 ms). The ANN_FLE fault location estimation modules are proposed for approximating the fault location. The performance of all the FLE modules is also evaluated with training and testing data. The performance of the fault location estimation modules is better with training data where 81% of the fault cases are within the ±1% error range but the performance w.r.t testing data is nominal where 53% of the fault cases are within ±5% error range. It can be concluded that the proposed protection scheme works efficiently for fault detection and classification with a single module and the performance of fault location estimation modules can be further improved with optimal tunning of ANN parameters.

*****

Chapter 4

A Novel Protection Scheme for Transmission Lines Connected to Solar Photovoltaic and Wind Turbine Farms Using Fuzzy Logic Systems and Bagged Ensemble Learning

4.1 Introduction

The global electrical energy demand is steadily increasing, driven by population growth, urbanization, and technological advancements. This escalating demand necessitates a sustainable energy for the future. The growing demand must be met besides addressing the challenge of climate change. To reduce the carbon emissions from conventional sources, nations across the globe are rapidly shifting towards renewable energy sources like solar and wind rather than fossil fuels for power generation. The integration of these inherently variable and geographically dispersed sources into the existing power grid poses significant challenges, especially in transmission line protection. Due to terrestrial and environmental conditions, renewable energy generation is not possible at all locations. The generated renewable power is to be transmitted to the load centres wherever it is required. The regional disparities in generation as well as demand necessitate the use of transmission lines.

The settings of conventional distance protection schemes are developed assuming the grid is solely supplied by the synchronous generators. Upon integration of renewables, the intermittent nature of renewable power sources creates problems to the distance relay operation that relies on the positive sequence components of voltage and current signals. The relay may issue false trips and experience underreach or overreach problems depending on the system operating conditions. Further, the faulty phase identification gets complicated due to the partial cancellation of positive and zero sequence components of currents during faults resulting in reduced fault currents than the healthy phase currents i.e. accounted for the control mechanisms of the voltage source converters associated with the renewable energy sources (RES) [119, 120].

This chapter presents an intelligent novel protection scheme with a fuzzy logic system to identify and classify the short circuit faults of the transmission line connected to RES (solar and wind power sources). The voltage signals of the bus connected to renewable energy sources are pre-processed with DFT are the inputs to the proposed Mamdani based fuzzy inference system for fault detection/classification. A bagged ensemble learning approach with regression decision trees is proposed for fault location estimation using the DFT processed voltage signals. The key points of the proposed protection method are:

- The proposed scheme of protection approach with FIS demonstrates robust performance in identifying and classifying various fault types, even under variable generation conditions of the RES connected to lines.
- This scheme achieved an accuracy of 99.56% in fault detection and classification utilizing only single end voltage data that eliminates the use of communication link. Hence no communication latency.
- The FIS based protection scheme is simple to implement and does not require any training for protection purpose.
- The bagged ensemble approach effectively reduces the estimation errors, ensuring a better approximation of the fault location that facilitates swift repair and restoration, minimizing downtime and enhancing grid resilience.
- The proposed approach demonstrates the potential of combining fuzzy logic, ensemble learning, and signal processing techniques for developing intelligent protection systems adaptable to modern power grids.

4.2 Details of Three-phase Transmission Line Connected to RES

In the present work, a 200 km length transmission line (400 kV and 50 Hz) connected to RES is considered. Fig. 4.1 depicts the single-line schematic representation of the transmission system model with RES blocks and block representation of the protection scheme proposed. The represented power transmission system is modelled and simulated utilizing the MATLAB/Simulink platform. A three-phase power source represented with Thevenin's equivalent having 1.25 GVA short circuit capacity and 10 X/R ratio is connected to one end of the line at bus B3 represents the 400 kV, 50 Hz grid. The RES are connected at the other end of the line at bus B1. The solar and wind powers of each 50 MW is integrated into the power system through the transmission line. The MATLAB components viz. distributed parameters line block based on Bergeron's line model and three-phase fault breakers are used to simulate the transmission line having shunt capacitance effect and various fault types respectively. The voltage samples collected at bus B1 are utilized for the proposed protection technique. The parameters of the transmission line are given in Appendix – III.

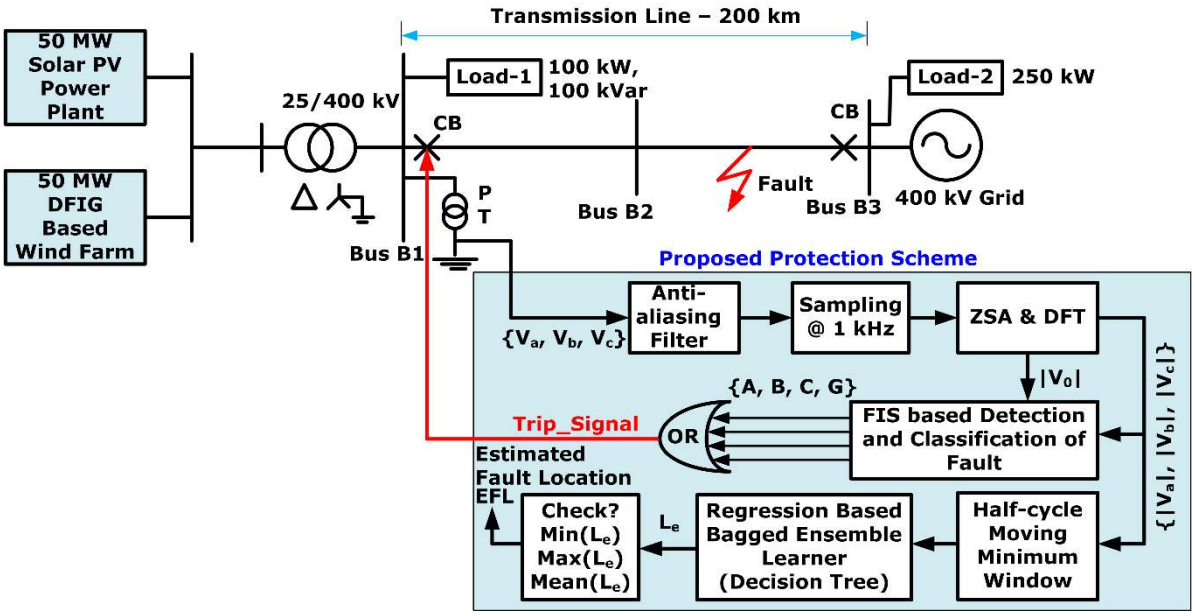

Fig. 4.1 Single-line schematic representation of power transmission system model along with block diagram of proposed protection method

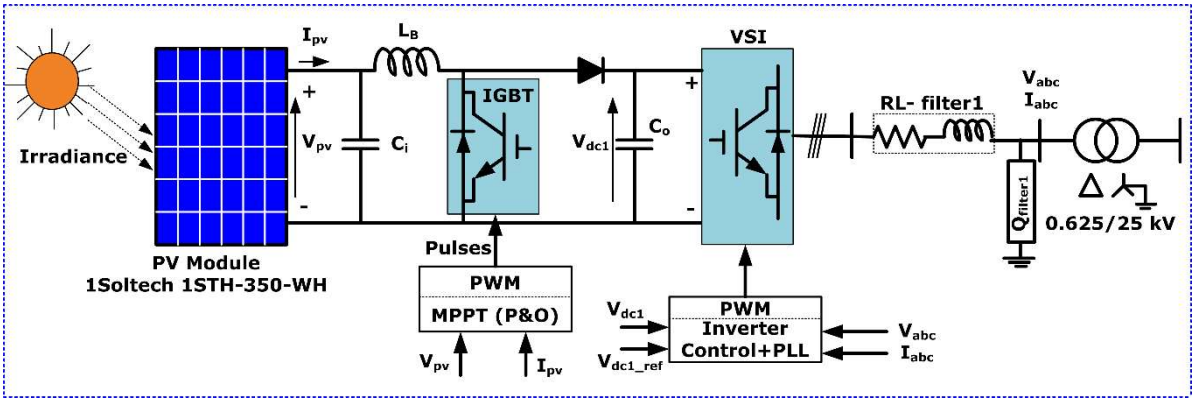

Fig. 4.2 Schematic representation of solar PV power source

The solar photovoltaic (PV) power plant rated with 50 MW power consists of PV module, DC-DC boost converter, and voltage source inverter with a step-up transformer. A schematic representation of the solar power plant is shown in Fig. 4.2. An aggregate model of the 50 MW solar power plant is developed in MATLAB/Simulink that constitutes 50 number of solar PV parallel arrays each of 1 MW rated power. Each array consists of 205 number of parallel strings and each string has 14 number of series connected modules. The solar PV power plant data and the specifications of the PV module are given in Appendix – IV. The DC-DC boost converter is used to boost the PV voltage and extract the maximum power from the PV plant with perturb and observe maximum power point tracking algorithm. The 2-level three-phase

voltage source inverter (VSI) and step-up transformer are used to interface/integrate the power of the PV plant into the power system. The block schematic of the inverter control is shown in Fig. 4.3. The details of the design aspects related to the PV system can be referred in [121, 122].

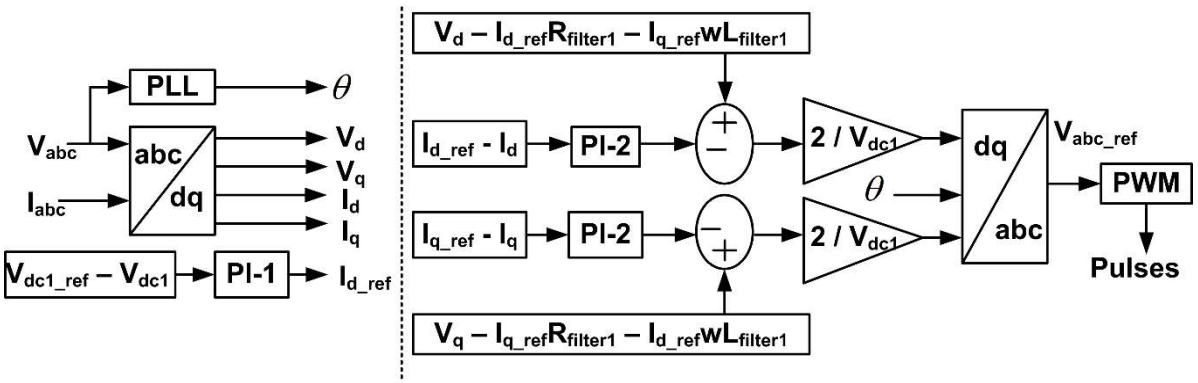

Fig. 4.3 Block schematic of inverter control

The wind power is generated using the doubly fed induction generators (DFIG). Fig. 4.4 presents the schematic representation of the DFIG based wind farm. An aggregate model of the 50 MW wind power farm is developed in MATLAB/Simulink. The DFIG based wind farm rated with 50 MW power consists of 33 number of wind turbine generators each of 1.5 MW rated power. The DFIG based wind farm data is given in Appendix – V. The wind turbine system, wound rotor induction generator, back-to-back converters (grid side converter (GSC) and rotor side converter (RSC)) with its associated control system, and the step-up transformer constitute the wind power farm. The power generated by the wind farm is fed to the power system through the step-up transformer where the stator windings are directly connected to the transformer and rotor windings are connected through the back-to-back converters. The 2-level converters are used for GSC and RSC that maintain the dc link voltage and control the rotor currents respectively. The block schematics of the converter control for RSC and GSC are shown in Fig. 4.5 and Fig. 4.6. The details of the design aspects related to the wind power system can be referred in [121, 122].

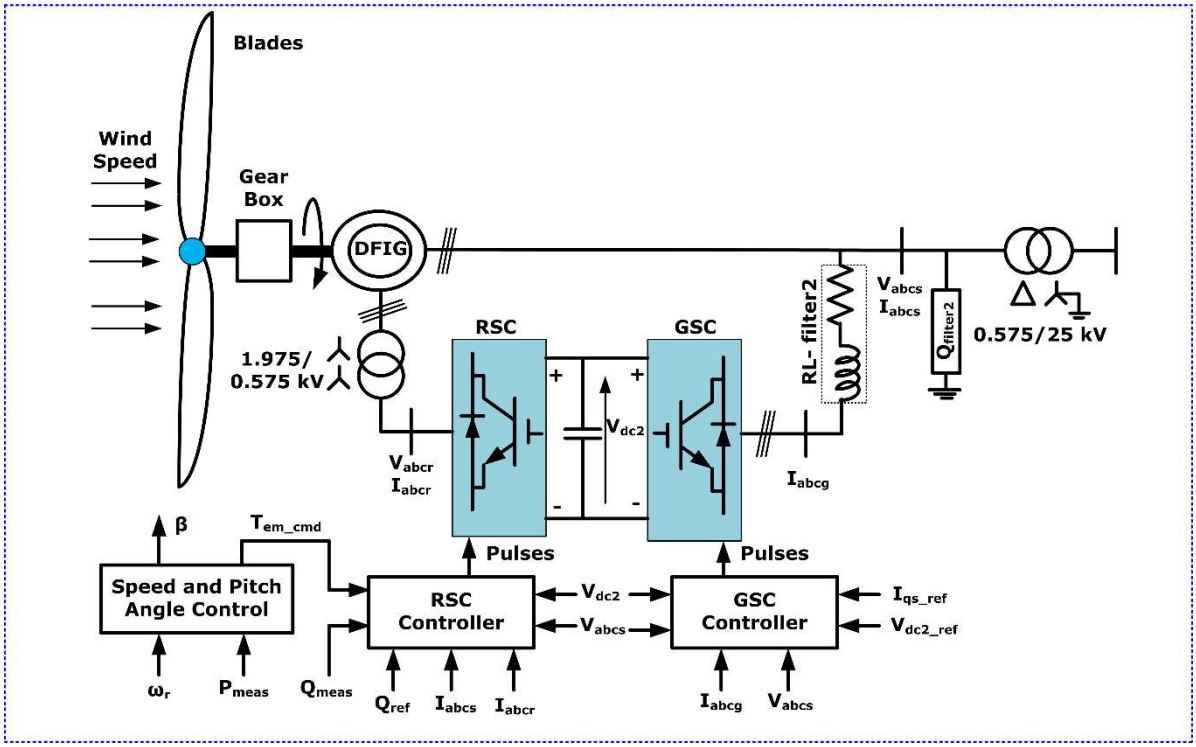

Fig. 4.4 Schematic representation of the DFIG based wind farm

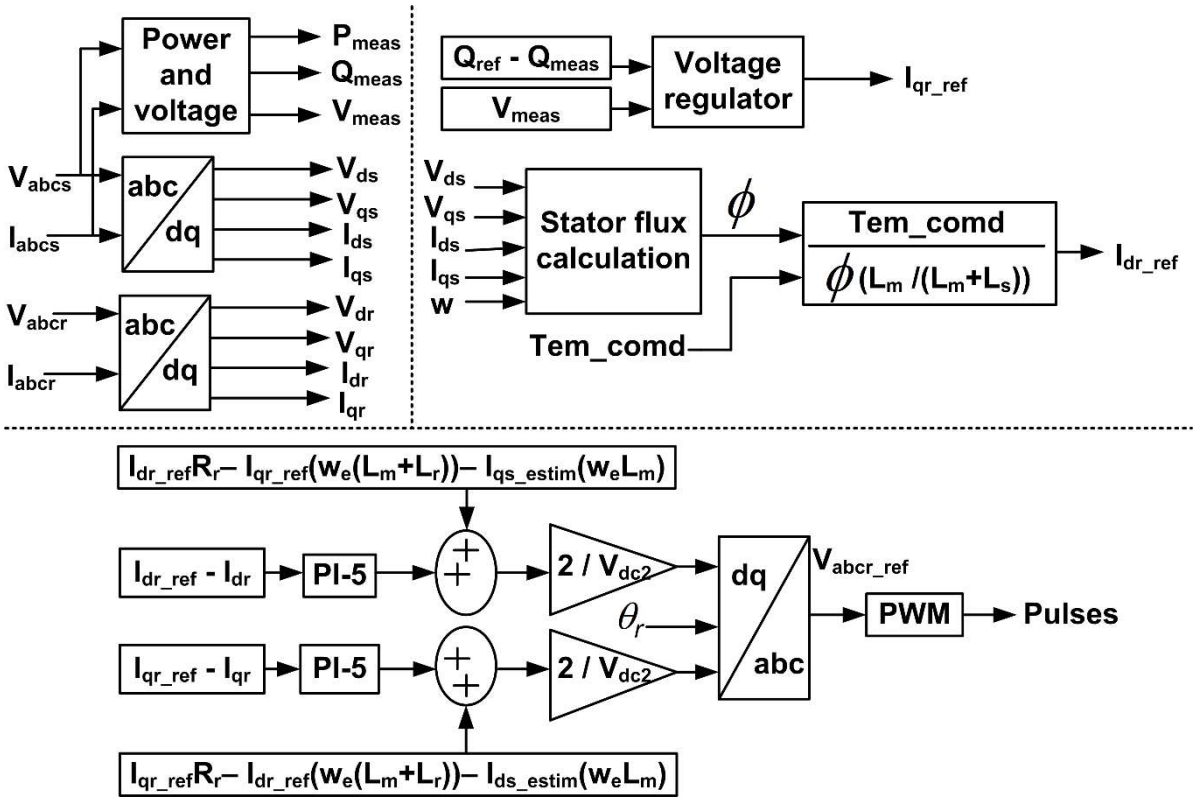

Fig. 4.5 Block schematic of RSC control

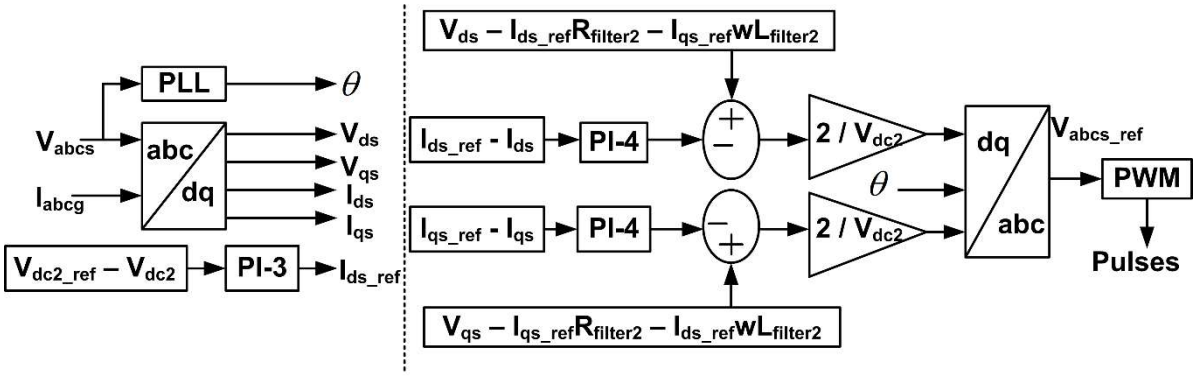

Fig. 4.6 Block schematic of GSC control

4.3 Development of Proposed Protection Scheme with FIS and Bagged Ensemble of Regression Trees

Generally, any digital scheme of protection involves majorly two stages. The first stage is the signal pre-processing to extract the relevant features useful for the protection task. The second stage is the implementation of the scheme of protection with the extracted features. In the present work, the simple and most widely applied discrete Fourier transform is employed as the signal processing technique and the scheme of protection is developed utilizing the fuzzy logic system and ensemble learning approach with features retrieved by DFT.

4.3.1 DFT Based Feature Extraction Process

The raw and unprocessed instantaneous fault information (either voltage or current data) captured at the relaying location are very transitory and oscillatory in nature due to which they cannot be directly used for the protection job. Hence, the raw fault data discretization and pre-processing with suitable digital signal processing technique is crucial. In the present study, the voltage samples collected at bus B1 are only employed for the protection job because the amount of current injected into the grid may vary depending upon the intermittent operating conditions of the RES. But, irrespective of RES operating conditions, the voltage at bus B1 is maintained almost invariable due to the control action of voltage source converters of RES. The initial stage of signal processing involves the filtering of three-phase voltage signals at bus B1 using a low pass Butterworth anti-aliasing filter of second-order with 480 Hz cut-off frequency to ensure the removal of higher order voltage harmonics. According to the Nyquist sampling criterion, the filtered voltage signal is sampled with a 1

kHz sampling frequency. Using the discrete Fourier transform, the amplitude of the voltage signal's fundamental component is extracted/determined from the discrete voltage samples. Eq. (4.1) gives $V_p(k)$, the discrete Fourier transform of $v_p(n)$ (discrete voltage samples) [91].

$$V_p(k) = \frac{1}{M}\sum_{n=0}^{M-1} v_p(n)\, e^{\frac{-j2\pi nk}{M}} \tag{4.1}$$

Where $V_p(k)$ is the voltage phasor, $v_p(n)$ is a discretized voltage signal, $p = a, b$, and c phases, $n, k = 0, 1, 2, 3, \ldots, M-1$ are sample numbers, order of frequency stamps, and M is the number of samples per cycle. The zero-sequence voltage is determined utilizing MATLAB's sequence analyser to ensure the ground involvement in the fault loop of grounded faults. Therefore, the features extracted relevant to the scheme of protection are the magnitudes of fundamental component and zero-sequence component of three-phase voltage samples viz. $\{|V_a|, |V_b|, |V_c|, and\ |V_0|\}$.

4.3.2 Proposed Protection Scheme for FDC and FLE

The fuzzy logic system is used for the detection and classification of short circuit faults of the transmission line. Fuzzy logic systems are one of the AI techniques that are based on the fuzzy logic mathematical framework which works on vague/imprecise input data to produce precise output mimicking human like reasoning. These are simple, flexible, and have an easily implementable structure. They can solve non-linear problems without intense computational effort regardless of the system's mathematical model. Fuzzy set theory forms the base for fuzzy logic concepts. Unlike the traditional binary logic where the possible outcomes are categorized as either completely true or false i.e. 1 or 0, fuzzy logic introduces the concept of partial truthiness or falseness ranging its degree from 0 to 1 that embraces the ambiguity of real-world problems. These rule-based systems make decisions using the fuzzy logic idea. The execution of these systems is based on a set of devised *"if-then"* fuzzy rules that establish conditional relationships mapping the input-output fuzzy sets represented by the membership functions. The execution involves processes like fuzzifying inputs and outputs, fuzzy inference processing, and defuzzification of outputs [8].

A single module of the Mamdani fuzzy inference system (FIS) is developed using MATLAB's Fuzzy Logic Toolbox to make decisions about the transmission line fault type and its occurrence. The FIS accepts four inputs $\{|V_a|, |V_b|, |V_c|, and\ |V_0|\}$ and provides four outputs *{A, B, C, and G}* to identify and classify the faults. The inputs and outputs are

organized into different fuzzy sets with the fuzzy linguistic variables labelled as *F (fault), VF (verge of fault),* and *UF (unfault)* for the inputs, and *L (Low), M (Medium),* and *H (High)* for the outputs. The fuzzy linguistic variables of the inputs and outputs are represented with the trapezoidal *(F, L,* and *H)* and triangular *(VF, UF,* and *M)* membership functions. Fig. 4.7 depicts the graphical representation of the fuzzification of inputs and outputs.

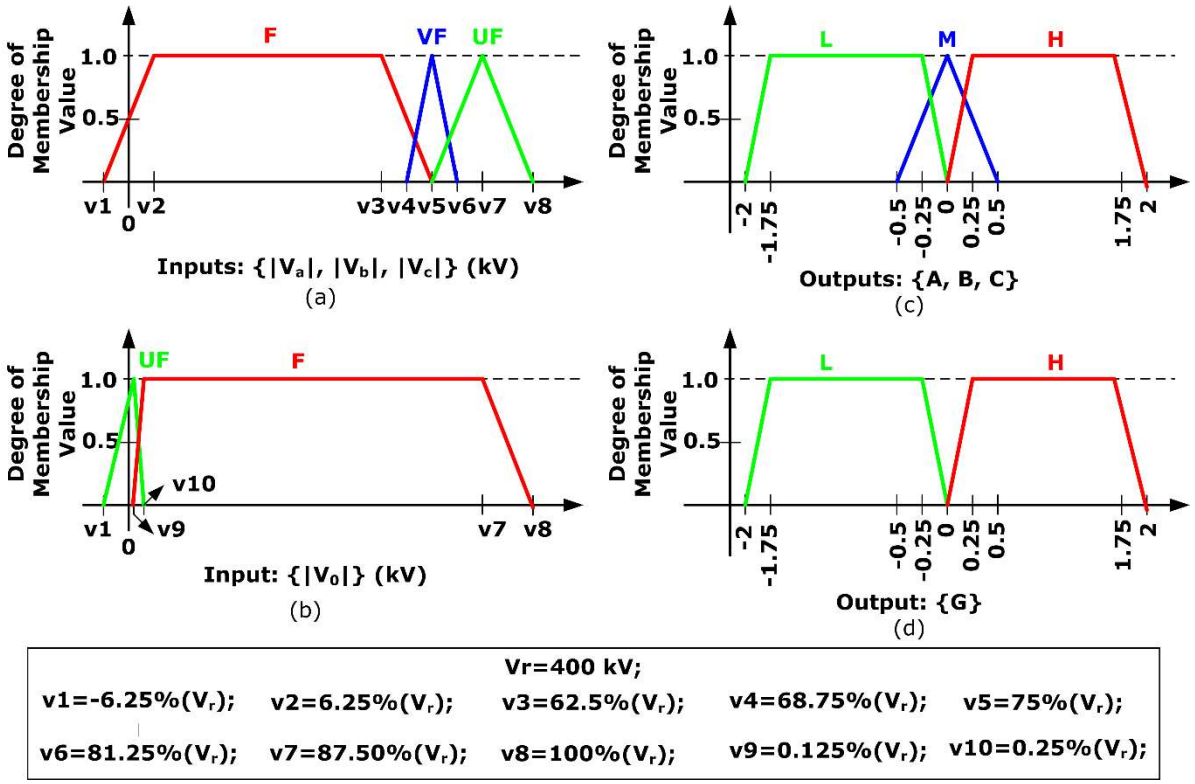

Fig. 4.7 Fuzzification of inputs and outputs

The suggested protection scheme employs 23 fuzzy rules that are formulated with the input-output fuzzy linguistic variables to detect/classify the faults. Table 4.1 presents the formulated fuzzy rule base of the scheme with rule no. #1 as *"If $|V_a|$ is UF and $|V_b|$ is UF and $|V_c|$ is UF then A is L, B is L, C is L"*. In a similar fashion, all other framed rules can be interpreted. The outputs *{A, B, and C}* are dedicated to detect the phase(s) is faulty or healthy represented with the output labels *"+1"* or *"-1"* respectively. Similarly, the output *{G}* is engaged in the detection of ground for the grounded faults. The centroid method of defuzzification is applied to the aggregated fuzzy outputs to deliver a crisp value that signifies the fault severity. Whenever a fault is detected, the faulty phase output of the FIS module shows *"High"* with the label *"+1"* and for the healthy phase the module output is *"Low"* with *"-1"*. The OR

operation is performed on the FIS outputs *{A, B, and C}* to issue the trip signal to the circuit breaker.

Table 4.1 Framed fuzzy rules

# Rule no.	Membership functions for								# Rule no.	Membership functions for							
	$\|V_a\|$	$\|V_b\|$	$\|V_c\|$	$\|V_0\|$	*A*	*B*	*C*	*G*		$\|V_a\|$	$\|V_b\|$	$\|V_c\|$	$\|V_0\|$	*A*	*B*	*C*	*G*
#1	*UF*	*UF*	*UF*	-	*L*	*L*	*L*	-	**#13**	*VF*	*VF*	*F*	-	*M*	*M*	*H*	-
#2	*VF*	*VF*	*VF*	-	*M*	*M*	*M*	-	**#14**	*UF*	*VF*	*F*	-	*L*	*M*	*H*	-
#3	*F*	*F*	*F*	-	*H*	*H*	*H*	-	**#15**	*VF*	*UF*	*F*	-	*M*	*L*	*H*	-
#4	*F*	*UF*	*UF*	-	*H*	*L*	*L*	-	**#16**	*F*	*F*	*UF*	-	*H*	*H*	*L*	-
#5	*F*	*VF*	*VF*	-	*H*	*M*	*M*	-	**#17**	*F*	*F*	*VF*	-	*H*	*H*	*M*	-
#6	*F*	*VF*	*UF*	-	*H*	*M*	*L*	-	**#18**	*UF*	*F*	*F*	-	*L*	*H*	*H*	-
#7	*F*	*UF*	*VF*	-	*H*	*L*	*M*	-	**#19**	*VF*	*F*	*F*	-	*M*	*H*	*H*	-
#8	*UF*	*F*	*UF*	-	*L*	*H*	*L*	-	**#20**	*F*	*UF*	*F*	-	*H*	*L*	*H*	-
#9	*VF*	*F*	*VF*	-	*M*	*H*	*M*	-	**#21**	*F*	*VF*	*F*	-	*H*	*M*	*H*	-
#10	*UF*	*F*	*VF*	-	*L*	*H*	*M*	-	**#22**	-	-	-	*UF*	-	-	-	*L*
#11	*VF*	*F*	*UF*	-	*M*	*H*	*L*	-	**#23**	-	-	-	*F*	-	-	-	*H*
#12	*UF*	*UF*	*F*	-	*L*	*L*	*H*	-									

This work employs a regression based bagged ensemble learning approach with decision trees strategy for estimation/prediction of fault location. The ensemble learning approach is one of the machine learning techniques i.e. used to improve the overall prediction accuracy and robustness of the model. An ensemble learner is one which combines the results of many learners to give a final output of high quality. In the bagged ensemble learning approach, the learners/models are independent of each other and are trained/processed parallelly on the training data set or subsets of training data that are obtained by sampling the initial training data set with replacement. Instead of single model training that may be prone to underfitting/overfitting due to data changes, the bagging ensemble process that trains multiple models avoids the overfitting issues making the system robust with good generalization performance. A pictorial representation of the bagged ensemble learner is shown in Fig. 4.8, where $D_{K,d}$ is the original training data set of K rows (instances) and d

columns (*d-1* features/attributes and the last column represents the target data), $D^1_{K1,d}$, $D^2_{K1,d}$, $D^3_{K1,d}$, ..., $D^n_{K1,d}$ are the subsets of training data, M_1, M_2, M_3, ..., M_n are individual models/learners, Y_1, Y_2, Y_3, ..., Y_n are the individual model outputs, and *n* is the number of learners in the ensemble. The *Y* is the final output of the ensemble. If the bagged ensemble is used for classification purpose, then the final aggregated output is based on the majority voting method and if it is a regression ensemble then the final aggregated output is the average of all the individual outputs [123, 124, 125].

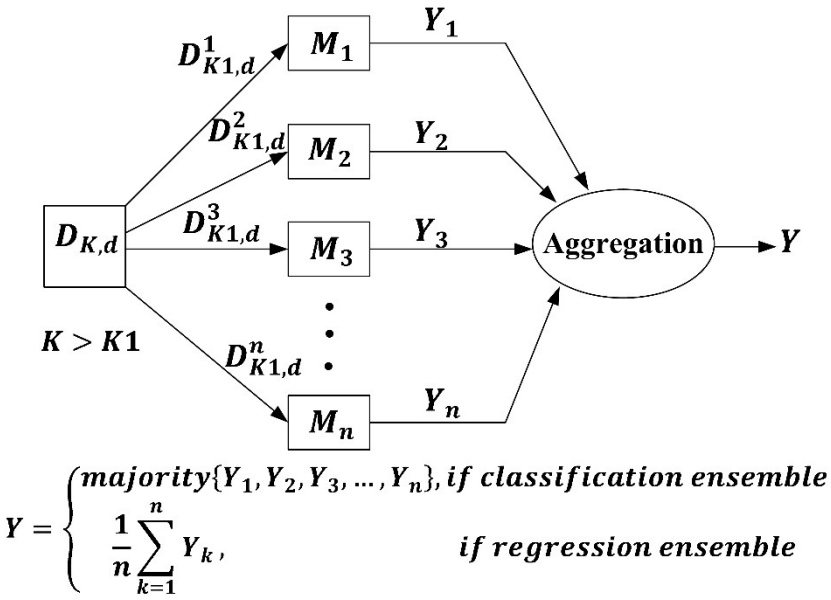

Fig. 4.8 Pictorial representation of bagged ensemble learner

In the proposed protection method, an ensemble of decision trees (regression) is implemented. Decision trees are one of the paradigms of data mining that are based on non-parametric supervised learning algorithms and are capable of effectively predicting input feature and output target relationships. The fundamental principle of growing decision trees is to *'divide and conquer'* the training data by recursively splitting/partitioning the data optimally using *'if-then'* conditions until the desired stopping criterion is reached. Impurity based calculations are employed for optimal splitting of the data to get a pure node in classification trees whereas minimum mean squared error of prediction is used to define the purity of split in regression trees. A pictorial representation of the decision tree growing is shown in Fig. 4.9 where the training data *D* contains features/attributes $(f_1, f_2, \dots, f_d)$ with *N* no. of instances, *Y* is the target data, and *S* is the potential splits obtained from *D*. The optimal splits and optimal features are derived from impurity-based calculations through the minimization of mean squared error of prediction. The process of splitting the data is

continued until the pure nodes are attained or the maximum depth of the tree is reached [13, 14, 126]. In Fig. 4.9, the pure node is represented with a circle and the impure node is represented with a rectangle.

$$D = \begin{bmatrix} f_1 & f_2 & . & . & f_d \\ & & a_{ij} & & \\ & & i = 1\ to\ N & & \\ & & j = 1\ to\ d & & \end{bmatrix} \quad Y = \begin{bmatrix} y_1 \\ y_2 \\ . \\ . \\ y_N \end{bmatrix} \quad S = \begin{bmatrix} S_1 & S_2 & . & . & S_d \\ & & s_{ij} & & \\ & & i = 1\ to\ N-1 & & \\ & & j = 1\ to\ d & & \end{bmatrix} \quad where\ S_j = \frac{a_{ij} + a_{(i+1)j}}{2}$$

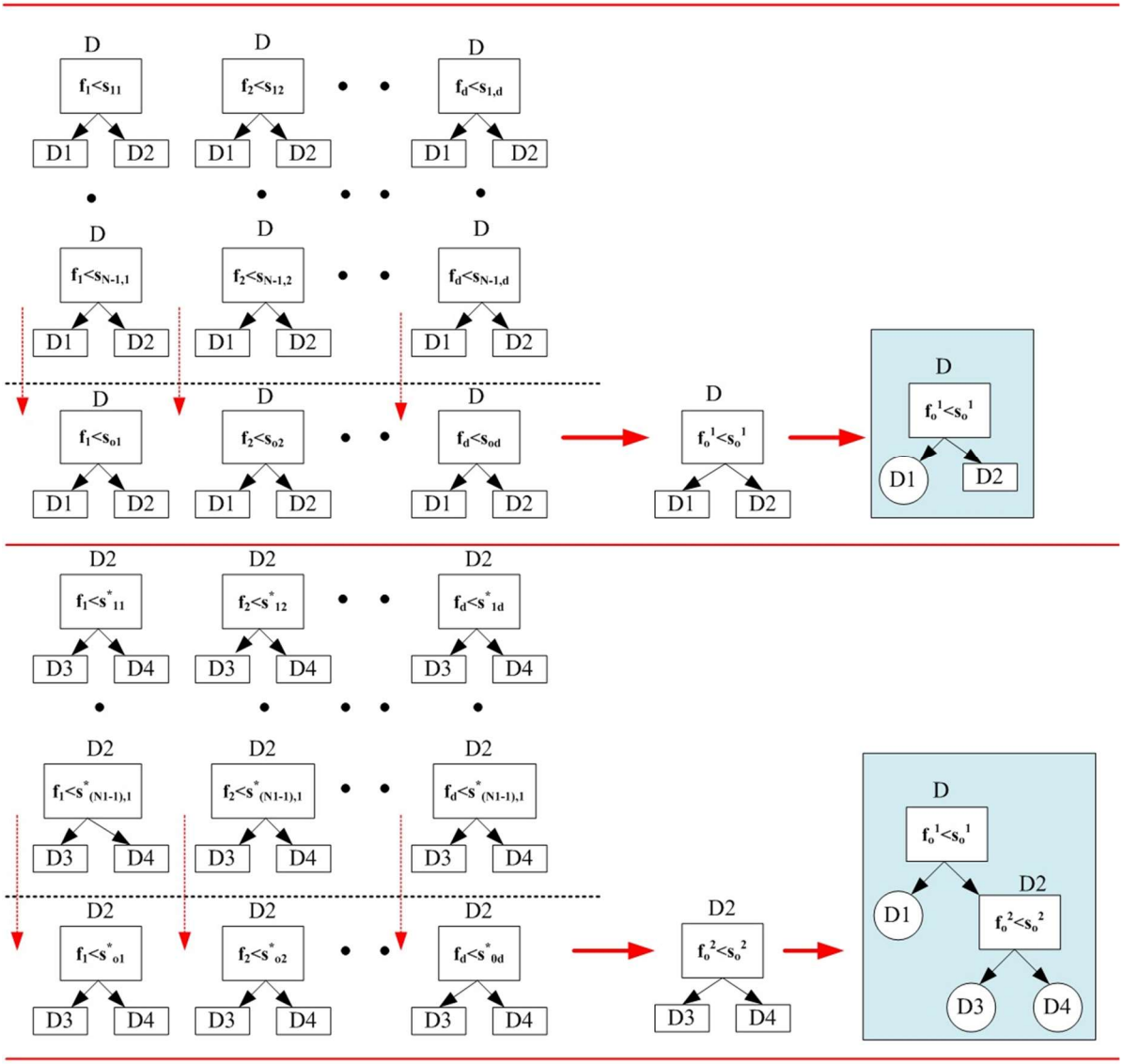

Fig. 4.9 Pictorial representation of decision tree growing

A bagged ensemble of 300 number of decision trees is implemented using the regression learner in MATLAB to estimate the location of the fault. An extensive number of fault simulations were conducted on the modelled system to generate the fault data for training the

bagged ensemble learner. A total of 3960 different fault cases were simulated considering the variations in different fault parameters viz. fault resistance, fault inception angle, fault location, and different fault types. Table 4.2 presents the details of fault parameters considered to generate the training data set. The size of the training data set is 39630*4, where the first three columns represent the half-cycle moving minimum window of the inputs *{|V_a|, |V_b|, and |V_c|}* and the last column represents the actual fault location (target). In the training data set, the actual fault location of no-fault cases is labelled as 400 km. The half-cycle post fault data (10 samples) is collected to construct the training data set. The bagged ensemble learner with different number of trees and minimum leaf sizes are trained on the generated data set through a series of pilot runs. The bagged ensemble learner with 300 number of trees and a minimum leaf size of one is found to be feasible. The estimated fault location (*EFL*) is derived from the minimum, maximum, and mean of the estimated location (L_e). Whenever a fault is detected (i.e. L_e < 400 km), then one cycle data of L_e is collected and the *EFL* is evaluated depending on the conditions given in Eq. (4.2) using the one cycle data. The training process took a time of 93.12 s to train the bagged ensemble model with the prediction metrics: root mean squared error of 0.996, mean squared error of 0.991 and mean absolute error of 0.719. All the simulations of the present work are carried out on the Intel® Core(TM) i5-10210U CPU @ 2.11 GHz processor with 8 GB RAM Windows 11 operating system. Fig. 4.10 presents the flowchart of the complete scheme of the suggested protection method and its block diagram is shown in Fig. 4.1.

Table 4.2 Fault parameters considered in the training data set

S. No.	Fault parameter	Variations
1.	Fault resistance (Ω)	0.01 Ω, 50 Ω, and 100 Ω (3 no.)
2.	Fault inception angle (°)	0° and 90° (2 no.)
3.	Fault location (km)	3 km, 6 km, 9 km, …, 194 km, and 197 km (66 no.)
4.	Fault types	10 (ABC, AB, BC, CA, ABG, BCG, CAG, AG, BG, and CG)
Therefore, total no. of fault cases considered = 3*2*66*10= 3960 and 3 - no fault case		

$$EFL = \begin{cases} Min(L_e), & if\ Min(L_e) \le 20\%(L_T)\ and\ Mean(L_e) \le 55\%(L_T) \\ Max(L_e), & if\ Min(L_e) > 20\%(L_T)\ and\ Mean(L_e) > 55\%(L_T) \\ Max(L_e) - Mean(L_e) + Min(L_e), & if\ Min(L_e) < 20\%(L_T)\ and\ Mean(L_e) > 55\%(L_T) \\ Max(L_e) - Mean(L_e) - Min(L_e), & if\ Min(L_e) > 20\%(L_T)\ and\ Mean(L_e) < 55\%(L_T) \end{cases} \quad (4.2)$$

Here, L_T, L_e, and EFL are the total length of the transmission line, estimated location, and estimated fault location in km respectively.

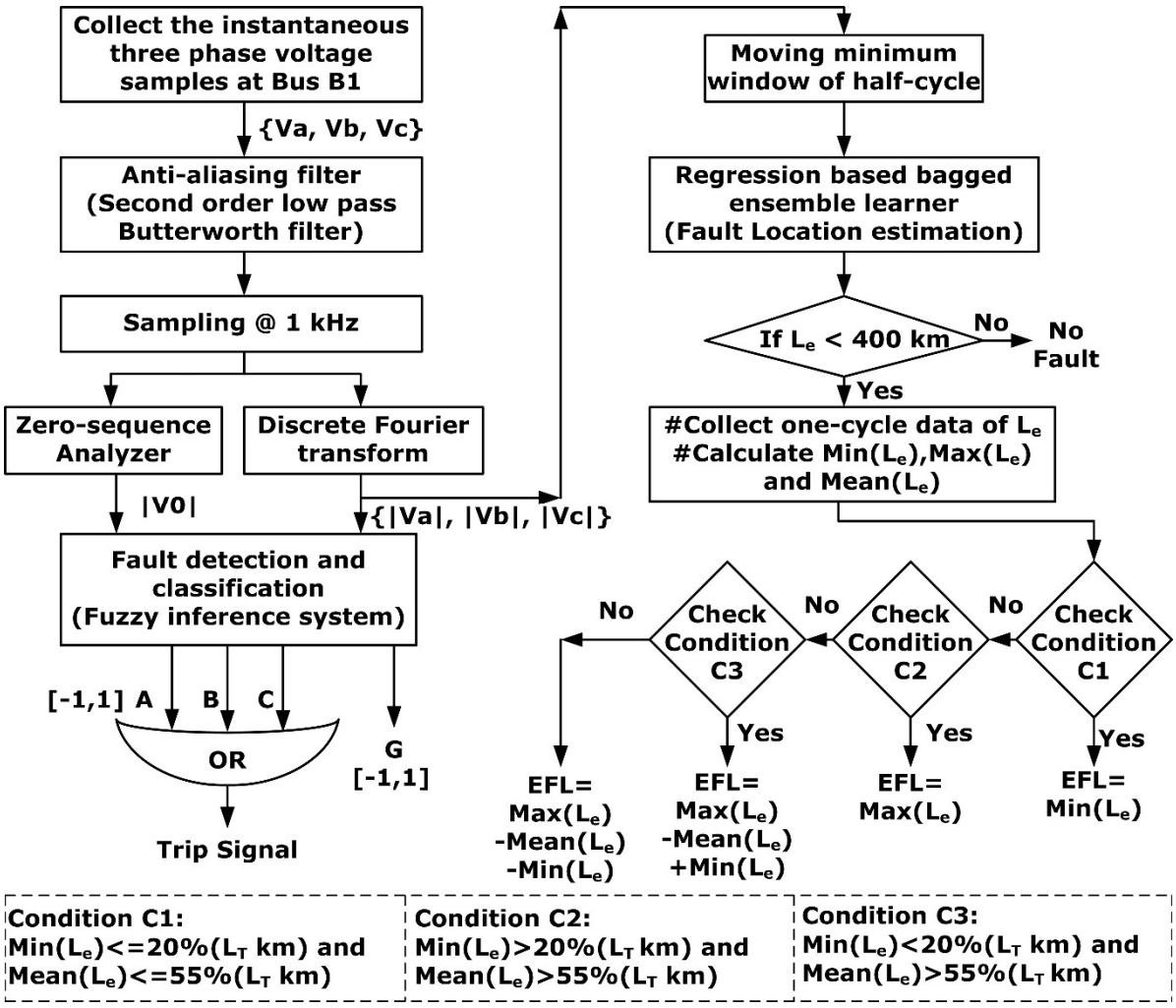

Fig. 4.10 Flowchart of the complete scheme of protection with FIS and bagged ensemble learning approach

4.4 Results and Discussion

The performance of the proposed scheme of protection is discussed in this section by carrying out extensive fault simulations on the simulated power system model. The suggested protection method utilizes FIS for the detection/classification of the fault and a regression based bagged ensemble approach for fault location estimation. The protection scheme's efficacy is evaluated for ten different types of short circuit faults simulated on the transmission line by varying different fault parameters (fault resistance, R_f (0 – 100 Ω), fault inception

angle, ϕ, (0° – 360°), and fault location, L_f (1 – 200 km)) with different solar irradiance and wind speed levels.

4.4.1 Performance Evaluation of FIS Module for Detection and Classification of Faults

Short circuit faults are stochastic in nature and can occur at location on any phase(s) of the transmission line. To evaluate the performance of the FIS based protection module different short circuit faults are simulated. An LG fault (AG) with fault resistance $R_f = 50\ \Omega$ and fault inception angle $\phi = 0°$ (time of fault, $T_f = 0.2$ s) is simulated at a fault location of 50 km from the bus B1 with solar irradiance of 1000 W/m^2 and wind speed of 15 m/s. The three-phase voltage, current, power, and magnitude of voltage features $\{|V_a|, |V_b|, |V_c|, and\ |V_0|\}$ measured at bus B1 are depicted in Fig. 4.11 for the above-mentioned fault.

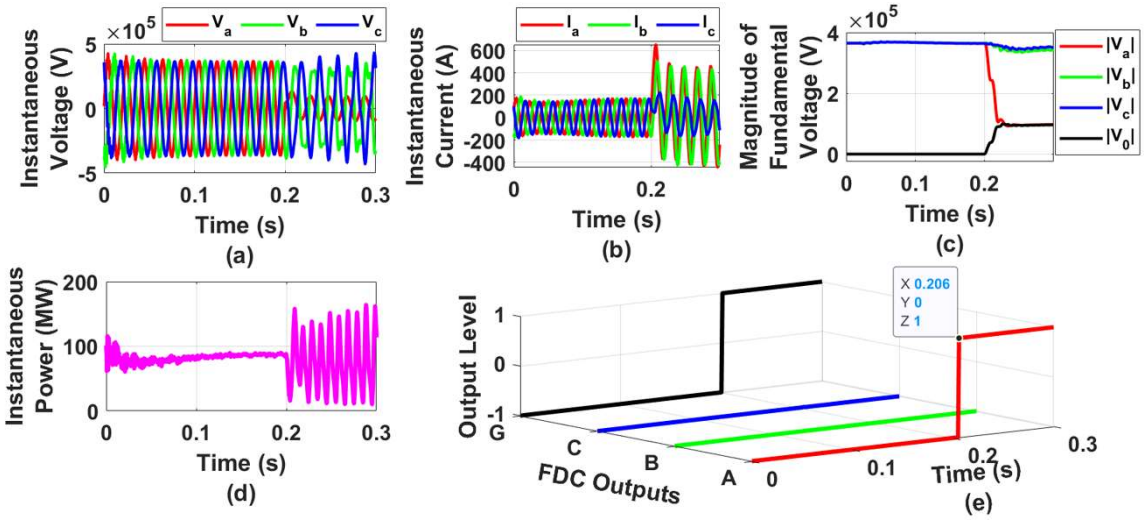

Fig. 4.11 AG fault with $R_f = 50\ \Omega$, $\phi = 0°$ ($T_f = 0.2$ s), $L_f = 50$ km, solar irradiance = 1000 W/m^2, and wind speed = 15 m/s. **(a)** and **(b)** Voltage and current waveforms at bus B1, **(c)** Voltage magnitudes of fundamental component and zero-sequence component, **(d)** Three phase power from renewables, and **(e)** FDC outputs

Fig. 4.11 (e) presents the FIS based protection module outputs *{A, B, C, G}* representing the fault detection and classification (FDC). From the FIS outputs, it can be observed that until 0.2 s the output level of all the output labels is *"-1"* (healthy condition) and after the occurrence of the AG fault at 0.2 s the output level of outputs *A* and *G* is *"+1"* (faulty condition) at 0.206 s indicates the instant of fault detection and its type. Hence, the proposed

protection scheme clearly identifies the fault type and its occurrence with the FDC time as 6 ms (FDC time = 0.206 ms – 0.2 ms = 6 ms) i.e. less than one cycle time (20 ms). Further, the performance of the proposed scheme is evaluated for different fault types with solar irradiance of 1000 W/m^2 and wind speed of 15 m/s for variations in fault resistance (Table 4.3), fault inception angle (Table 4.4), and fault location (Table 4.5). The L_f = 50 km and ϕ = 0° are kept constant in Table 4.3, the R_f = 50 Ω and L_f = 105 km are kept constant in Table 4.4, and the R_f = 20 Ω and ϕ = 0° are kept constant in Table 4.5 for the tabulated results.

Table 4.3 Performance results of the proposed FIS protection module for varying fault resistance

Solar irradiance = 1000 W/m^2 and wind speed =15 m/s							**L_f = 50 km and ϕ = 0° (T_f = 0.2 s)**			
S. No.	**Fault type**	**R_f (Ω)**	**FIS based FDC outputs**				**FDC time (ms)**			
			A	***B***	***C***	***G***	***A***	***B***	***C***	***G***
1.	AG	0.01 Ω	1	-1	-1	1	5 ms	-	-	1 ms
2.	BG	50 Ω	-1	1	-1	1	-	3 ms	-	1 ms
3.	ABG	50 Ω	1	1	-1	1	5 ms	3 ms	-	1 ms
4.	BCG	100 Ω	-1	1	1	1	-	3 ms	8 ms	1 ms
5.	AB	5 Ω	1	1	-1	-1	6 ms	4 ms	-	-
6.	ABC	10 Ω	1	1	1	-1	6 ms	3 ms	8 ms	-

Table 4.4 Performance results of the proposed FIS protection module for varying fault inception angle (FIA)

Solar irradiance = 1000 W/m^2 and wind speed =15 m/s							**R_f = 50 Ω and L_f = 105 km**			
S. No.	**Fault type**	**FIA (ϕ°) (T_f (s))**	**FIS based FDC outputs**				**FDC time (ms)**			
			A	***B***	***C***	***G***	***A***	***B***	***C***	***G***
1.	AG	0° (0.2 s)	1	-1	-1	1	6 ms	-	-	2 ms
2.	ABG	45° (0.2025 s)	1	1	-1	1	3.5 ms	8.5 ms	-	2.5 ms
3.	AB	90° (0.205 s)	1	1	-1	-1	10 ms	8 ms	-	-
4.	ABC	180° (0.21 s)	1	1	1	-1	6 ms	3 ms	8 ms	-
5.	BCG	270° (0.215 s)	-1	1	1	-1	-	8 ms	4 ms	1 ms

Table 4.5 Performance results of the proposed FIS protection module for varying fault location

Solar irradiance = 1000 W/m^2 and wind speed =15 m/s			**R_f = 20 Ω and ϕ = 0° (T_f = 0.2 s)**							
S. No.	**Fault type**	**L_f (km)**	**FIS based FDC outputs**				**FDC time (ms)**			
			A	***B***	***C***	***G***	***A***	***B***	***C***	***G***
1.	CG	5 km	-1	-1	1	1	-	-	7 ms	1 ms
2.	ABG	50 km	1	1	-1	1	6 ms	3 ms	-	1 ms
3.	ABC	100 km	1	1	1	-1	6 ms	3 ms	8 ms	-
4.	BC	150 km	-1	1	1	-1	-	4 ms	9 ms	-
5.	AG	197 km	1	-1	-1	1	5 ms	-	-	2 ms

Further, the performance of the proposed FIS protection module is evaluated for faults with different solar irradiance and wind speed levels. Fig. 4.12 depicts the results of the proposed scheme for the LLG fault (ABG) with the following parameters: L_f = 90 km, R_f = 80 Ω, T_f = 0.5 s (ϕ = 0°), solar irradiance = 500 W/m^2, and wind speed = 8 m/s. From Fig. 4.12 (d), it can be observed that the ABG fault is detected and classified within 7 ms after the inception of the fault. Similarly, Fig. 4.13 depicts the results of the proposed scheme for the LLL fault (ABC) with the following parameters: L_f = 150 km, R_f = 30 Ω, T_f = 0.5 s (ϕ = 0°), solar irradiance = 1200 W/m^2, and wind speed = 20 m/s. The ABC fault is identified in 8 ms after the inception of the fault.

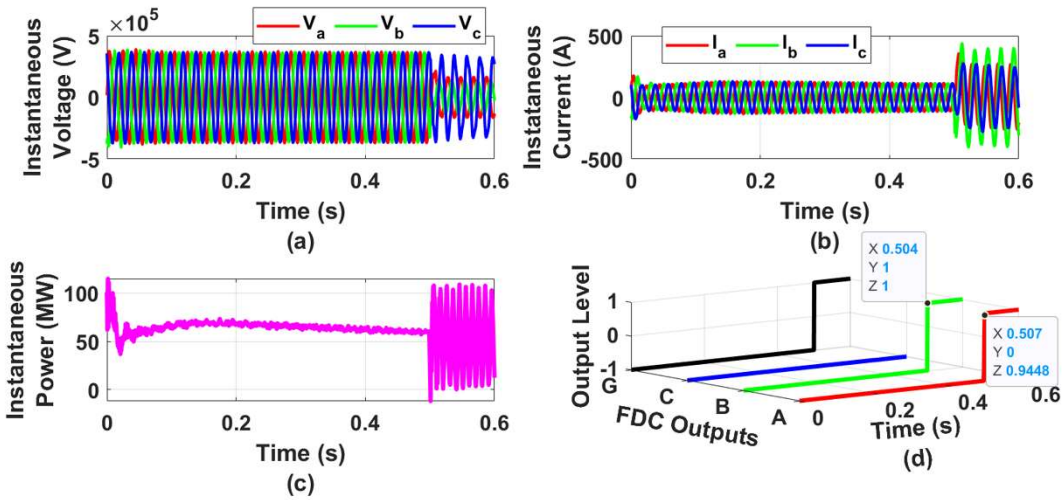

Fig. 4.12 ABG fault with R_f = 80 Ω, ϕ = 0° (T_f = 0.5 s), L_f = 90 km, solar irradiance = 500

W/m^2, and wind speed = 8 m/s. **(a)** and **(b)** Voltage and current waveforms at bus B1, **(c)** Three phase power from renewables, and **(d)** FIS based FDC outputs

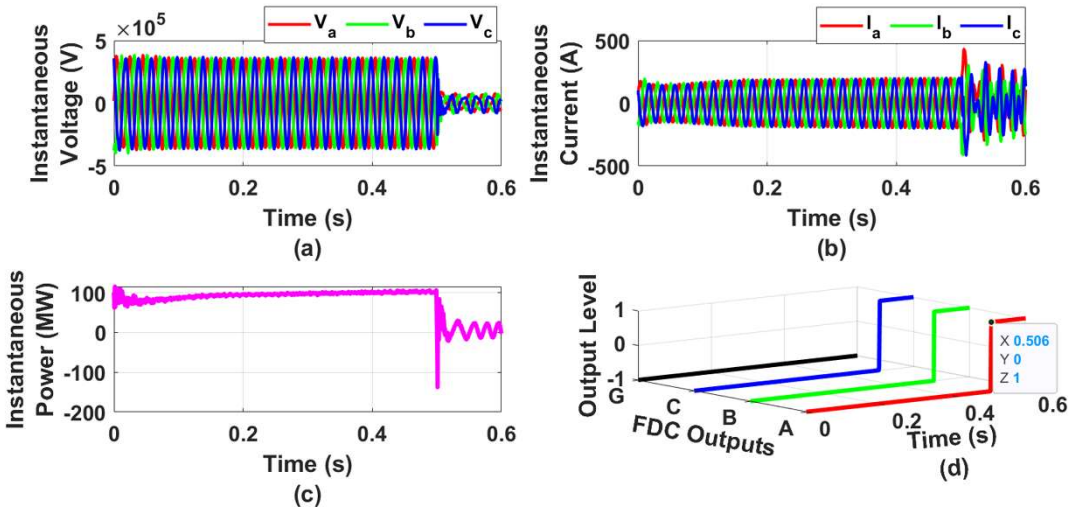

Fig. 4.13 ABC fault with R_f = 30 Ω, ϕ = 0° (T_f = 0.5 s), L_f = 150 km, solar irradiance = 1200 W/m^2, and wind speed = 20 m/s. **(a)** and **(b)** Voltage and current waveforms at bus B1, **(c)** Three phase power from renewables, and **(d)** FDC outputs

Table 4.6 Performance results of the proposed FIS protection module for varying fault parameters (solar irradiance = 500 W/m^2 and wind speed = 8 m/s)

Solar irradiance = 500 W/m^2 and wind speed = 8 m/s											
S. No.	**Fault type**	***L_f* (km)**	***R_f* (Ω)**	**FIA (ϕ°) (T_f (s))**	**FIS based FDC outputs**				**FDC time (ms)**			
					A	***B***	***C***	***G***	***A***	***B***	***C***	***G***
1.	AG	50 km	50 Ω	0° (0.5 s)	1	-1	-1	1	6 ms	-	-	1 ms
2.	ABG	90 km	80 Ω	0° (0.5 s)	1	1	-1	1	7 ms	4 ms	-	1 ms
3.	AB	130 km	15 Ω	90° (0.505 s)	1	1	-1	-1	10 ms	8 ms	-	-
4.	ABC	180 km	10 Ω	180° (0.51 s)	1	1	1	-1	6 ms	3 ms	8 ms	-
5.	BG	10 km	100 Ω	270° (0.515 s)	-1	1	-1	1	-	8 ms	-	1 ms
6.	BCG	190 km	100 Ω	360° (0.52 s)	-1	1	1	1	-	2 ms	9 ms	1 ms

Table 4.6 and Table 4.7 showcase the performance of the proposed method under varying fault conditions. Table 4.6 presents results for solar irradiance of 500 W/m² and wind speed of 8 m/s, while Table 4.7 focuses on solar irradiance of 1200 W/m² and wind speed of 20 m/s.

Both tables explore the impact of different fault types and variations in fault parameters. The results presented showcase the effectiveness of the proposed FIS protection module even under different operating conditions of the RES for varying transmission line fault conditions.

Table 4.7 Performance results of the proposed FIS protection module for varying fault parameters (solar irradiance = 1200 W/m^2 and wind speed = 20 m/s)

Solar irradiance = 1200 W/m^2 and wind speed = 20 m/s												
S. No.	**Fault type**	**L_f (km)**	**R_f (Ω)**	**FIA (ϕ°) (T_f (s))**	**FIS based FDC outputs**				**FDC time (ms)**			
					A	***B***	***C***	***G***	***A***	***B***	***C***	***G***
1.	ABC	150 km	30 Ω	0° (0.5 s)	1	1	1	-1	6 ms	3 ms	8 ms	-
2.	CAG	70 km	70 Ω	0° (0.5 s)	1	-1	1	1	6 ms	-	8 ms	1 ms
3.	CG	25 km	55 Ω	90° (0.505 s)	-1	-1	1	1	-	-	4 ms	1 ms
4.	BC	160 km	25 Ω	180° (0.51 s)	-1	1	1	-1	-	2 ms	7 ms	-
5.	ABG	197 km	100 Ω	270° (0.515 s)	1	1	-1	1	9 ms	9 ms	-	2 ms
6.	AG	3 km	0.01 Ω	360° (0.52 s)	1	-1	-1	1	3 ms	-	-	1 ms

Further, the reliable operation of the proposed scheme of protection is assessed in terms of accuracy and dependability with the help of a confusion matrix. The accuracy and dependability are calculated using Eq. (4.3) and Eq. (4.4). The confusion matrix is developed for the fault cases that are described in Table 4.2 (3963 fault cases) and Table 4.10 (2400 fault cases). The number of true and detected fault cases are segregated into LG, LLG, LL, LLL, and NF fault types depicted in Table 4.8 are listed in the confusion matrix. The three no-fault cases (NF) are the different operating conditions of RES with no fault on the transmission line. The accuracy and dependability of the proposed scheme are found to be 99.56% given in Table 4.9.

$$Accuracy = \frac{total\ no.of\ cases\ detected\ correctly}{total\ no.of\ fault\ and\ no\ fault\ cases} \times 100 \tag{4.3}$$

$$Dependability = \frac{total\ no.of\ fault\ cases\ detected\ correctly}{total\ no.of\ actual\ fault\ cases} \times 100 \tag{4.4}$$

Table 4.8 Confusion matrix for FDC

		Detected faults					
		LG	**LLG**	**LL**	**LLL**	**NF**	**Total**
True faults	**LG**	1908	-	-	-	-	1908
	LLG	-	1880	-	28	-	1908
	LL	-	-	1908	-	-	1908
	LLL	-	-	-	636	-	636
	NF	-	-	-	-	3	3
Total no. of fault cases = 6363							

Table 4.9 Performance index of FIS based protection module

S. No.	Performance index
1.	Accuracy = $\frac{6335}{6363} \times 100 = 99.56\%$
2.	Dependability = $\frac{6332}{6360} \times 100 = 99.56\%$

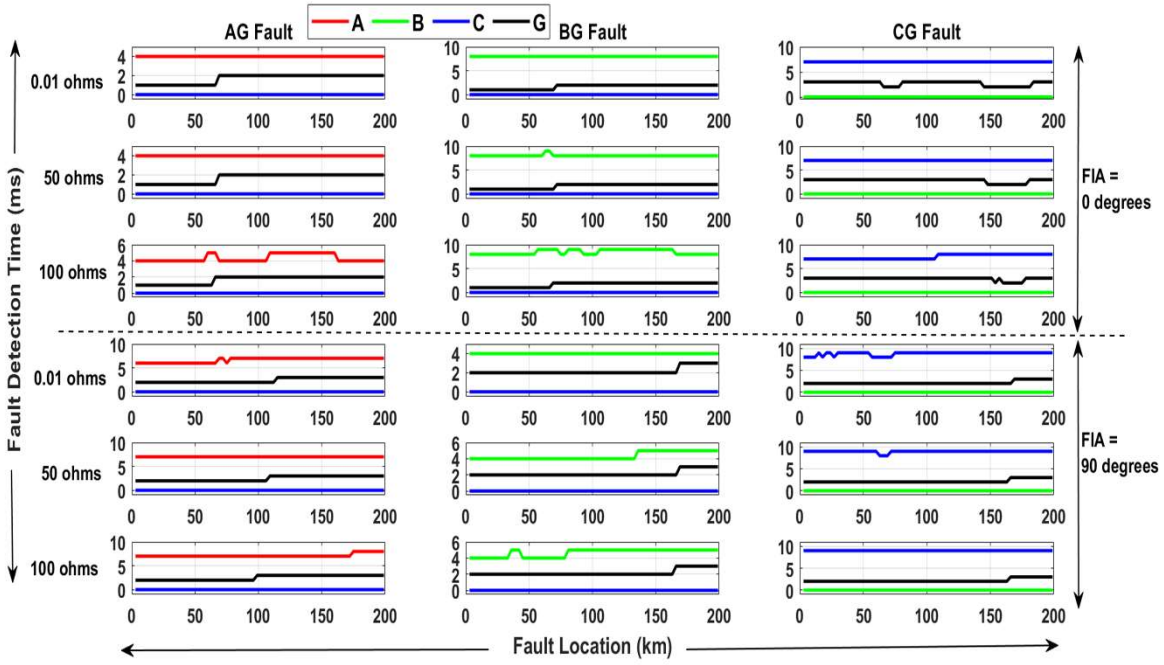

Fig. 4.14 Fault detection time of the proposed protection module with FIS for LG fault cases of Table 4.2

The response or fault detection time of the proposed FIS based protection module for different LG fault cases that are detailed in Table 4.2 is shown in Fig. 4.14. The x-axis represents the variation in fault location and the y-axis denotes fault detection time. The fault inception angle for the first and last three rows of figures are 0° and 90° respectively. The fault resistance is 0.01 Ω (for 1st and 4th rows), 50 Ω (for 2nd and 5th), and 100 Ω (for 3rd and 6th rows). From Fig. 4.14, it can be observed that the different LG fault cases (AG faults in column-1, BG faults in column-2, and CG faults in column-3) are detected within half-cycle time. The fault detection time is also evaluated for the other fault cases in Table 4.2 and Table 4.10. It is noticed that the fault detection time is well within half-cycle time for all the LG, LLG, and LLL fault cases and one-cycle time for LL fault cases. The accuracy achieved and fault detection time of one-cycle time demonstrates the reliable operation of the proposed FIS protection module.

4.4.2 Performance Evaluation of Regression Tree Based Bagged Ensemble Learning Module for Fault Location Estimation

The effectiveness of the proposed fault location module is assessed for diverse fault cases considering varying fault locations using the percentage error metric defined in Eq. (4.5). This metric is the percentage error in estimated fault location that compares the estimated fault location *(EFL)* with the actual fault location (*AFL)*, normalized by the total line length *(L_T)*.

$$\%\ Error\ in\ the\ estimated\ fault\ location\ (\%E) = \frac{EFL - AFL}{L_T} \times 100 \tag{4.5}$$

An LG fault (AG) with R_f = 0.01 Ω and ϕ = 0° is simulated at 9 km *(AFL)* from bus B1. Fig. 4.15 presents the output *(L_e)* of regression based bagged ensemble learner towards the fault location estimation. When the system is healthy, the proposed bagged ensemble fault locator outputs 400 km. In case of a faulty condition, the proposed fault location module estimates fault location close to *AFL* i.e. 8.551 km with a -0.2245% error in the *EFL.* Similarly, Fig. 4.16 and Fig. 4.17 depict the outputs of the fault location module for the LLG fault (ABG fault with R_f = 90 Ω and ϕ = 0°) and a triple line fault (ABC fault with R_f = 0.01 Ω and ϕ = 0°) simulated at 104 km *(AFL)* and 196 km *(AFL)* respectively. The *EFL* is found to be 108.13 km (*%E* = 2.065%) for the ABG fault and 193.10 km (*%E* = -1.45%) for the ABC fault with the proposed method of location estimation. In all the above-mentioned fault cases (AG, ABG, and ABC), the solar irradiance = 1000 W/m^2 and wind speed = 15 m/s.

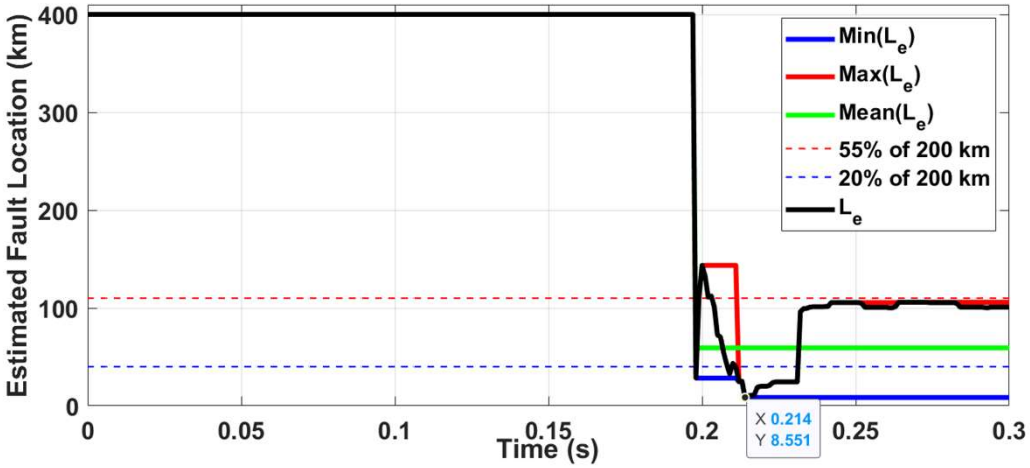

Fig. 4.15 Estimated fault location for AG fault with R_f = 0.01 Ω, ϕ = 0° and AFL = 9 km

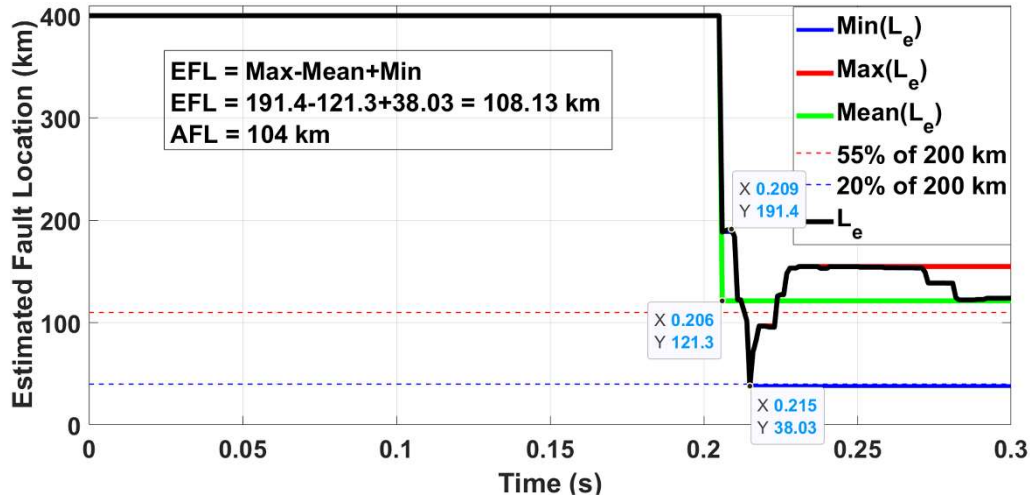

Fig. 4.16 Estimated fault location for ABG fault with R_f = 90 Ω, ϕ = 0° and AFL = 104 km

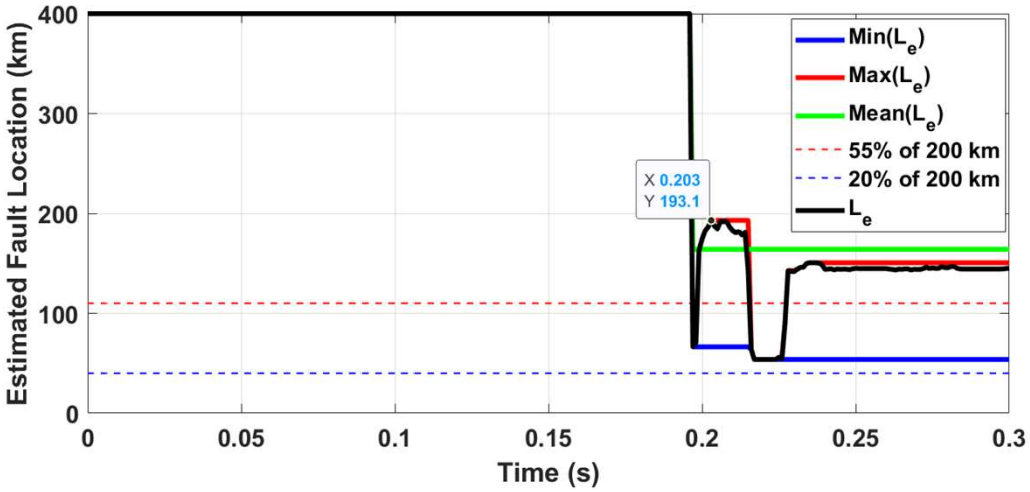

Fig. 4.17 Estimated fault location for ABC fault with R_f = 0.01 Ω, ϕ = 0° and AFL = 196 km

To assess the effectiveness of the proposed fault location module, a testing data set is created by simulating different types of faults and Table 4.10 gives the details of fault parameters considered that counts for 2400 different fault cases. Fig. 4.18 presents the scatter plot of percentage error in the estimated fault location for different faults mentioned in Table 4.10. It is noticed that the *%E* lies in the band of +/-5% with the proposed method. Table 4.11 presents the results of the estimated fault location for different faults. Further, to assess the reliability of the fault location module, the Chi-square error analysis is performed on 400 *EFL* errors that are obtained by randomly simulating the faults at different locations along the transmission line. Table 4.12 presents the Chi-square test for reliability analysis of the proposed fault location estimation method. The low difference between the observed and expected number of errors showcases the efficacy of the proposed method and the Chi-square value (D^2) falls in the 5% band of significance level [127].

Table 4.10 Fault parameters considered in the testing data set

S. No.	Fault parameter	Variations
1.	Fault resistance (Ω)	30 Ω, 60 Ω, and 90 Ω (3 no.)
2.	Fault inception angle (°)	45° and 180° (2 no.)
3.	Fault location (km)	5 km, 10 km, 15 km, …, 190 km, and 195 km (40 no.)
4.	Fault types	10 (ABC, AB, BC, CA, ABG, BCG, CAG, AG, BG, and CG)

Therefore, the total no. of fault cases considered = 3*2*40*10= 2400

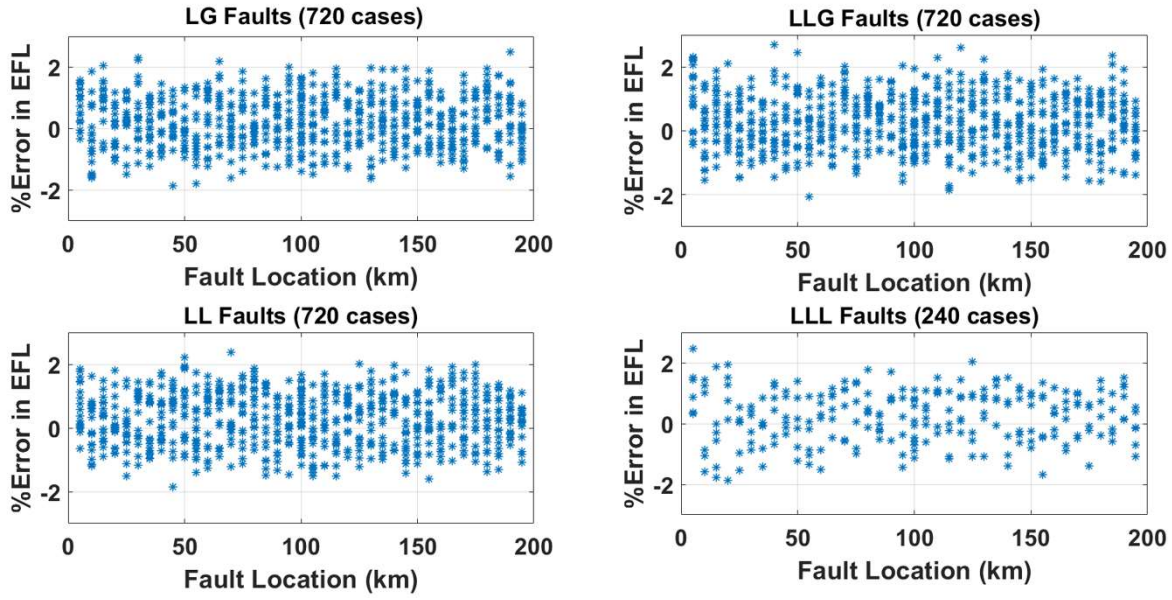

Fig. 4.18 Percentage error in estimated fault location for all fault cases of Table 4.10

Table 4.11 Performance of the proposed bagged ensemble learner module for different faults

S. No.	Fault type	*AFL* (km)	R_f (Ω)	FIA (ϕ°)	*EFL* (km)	% Error
1.	AG	5 km	50 Ω	0°	5.38 km	0.19%
2.	ABG	70 km	0.01 Ω	0°	71.74 km	0.87%
3.	AB	120 km	20 Ω	0°	116.45 km	-1.76%
4.	ABC	190 km	0.01 Ω	0°	191.27 km	0.64%
5.	BG	50 km	60 Ω	90°	45.66 km	-2.17%
6.	BCG	100 km	100 Ω	90°	99.31 km	-0.35%
7.	BC	150 km	10 Ω	90°	144.73 km	-2.64%
8.	ABC	30 km	15 Ω	90°	30.87 km	0.44%
9.	CG	130 km	100 Ω	270°	127.65 km	-1.18%
10	CAG	80 km	90 Ω	270°	79.48 km	-0.26%
11.	CA	195 km	25 Ω	270°	193.19 km	-0.91%
12.	ABC	197 km	10 Ω	270°	193.35 km	-1.825%

Table 4.12 Chi-square test for fault location estimation reliability analysis

Interval number *(i)*	% Error interval	No. of observed errors (N_{oi})	No. of expected errors (N_{ei})	$\frac{(N_{oi}-N_{ei})^2}{N_{ei}}$
1	-4.5 to -3.5	7	5	0.8
2	-3.5 to -2.5	22	19	0.4737
3	-2.5 to -1.5	39	46	1.0652
4	-1.5 to -0.5	78	82	0.1951
5	-0.5 to 0.5	104	101	0.0891
6	0.5 to 1.5	86	83	0.1084
7	1.5 to 2.5	44	46	0.087
8	2.5 to 3.5	20	18	0.2222

$$D^2 = \sum_{i=1}^{8} \frac{(N_{oi} - N_{ei})^2}{N_{ei}} = 3.0407$$

4.4.3 Comparison of the Proposed Protection Scheme

A comparison of the proposed scheme of protection is discussed in this section in terms of protection and feature extraction techniques, protection tasks implemented, type of RES integrated, and FDC accuracy. Table 4.13 provides a comparison of different protection schemes with the proposed method. All the protection methods mentioned in Table 4.13 are training-based artificial intelligent methods for the detection and classification of faults except the proposed one. The training-based methods require large sets of training data considering different operating conditions to train the models for achieving high performance and accuracy of the trained models in the protection tasks. The proposed scheme is implemented with the fuzzy inference concept for fault detection and classification that do not require any training of the module. Further, the FDC accuracy is comparably high with other training-based techniques.

Table 4.13 Comparison with other protection schemes

Comparison term	**Reference**						
	[63]	[64]	[128]	[129]	[130]	[131]	Proposed
Protection technique based on	SVM	ANN	SVM and GPR	Rotation forest	Decision tree and SVM	Random forest	FIS and regression based bagged ensemble learner
Signal pre-processing or features utilized	Transient motoring index of currents	MODWT; energy of detail coefficients of voltage and current	RMS of voltages and currents	DWT; standard deviation of approximate coefficients of voltage and current	DFT; amplitude and phase angle of voltage and current phasors	Positive sequence currents and empirical mode decompositi on of grid side currents	DFT; magnitudes zero-sequence and fundamental components of phase voltages
Protection tasks	FDC	FD of symmetrical faults only	FDC and FLE	FDC	FDC and FLE	FDC and FLE	FDC and FLE
FDC accuracy	99.84%	98.40%	99.50%	99.43%	97.9%	99.95%	99.56%
FDC time	10 ms	-	20 ms	16.67 ms	-	8 ms	20 ms
PV and/or wind power integration	Wind power	Wind power	- (DGs)	PV and wind power	Wind power	Wind power	PV and wind power

FD: Fault detection, FDC: Fault detection and classification, and FLE: Fault location estimation

4.5 Summary

In this chapter, an FIS based protection module for the detection/classification of short circuit faults and a bagged ensemble learning approach with regression trees for approximating actual fault location has been proposed for the transmission line connected to RES (solar PV and DFIG based wind power). The proposed protection modules utilize only the DFT processed three-phase voltage information of a single bus (i.e. connected to RES). Hence, the communication link is not required and there is no communication latency. The proposed FIS based protection module effectively detects the fault occurrence and classifies the different short circuit fault types within one cycle time (20 ms) following the fault inception even for varying fault parameters under different operating conditions of RES. This showcases that the proposed detection/classification scheme is passive/robust to fault parameter variations and RES power intermittences. The performance index indicates the efficacy of the FDC scheme with an accuracy of 99.56% calculated with the help of a confusion matrix. The proposed fault location module with the bagged ensemble of regression trees successfully predicts the actual fault location with minimal error. The percentage error in the estimated fault location is within ±5% error band even for various faults with varying fault parameters demonstrating the adaptability to diverse fault scenarios. Further, the reliability of the fault location estimation module is confirmed through the statistical analysis with the Chi-square test (D^2 = 3.0407) on location errors falling in the 5% band of the significance level. The proposed approach exemplifies the potential of combining fuzzy logic, ensemble learning, and signal processing techniques for developing intelligent protection systems adaptable to modern power grids.

*****

Chapter 5

Frequency Control of an Islanded Microgrid with Multi-stage PID Control Approach Using Moth Flame Optimization Algorithm

5.1 Introduction

The supply of power from traditional generating units to distant areas and islands is expensive, unreliable, and damaging to the environment under the current situation of contemporary power systems [132]. Under these circumstances, microgrids (MGs) offer reliable and cost-effective power solutions for supplying the required excess power demand to remote areas. Microgrid is a combination of diesel engine generators (DEGs), loads, renewable energy sources (RES), and various energy storage systems. An MG acts like a single controllable unit that contains a group of distributed energy sources to supply the excess demand from the different connected loads (residential, commercial, or small industrial loads). It could be regarded as a small-scale local grid with control capabilities at low voltage distribution levels [133].

In traditional power systems, the frequency regulation job is simple as the disturbance arises due to the stochastic loads only. But in an islanded MG; the frequency control problem is always a concerning challenge for the operators that account for some intrinsic attributes of the system viz. functional complexity, variable structure, and diversity in the generation. These attributes introduce rapidly changing operational points of the system [134]. Moreover, the rapid growth in the increased penetration levels of RES into MG will result in low inertia of the MG system. The low inertia of the MG system, stochastic loads, and intermittent/discontinuous generation of renewables will create complications in the frequency control of an islanded MG. Massive frequency deviations will cause stability and reliability problems and sometimes may lead to MG blackout. Although the PID controllers are simple in structure, reliable, and better at performance with fair cost, the classical PI/PID controllers fail to provide a satisfactory response for MG frequency control under these rapid changes in MG operating conditions [135]. Therefore, an intelligent and robust controller is required to regulate the frequency of an islanded MG.

The selection of appropriate optimal techniques for modifying the control parameters is crucial to improvise the MG's dynamic response. The use of an appropriate algorithm for optimizing the controller's parameters (gain constants) could enhance the system's response in terms of low overshoots, reduced error values and fast settling times. Therefore, in the present chapter, a newly developed and powerful moth flame optimization (MFO) algorithm is presented to optimize the multi-stage PID (MPID) controller gain constants. This chapter

investigates the frequency dynamics of an MG having DEG, PV (photovoltaic), WTG (wind turbine generator), and PHEVs (plug-in hybrid electric vehicles) operating in islanded mode. The coordinated control of DEG and PHEV with the MPID controller is studied using the MFO algorithm.

The key points of this chapter are listed below:

- The performance of differently tuned PID controllers (GOA, TLBO, PSO, and MFO) is demonstrated and compared through the MATLAB/Simulink simulation results to show the superiority and feasibility of the MFO algorithm over the other powerful and well-known meta-heuristic techniques.
- An MFO-tuned MPID controller has been proposed for mitigating the oscillations in the frequency dynamics of the modelled Bella Coola MG incorporating RES and PHEVs. The MFO algorithm is applied to optimize the MPID controller's gain constants.
- The MPID controller's robustness is evaluated by taking into consideration the simultaneous changes in RES, load dynamics, and MG and PHEV uncertainties in a single controller framework.
- The effect of PHEVs in the secondary and primary frequency control loops (SFC and PFC) of an islanded MG has been analyzed with RES and load disturbances to choose the better control action.

5.2 Details of Mathematical Model of Investigated MG

Fig. 5.1 shows the simplified form of the Bella Coola hybrid MG mathematical model under investigation. The present model comprises DEG, PHEV aggregator and RES (wind and solar power output) [136]. This study considers WTG and PV powers to be uncontrolled power sources (as disturbances). The advantages of using renewable energy are hindered, as frequency deviations limit the MPPT output power when they participate in frequency control. So, in this work, based on load changes and available PV/WTG powers, the diesel engine generator and PHEVs manage the power balance in the MG that is achieved through the suggested controller. Table 5.1 contains the parameters of the MG test system. From Fig. 5.1, the generation-load balance equation is:

$$\Delta P_{DEG} + \Delta P_{PHEV} + \Delta P_{WTG} + \Delta P_{PV} = \Delta P_L \tag{5.1}$$

The expression for deviation in the MG frequency (Δf) caused by the RES and load disturbances is given in Eq. (5.2) and B is the frequency bias factor ($B = D + 1/R$).

$$\Delta f = \frac{1}{Ms+D}(\Delta P_{DEG} + \Delta P_{WTG} + \Delta P_{PV} - \Delta P_{PHEV} - B\Delta f - \Delta P_L) \tag{5.2}$$

The proposed coordinated control's aim is to minimize the frequency deviations of MG under critical operating scenarios with the proposed MPID controller. In this work, only DEG and PHEVs are responsible for power balance. Therefore, the PV and WTG sources are modelled as disturbances in LFC analysis.

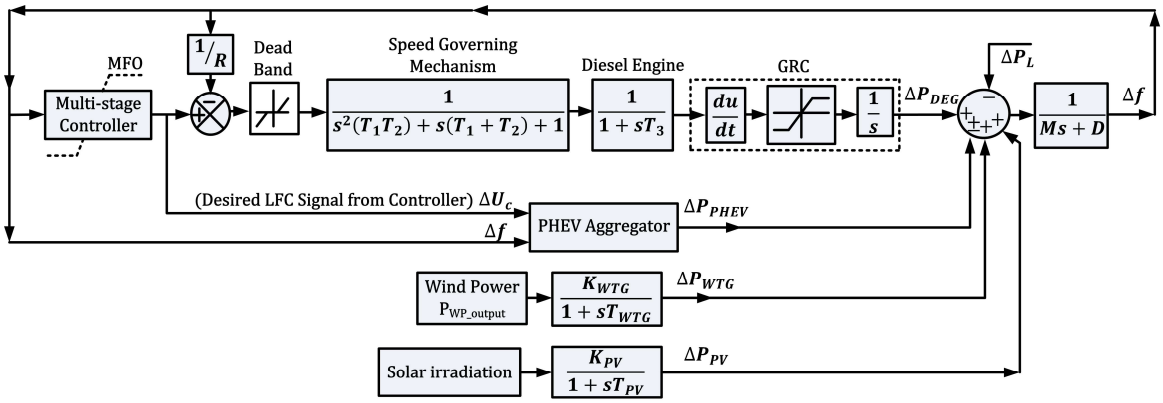

Fig. 5.1 MG mathematical model

Table 5.1 MG system parameters [85]

Parameter	Value	Parameter	Value	Parameter	Value
M (s)	0.1667	T_{PHEV} (s)	0.1	N_{EV}	600
D (puMW)	0.015	T_{WTG} (s)	2	R, R_{av} (Hz/puMW)	2.4
T_1 (s)	0.025	T_{PV} (s)	1.8	P_{max} (kW)	5
T_2 (s)	2	K_{WTG}	1	Δf_u (Hz)	0.1
T_3 (s)	3	K_{PV}	1	Δf_l (Hz)	0.1

5.2.1 DEG Model

Since the power generation from the solar PV and WTG systems is stochastic, DEG forms the best means of supplying reliable and quality power to the essential loads in a standalone

MG. A speed governing mechanism and diesel engine combination form the diesel engine generator system. The DEG mathematical model is given in Fig. 5.2 [137].

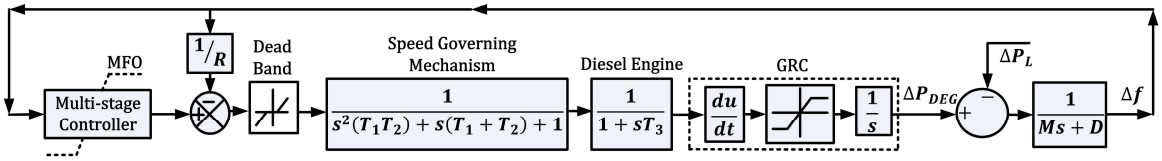

Fig. 5.2 DEG mathematical model

5.2.2 WTG Model

The mechanically produced output power of a WTG is highly inconsistent since it depends on the stochastic wind speeds and is given by:

$$P_{wp} = 0.5\rho A V_w^3 C_p(\beta, \lambda) \tag{5.3}$$

where,

P_{wp} = power output of windmill, ρ = air density (kg/m^3), V_w = speed of wind (m/s), A = rotor swept area (m^2), and C_p = power coefficient (function of tip speed ratio, λ and blade pitch angle, β (deg)). R = radius of the blade (m) and ω = angular velocity of the blade (rad/s). The C_p can be expressed as:

$$C_p(\beta, \lambda) = \left(\frac{25.52}{\gamma} - 1.1 - 0.088\beta\right) exp^{-125/\gamma} \tag{5.4}$$

$$\gamma = 1 \Big/ \left[\frac{1}{\lambda + 0.08\beta} - \frac{0.035}{1 + \beta^3}\right]$$

$$\lambda = \frac{R\omega}{V_w}$$

The WTG linear model can be represented as [138]:

$$TF_{WTG} = \frac{\Delta P_{WTG}}{P_{WP_{output}}} = \frac{K_{WTG}}{1 + ST_{WTG}} \tag{5.5}$$

Fig. 5.3 depicts the model for the generation of wind output power variations mathematically.

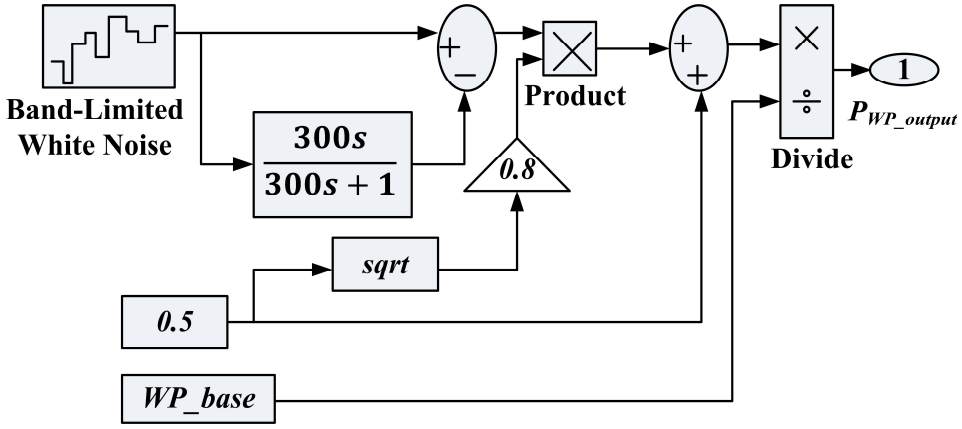

Fig. 5.3 Mathematical model for wind output power with random wind velocity pattern generation

5.2.3 PV Model

The extraction of electrical energy from photons takes place in the PV cells that are made from a semiconductor material. The possibility of the desired level of installation capability of PV sources is the key benefit of photovoltaics. The power generated from a PV source depends on the amount of solar irradiation and temperature. If 25°C ambient temperature is maintained then P_{PV} varies linearly with the irradiation constant (φ) only [138].

$$P_{PV} = P_{solar}\left(\frac{\varphi}{\varphi_{STC}}\right)(1 + K_t[T_a + 0.0256\varphi\Delta\varphi - T_{STC}]) \tag{5.6}$$

The ΔP_{PV} with respect to $\Delta\varphi$ can be computed using Eq. (5.7):

$$\Delta P_{PV} = \left(\frac{P_{solar}}{\varphi_{STC}}\right)(\Delta\varphi + K_t[\Delta\varphi T_a + \varphi\Delta T_a + 0.0512\varphi\Delta\varphi - T_{STC}\Delta\varphi]) \tag{5.7}$$

The PV system's first-order model can be represented as [139]:

$$TF_{PV} = \frac{\Delta P_{PV}}{\Delta\varphi} = \frac{K_{PV}}{1+sT_{PV}} \tag{5.8}$$

Fig. 5.4 depicts the mathematical model for PV output power with random solar irradiation pattern generation [83]. The power data used for the WTG power and PV power can be found in [139].

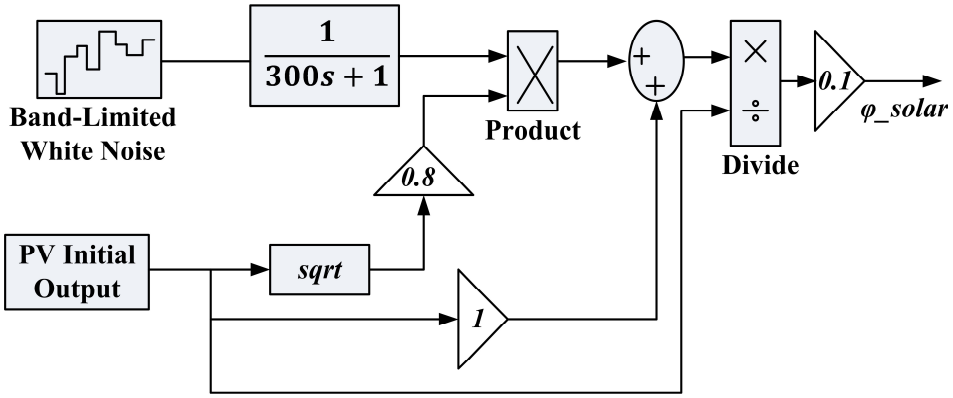

Fig. 5.4 Mathematical model for PV output power with random solar irradiation pattern generation

5.2.4 PHEV Model

Fig. 5.5 illustrates the PHEV aggregator's mathematical model for LFC studies. Due to their slow discharge rate, quick response time, and dispersed availability, PHEVs are a great energy storage alternative for LFC needs. The output power from the PHEV aggregator based on frequency deviation is as follows (ΔP_{PHEV}):

$$\Delta P_{PHEV,i} = \begin{cases} K_{EV,i}\Delta f; \ \left|K_{EV,i}\Delta f\right| \le P_{max} \\ P_{max}; \ K_{EV,i}\Delta f > P_{max} \\ -P_{max}; \ K_{EV,i}\Delta f < -P_{max} \end{cases} \tag{5.9}$$

$$\Delta P_{PHEV,AG} = N_{EV} * \Delta P_{PHEV,i} \tag{5.10}$$

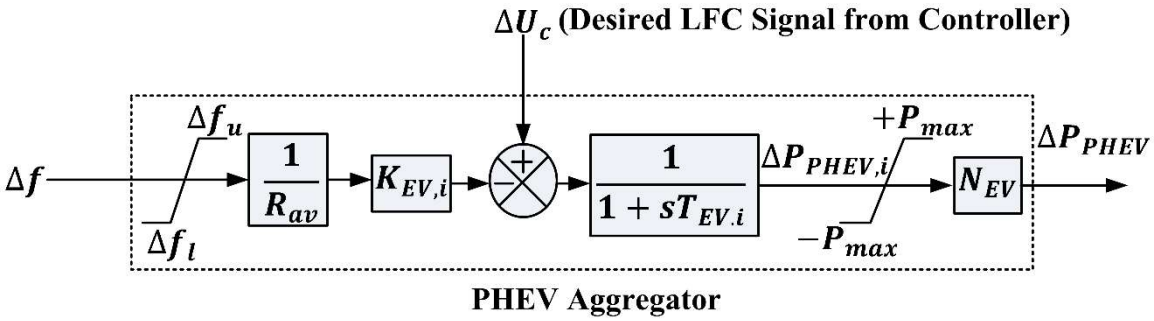

Fig. 5.5 PHEV aggregator model for frequency control studies

The controller's command signal (ΔU_c) is used to determine whether the ΔP_{PHEV} will be used for charging/discharging [140]. P_{max} is the maximum power available from an individual EV, $K_{EV,i}$ represents the single EV's participation gain. The battery's state of charge

(SOC) determines the value of $K_{EV,i}$. Fig. 5.6 shows the $K_{EV,i}$ vs SOC of PHEV [141]. N_{EV} denotes the number of EVs, R_{av} denotes the droop characteristics of the PHEV aggregator and $T_{EV,i}$ is the battery time constant.

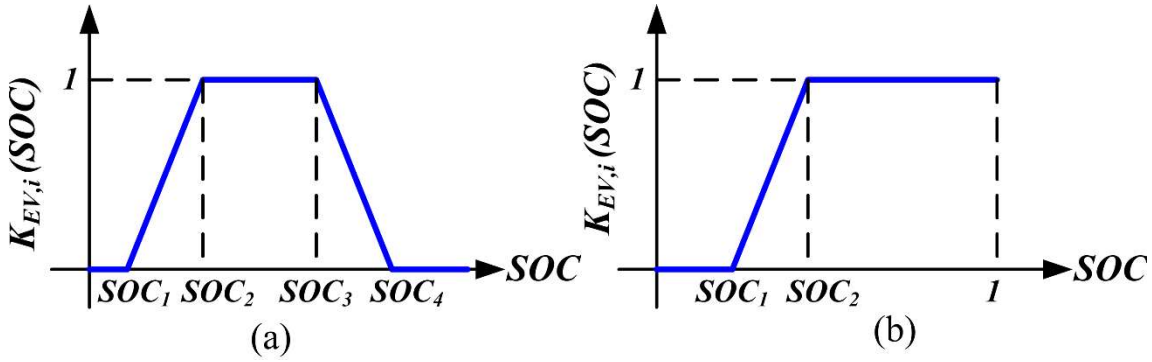

Fig. 5.6 $K_{EV,i}$ vs. SOC a) Discharge mode, b) Idle mode

5.3 Development of Proposed Moth Flame Optimization Based MPID Controller

The escalating complexity of power systems requires a quick and precise refining of the controller's gain constants to achieve a better LFC response. To address this problem, many swarm-intelligent strategies for PI/PID controller tuning have been suggested in the literature. The fundamental characteristics of these algorithms are the absence of derivatives and non-dependence on the plant model. A few of them are PSO, TLBO, GA, CSO, HSO and GOA. The NFL (no free lunch) theorem states that no single swarm-intelligent approach has the potential solution to solve all engineering optimization issues and that there is always an opportunity for improvement. So, for fine-tuning the MPID controller, a recently developed and powerful MFO is used. Mirjali et al. developed MFO in 2015, which imitates the social behaviour of moth flames. This algorithm was benchmarked on various standard test problems and verified its performance quantitatively and qualitatively with different optimization approaches in the literature. This method was used extensively to solve different engineering problems because of its merits viz. quick convergence, few controlling factors, straightforward implementation structure and simplicity [142 – 144].

5.3.1 Mathematical Modelling of MFO

This algorithm mimics the flying characteristics of moths. Moths are flying insects that belong to the same class as butterflies. The swarming behaviour is a unique feature of the

moths that is found at both stages of the moth's evolution (nymph/larval and adult stages). Moreover, moths exhibit special navigation paths at night by nature called transverse orientation. The moths follow a specific path with respect to the moonlight during their travel in the night. When moths are far away from any light, they travel long distances in a straight line (single direction) based on moonlight. Once they come too close to a light source, they fly spirally around it and finally reach convergence after certain modifications.

This algorithm can be divided into two components, called moths and flames, either of them is regarded to be the solution. The moths and flames are viewed as search agents and elite positions explored during the iterations in this algorithm. Thus, flames can be regarded as flags that moths drop when exploring the search space. So that flames can never lose their best position during the population update and while finding the global best solution. Below is an illustration of the mathematical model used to replicate the swarming behaviour of moths:

The moths are initialized as follows for the first iteration:

$$M = \begin{bmatrix} m_{1,1} & \cdots & m_{1,d} \\ \vdots & \ddots & \vdots \\ m_{n,1} & \cdots & m_{n,d} \end{bmatrix} \tag{5.11}$$

Where M is the matrix of moth population, d is the dimension of search space which depends on the no. of optimization variables and n represents the total no. of moths.

Based on the fitness function and its value, the moths can be sorted in ascending/descending order. Eq. (5.12) represents the objective value of moth's population.

$$OM = (OM_1, OM_2 \ldots \ldots OM_n\ )^T \tag{5.12}$$

Similarly, the flame matrix can be updated as:

$$F = \begin{bmatrix} f_{1,1} & \cdots & f_{1,d} \\ \vdots & \ddots & \vdots \\ f_{n,1} & \cdots & f_{n,d} \end{bmatrix} \tag{5.13}$$

Based on the fitness function and its value, the flames can be sorted in ascending/descending order. Eq. (5.14) represents the objective value of flame's population.

$$OF = (OF_1, OF_2 \ldots \ldots OF_n\ )^T \tag{5.14}$$

The typical structure of MFO can be expressed with three approximations as follows:

$$MFO = (I, P, T) \tag{5.15}$$

Where *I*: Initialization; *P*: Position update, *T*: Termination

In Eq. (5.15), *I* denotes the initialization of the population, which can be defined as:

$$M_{i,j} = lb(i) + \Big(randomno\big(1, N_{pop}\big)\Big)\big(ub(i) - lb(i)\big) \tag{5.16}$$

Where N_{pop} denotes the population size, *ub* is the upper limit boundary, and *lb* is the lower limit boundary.

In Eq. (5.15), *P* denotes the position update of moths. The position update of the moth with respect to flames can be updated by using Eq. (5.17)

$$M_i = S\big(M_i, F_j\big) \tag{5.17}$$

The logarithmic spiral function *(S)* is used as the key updating strategy because the algorithm is based on the moth's transverse orientation around a flame and can be written as follows:

$$S\big(M_i, F_j\big) = F_j + D_i e^{bt} \cos(2\pi t) \tag{5.18}$$

Where F_j denotes the position of the j^{th} flame and M_i indicates the position of i^{th} moth, '*t*' indicates a random number in [-1, 1], and 'b' defines the shape of the logarithmic spiral. D_i is the distance of the i^{th} moth from the j^{th} flame, which is defined as:

$$D_i = \big|F_j - M_i\big| \tag{5.19}$$

The moth's position is updated with respect to flame during exploration and exploitation [145]. The exploitation is taken care by the logarithmic spiral function and it takes place if the subsequent point is located between the moth and flame. Exploration is taken care by the distance term, D_i. In any swarm intelligence algorithm, an optimal trade-off between exploitation and exploration is needed to obtain global optimization. In this algorithm, the value of *'t'* and number of flames reduces from iteration to iteration to have an equalized effect on exploitation and exploration, as stated in Eq. (5.20) and Eq. (5.21).

$$flame\_no = round\left(J - i\left(\frac{J-1}{T}\right)\right) \tag{5.20}$$

$$t = 1 - randomno\left(2 + \frac{i}{T}\right) \tag{5.21}$$

where *J* specifies the maximum no. of flames, *T* is the maximum count of iterations and *i* is the present iteration.

5.3.2 Proposed Multi-stage PID (MPID) Controller Using MFO

An MPID controller is a union of PD and PI controllers in tandem. Fig. 5.7 illustrates the structure of an MPID controller. The PD controller in the initial stage receives an error (Δf) as its input and the PI controller in the final stage receives input from the output of the initial stage [83]. The MPID controller output (ΔU_c) is a reference power command signal for DEG and PHEVs. The key benefit of an MPID controller is that the system can utilize the best features of both controllers. At first, the PD controller is used to produce constant output to improve the transient response and later the steady-state error is reduced with the integral component of the PI controller. So, in this controller, the integral term is absent during the transient state. This overcomes the restriction of a traditional PID controller, which includes the incorporation of an integral component during the transient state.

The control signal fed to DEG and PHEV through the MPID controller can be expressed as [83]:

$$\Delta U_c = \left(K_P + K_D \frac{sN}{s+N}\right)\left(1 + K_{PP} + \frac{K_I}{s}\right)\Delta f \tag{5.22}$$

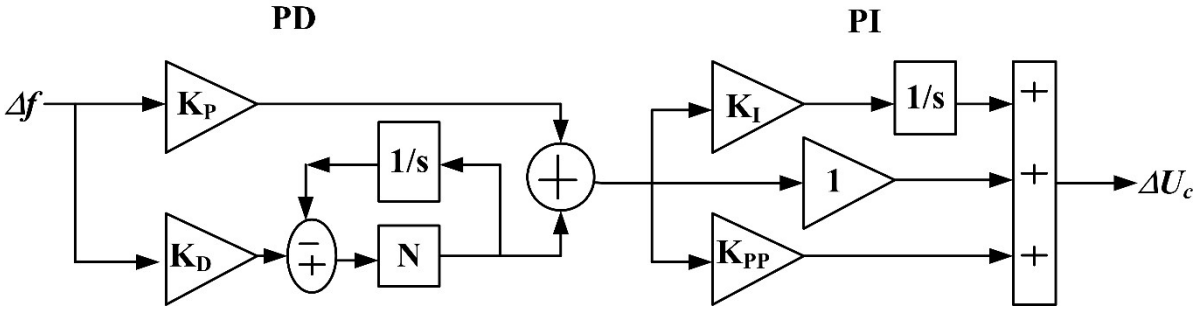

Fig. 5.7 Mathematical model of MPID controller

5.3.2.1 Optimizing MPID controller with MFO algorithm

The following steps are an explanation of the process for optimizing the proposed MPID controller with MFO:

Step 1: **Random initialization:** In the first iteration, generate a random population by using Eq. (5.11) & Eq. (5.16). Since the proposed controller has ($K_P, K_D, K_{PP}, K_I,$ *and* N) as 5

controller parameters, the population size is taken to be 100×5. Here, 100 stands for the population of moths and 5 for the dimensional size of the search space.

Step 2: **Objective/fitness assessment:** Simulate the developed model to evaluate the population's performance with the fitness function (integral time absolute error (ITAE)) given in Eq. (5.23).

$$ITAE = min \int_0^{t_{sim}} t|\Delta f|dt \tag{5.23}$$

Subjected to the optimization of $0.01 \leq K_{P,}K_{PP}, K_I, K_D \leq 2$ and $0 \leq N \leq 200$ [85]. Where 't_{sim}' denotes the total simulation time. The Δf value will be obtained from the Simulink model shown in Fig. 5.1.

Step 3: **Selection:** Based on the fitness value (ITAE), flag the best positions by flames.

Step 4: **Update the MFO algorithm-specific parameters:** At each iteration, calculate the value of *D* for the corresponding moth and update the number of flames, and value of *t* using Eq. (5.19), Eq. (5.20) & Eq. (5.21).

Step 5: **Population update:** Based on the values of *D*, *F* and *t* estimate the updated position of the moth with respect to the best flame's position using Eq. (5.18).

Step 6: **Stopping rule:** When the current iteration exceeds the maximum iteration count, the optimal parameters for the controller are the most optimal solution achieved till the last iteration that corresponds to the optimal value of ITAE. Show the optimized $K_{P,}K_{PP}$, K_I, K_D, *N,* and ITAE values.

5.4 Results and Discussion

The simulation studies are performed on the Bella Coola MG having different renewable energy sources and PHEVs that are modelled in the MATLAB Simulink platform. An extensive investigation of the simulation outcomes of an islanded MG's frequency deviations are provided in this section. The MG frequency deviations are analyzed with variations in the load (ΔP_L), RES power disturbances (solar power (ΔP_{PV}) and wind power (ΔP_{WTG})) and with the parametric uncertainties of MG and PHEV. The performance of the MFO-optimized MPID controller is presented for the aforementioned disturbances. Initially, to examine the supremacy of the MFO algorithm over other popular metaheuristic algorithms (PSO, TLBO, and GOA), the performance of different PID controllers is assessed with step

load and multiple step load perturbations. Later, the performance of MFO optimized PID and MPID controllers is evaluated for several operating scenarios that have been created and tested on Bella Coola MG. Further, the presence of PHEVs in primary and secondary frequency control loops is presented. Finally, the stability analysis and comparison results are presented.

5.4.1 Performance Evaluation of the Proposed Controller Under Different Operating Conditions

i) Initial case: Dynamic response evaluation of various meta-heuristic-based PID controllers against step load and multi-step load disturbances (ΔP_L)

The initial case is meant to demonstrate the effectiveness of the MFO-based PID controller above the other well-known meta-heuristic optimized PID controllers in the literature. In the present operating scenario, a 10% step change in load demand is considered and the PID controllers' parameters are optimized using the meta-heuristic algorithms considering the ITAE as the fitness function. The ITAE characteristics of differently tuned PID controllers are shown in Fig 5.8. Table 5.2 denotes the optimized parameters of the PID controller with various meta-heuristic techniques. Fig. 5.9 displays the frequency perturbation response of the MG for the operating conditions of step load change case using various PID controllers. Table 5.3 represents the comparative performance analysis of differently tuned PID controllers, considering Fig. 5.9 with regard to ITAE value, settling time and overshoot/undershoots.

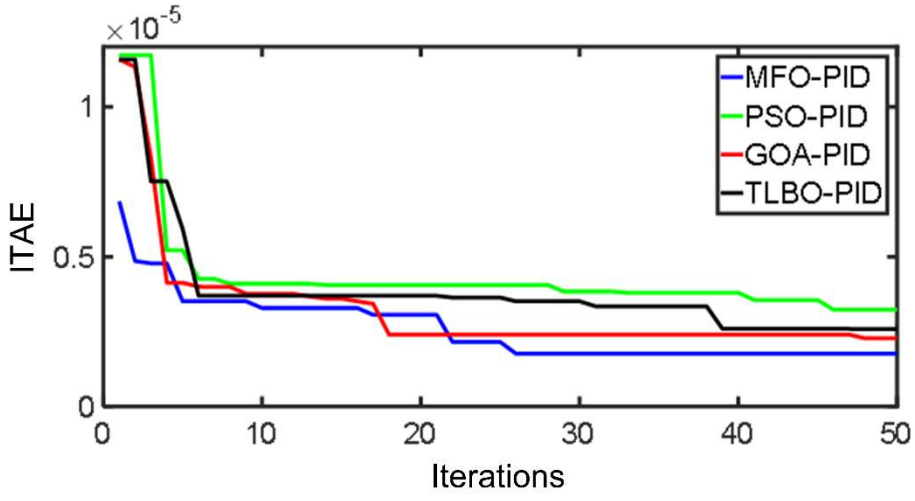

Fig. 5.8 ITAE performance characteristics

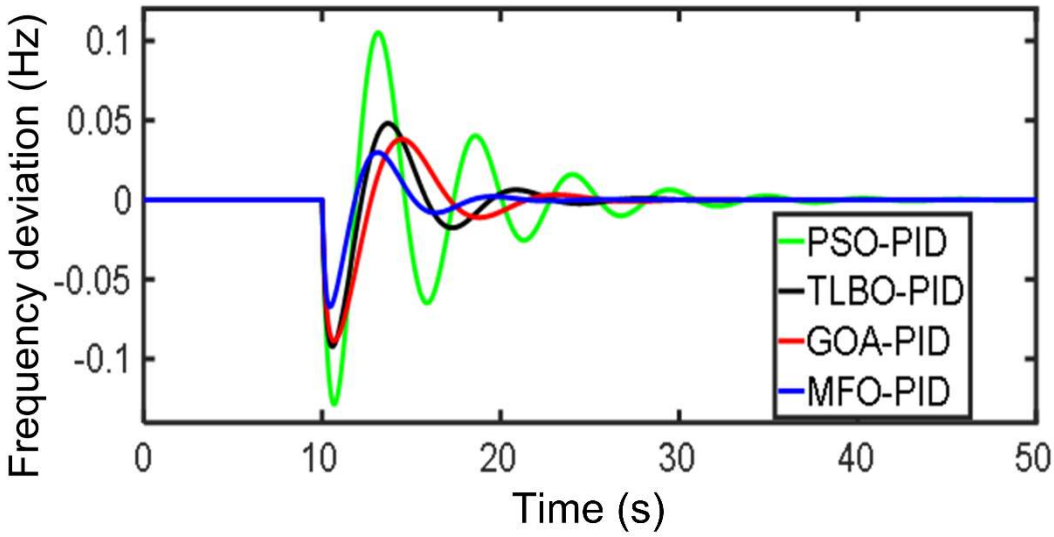

Fig. 5.9 MG frequency perturbation response for 10% step load change

Table 5.2 Optimized gains of various controllers

Methods	Optimized Gains			
	K_P	K_I	K_D	N
PSO-PID	1.0329	1.6248	1.1992	100.2266
TLBO-PID	1.1922	0.8718	1.8374	119.4526
GOA-PID	1.39556	1.42816	1.90277	59.623
MFO-PID	1.8230	1.5632	1.7258	28.5346

Table 5.3 Comparative analysis of differently optimized PID controllers for step load change case of operating conditions

Optimizing Method-PID	Performance Analysis Terms			
	Peak Undershoot (Hz)	Peak Overshoot (Hz)	Settling Time (s)	Integral Time Absolute Error
PSO-PID	-0.12	0.1	21	0.000043
TLBO-PID	-0.095	0.05	13	0.000038
GOA-PID	-0.093	0.045	11	0.000032
MFO-PID	-0.06	0.03	9	0.000021

From the above results, it is evident that the elite performance of the MFO-PID is visible from the MG dynamic response following a step load perturbation. The MFO-PID controller

minimizes the frequency drop and improves the settling times far better than others. To have a next-level comparison, multi-step load disturbances are considered as depicted in Fig. 5.10 (a) and Fig. 5.10 (b) depicts the MG frequency response with differently tuned controllers. In this case also, the MFO-PID controller offers superior performance than the other controllers. It is evident that the adopted MFO algorithm is well suited for this problem, hence the MFO algorithm is employed to optimize the proposed MPID's gain constants to have better control of MG frequency deviations. From the next case onwards, the proposed MFO MPID controller and the MFO PID controller are contrasted to provide a better perspective of the results view.

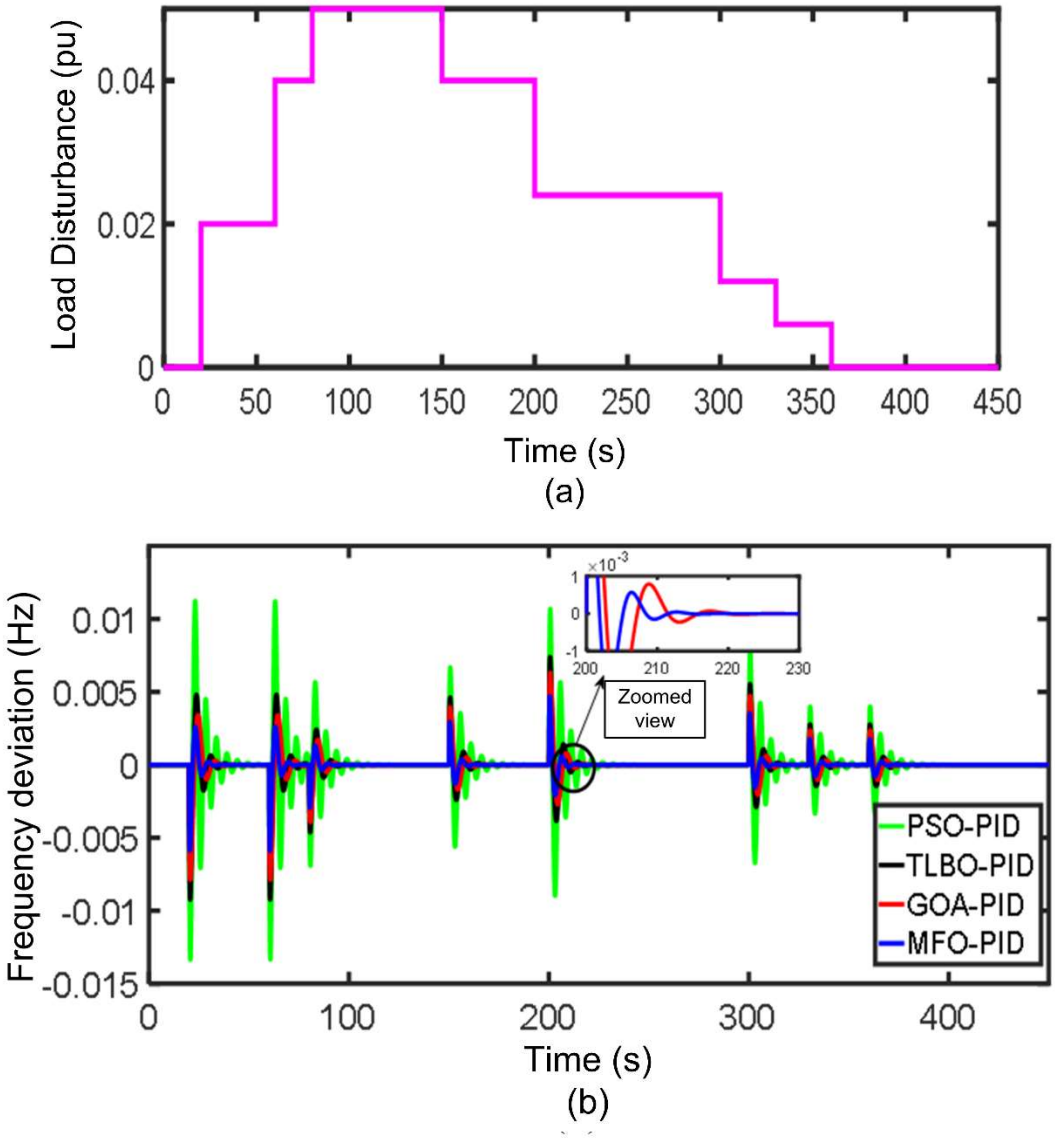

Fig. 5.10 Dynamic response of various controllers: **a)** Multistep load disturbances in MG **b)** Frequency perturbation response of MG

ii) Case-1: Dynamic response evaluation of MFO optimized multi-stage PID controller considering multiple power disturbances (concurrent changes in ΔP_L, ΔP_{PV} and ΔP_{WTG}) and parametric uncertainties of MG and PHEV

This case is meant to demonstrate the effectiveness of the multi-stage PID controller over the PID controller using the MFO algorithm. The parameters of MPID and PID controllers are optimized considering the simultaneous disturbances in load, solar, and wind powers along with parametric uncertainties of MG and PHEV using ITAE as the fitness function. Fig. 5.11 shows the multiple power fluctuations (LD = load disturbance, WD = wind disturbance, and PVD = photovoltaic disturbance) and Table 5.4 presents the percentage of parametric uncertainties considered for the MG and PHEV aggregator. Fig. 5.12 shows the ITAE characteristics of the proposed MFO-MPID and MFO-PID controllers. Table 5.5 presents the optimal gain constants of the two controllers.

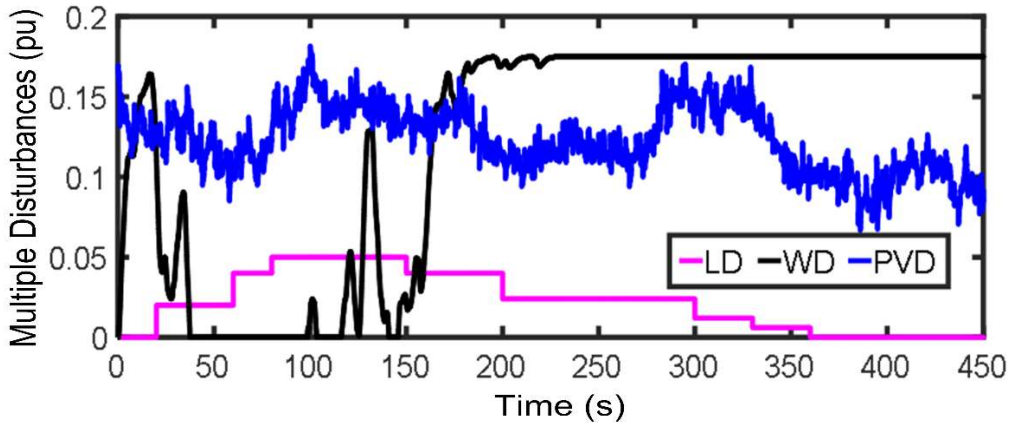

Fig. 5.11 Concurrent power fluctuations (multiple disturbances) in MG

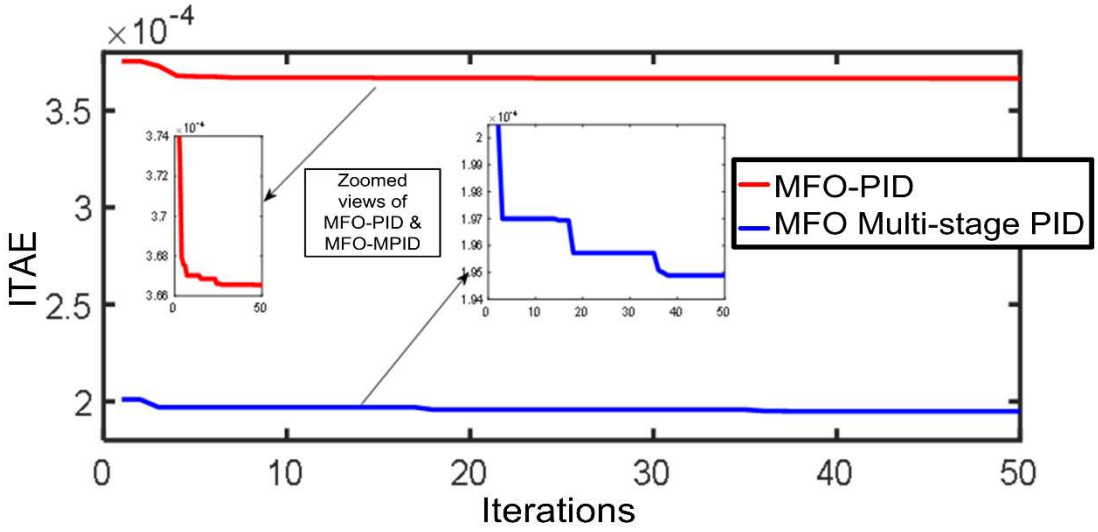

Fig. 5.12 MFO PID and MPID controllers' ITAE performance evaluation with case-1 conditions

Table 5.4 Percentage uncertainties in MG and PHEVs

Parameters	Percentage variation	Actual
K_{EV}	-30 %	1
R_{av} *(Hz/puMW)*	-50 %	2.4
T_{EV} *(s)*	+50 %	0.1
M (s)	-20 %	0.1667
D (puMW)	-20 %	0.015
R (Hz/puMW)	+20 %	2.4

Table 5.5 MFO PID & MPID controllers' optimized gains

Controller	Controller parameters				
	K_P	K_I	K_{PP}	K_D	N
MFO-PID	1.1334	1.3196	-	1.9169	144.3923
MFO-MPID	1.4922	1.6656	0.0774	2	134.2390

The purpose of this case is to examine how well an MPID controller outperforms the PID controller in the context of various disturbances, MG, and PHEV uncertainties. Fig. 5.13 depicts the frequency perturbation response of both controllers in this context. It can be observed that there is an improved performance of the proposed multi-stage PID controller than the PID in minimizing the frequency deviations of the MG.

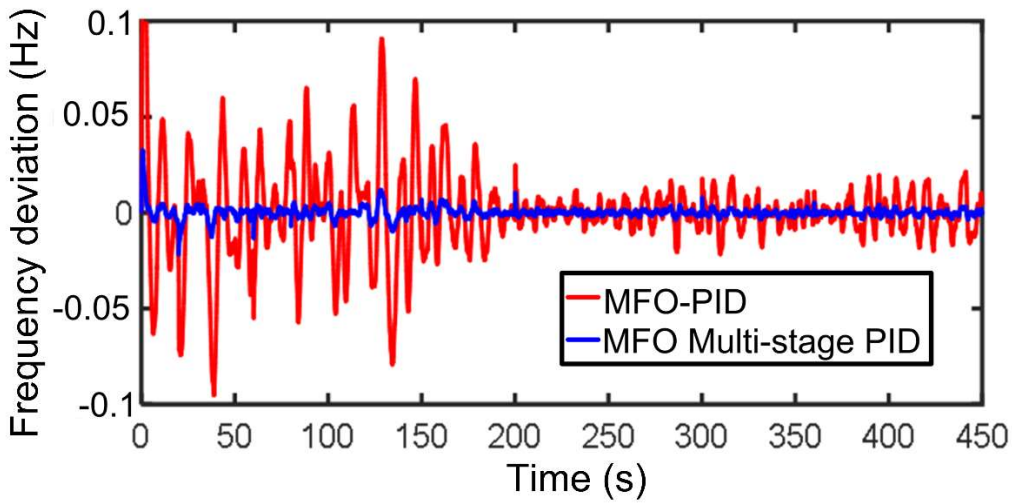

Fig. 5.13 Frequency perturbation response of MG against multiple power disturbances and parametric uncertainties

iii) Case-2: Response evaluation of the proposed controller under multiple power disturbances (concurrent changes in ΔP_L, ΔP_{PV} and ΔP_{WTG})

In case-2, the changes in load, solar and wind power disturbances are considered concurrently in MG. The concurrent power changes in MG are depicted in Fig. 5.11 and the MG frequency perturbation response is shown in Fig. 5.14.

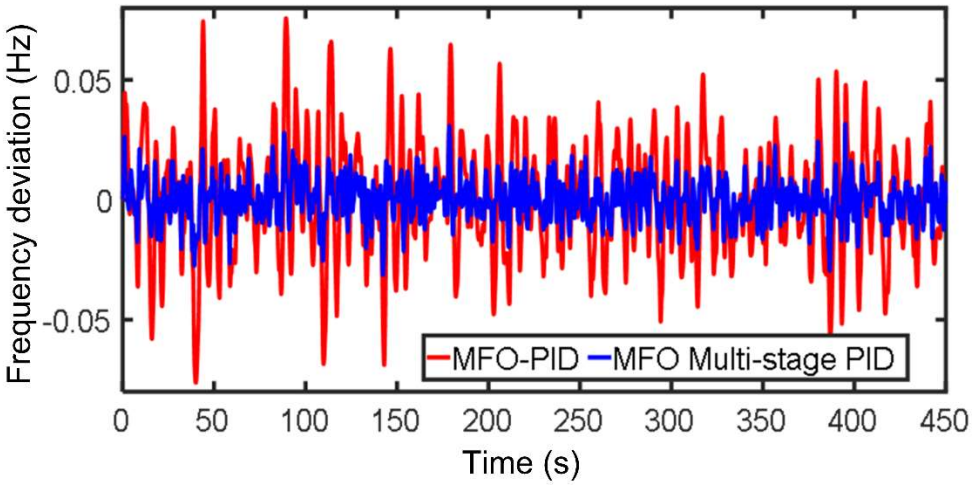

Fig. 5.14 MG frequency perturbation response for multiple power disturbances

iv) Case-3: Response evaluation of the proposed controller under solar power disturbances (ΔP_{PV})

In case-3, only solar disturbances are considered in MG. Fig. 5.15 (a) depicts the random change in solar irradiation power and the respective MG frequency deviations are shown in Fig. 5.15 (b).

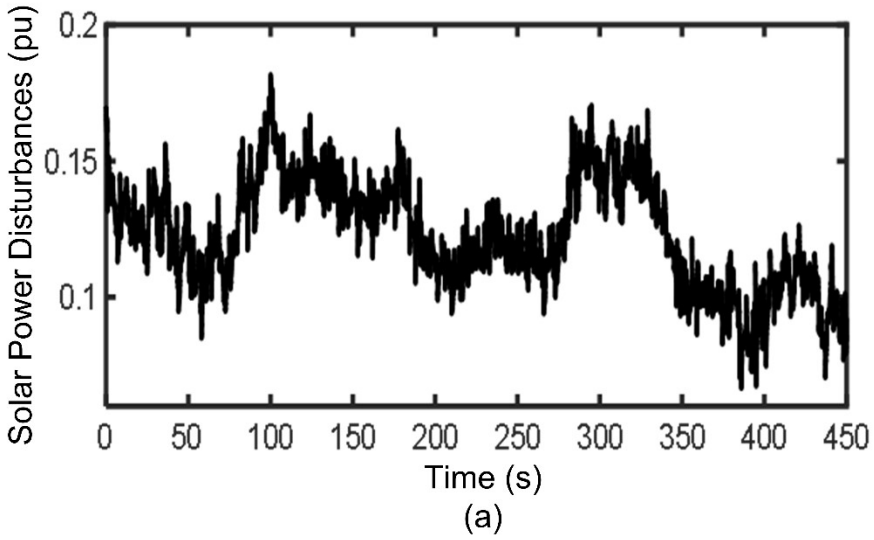

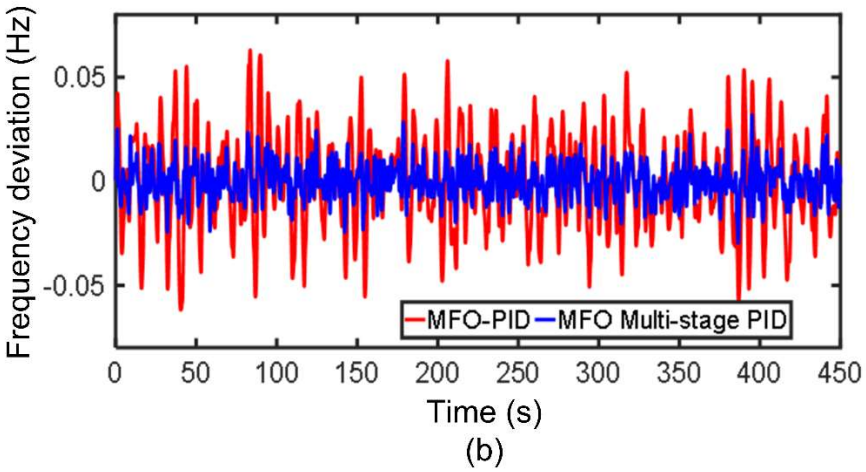

Fig. 5.15 a) Fluctuations of solar power in MG **b)** MG frequency perturbation response for case-3

v) Case-4: Response evaluation of the proposed controller to wind power fluctuations (ΔP_{WTG})

For this case-4, only ΔP_{WTG} is considered in MG. The random fluctuations in wind power are shown in Fig. 5.16 (a) and Fig. 5.16 (b) depicts the corresponding response of frequency deviation in the MG.

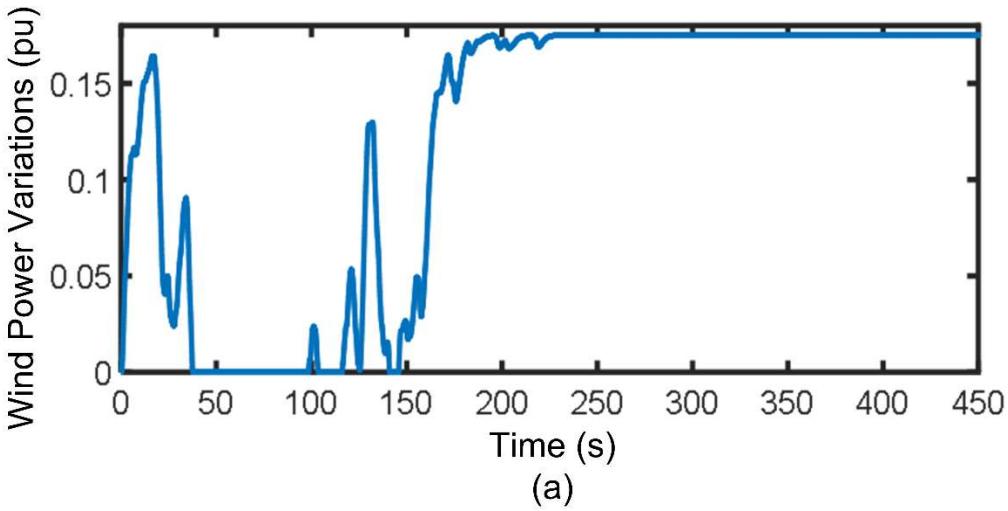

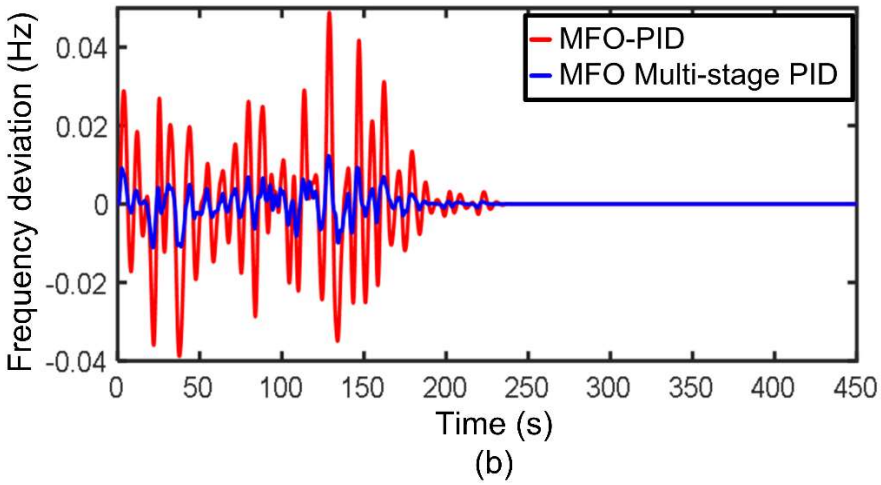

Fig. 5.16 a) Fluctuations of wind power in MG **b)** MG frequency perturbation response for case-4

From the results of the above cases-1, 2, 3, and 4, it is understood that the proposed MFO optimized multi-stage PID controller is performing better in mitigating the MG frequency deviations than the PID controller. Table 5.6 portrays the dynamic performance evaluation of both controllers in terms of peak undershoot, peak overshoot, and ITAE value. Table 5.6 results convey that the suggested MFO-MPID controller enhances the performance of MG over the MFO-PID controller when subjected to RES/load disturbances. The case-1 result also reveals that the suggested controller showed a good level of resilience towards the considered parametric uncertainties. Also, it is clear from ITAE performance characteristics that, in comparison to the PID controller, the ITAE value is still reduced with proper use of the PID controller in multi-stages. Therefore, the MFO-MPID controller can be utilized for the control of modern power systems incorporating high renewable energy content.

Table 5.6 Dynamic performance evaluation of MFO PID & MPID controllers against the cases 1, 2, 3, and 4 operating conditions

Cases	Peak Undershoot (Hz)		Peak Overshoot (Hz)		ITAE	
	MFO-PID	MFO MPID	MFO-PID	MFO MPID	MFO-PID	MFO MPID
Case-1	-0.1	-0.0357	0.09	0.032	0.0003623	0.0002384
Case-2	-0.058	-0.035	0.056	0.03	0.000283	0.000212
Case-3	-0.055	-0.032	0.052	0.028	0.000250	0.000190
Case-4	-0.039	-0.011	0.042	0.012	0.000216	0.000152

vi) Case-5: Impact of PHEVs in the SFC and PFC loops (Primary Frequency Control)

This case's objective is to investigate the impact of PHEVs on the dynamic frequency control in the SFC loop with a control signal from the MPID controller versus the impact of PHEVs in the PFC loop. This can be illustrated with the help of the PHEV aggregator model (in Fig. 5.5). In the suggested method, the control signal for PHEV aggregator output power is obtained from the MFO-optimized MPID controller. Whereas in the PFC loop, there will be no control signal for PHEV output power and the P_{PHEV} is obtained from droop characteristics of the PHEV aggregator (R_{av}). The MG frequency perturbation response under case-5 conditions is depicted in Fig. 5.17. The input disturbances for this case are same as case-1 conditions. As seen in Fig. 5.17, with the suggested approach the MG frequency deviations are significantly reduced over the PHEV aggregator in the PFC loop. This due to proper coordination is established by the proposed controller between DEGs and PHEVs in the SFC loop.

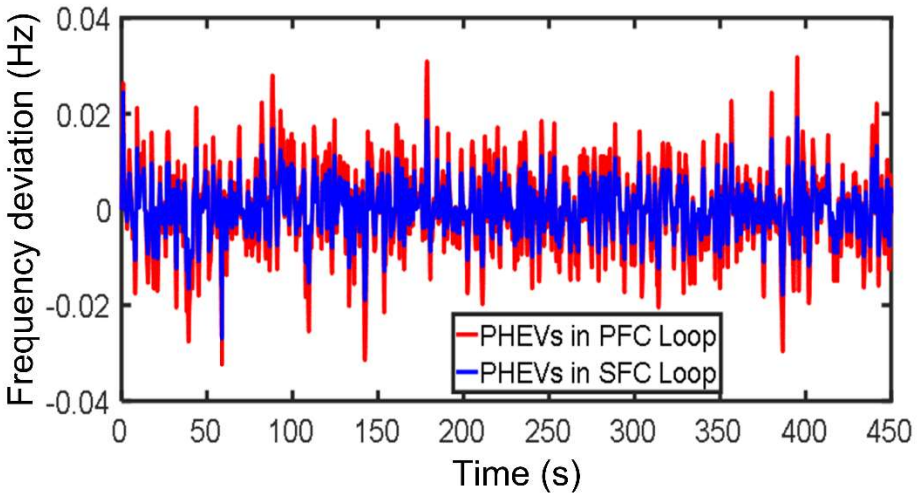

Fig. 5.17 Impact of PHEV aggregator due to the proposed method on the frequency response of MG over the generalized methods in literature [146]

Observations from the simulation results

The following observations have been noticed from various operating cases.

i. From initial case conditions, it is noticed that the MFO-PID controller exhibits an improvement in undershoot (50%, 36.84% and 35.48%), overshoot (70%, 40%, and 33.33%) and settling times (57.14%, 30.77% and 18.18%) over PSO-PID, TLBO-PID and GOA-PID controllers respectively. The above quantitative results confirm

that the proposed MFO algorithm is precisely adaptable to the present MG frequency control problem.

ii. Upon comparison with the MFO-PID controller, it has been noticed that the suggested MFO-MPID controller reduces the ITAE value by at least 24% for the operating conditions of cases 1, 2, 3, and 4.

iii. Finally, from the conditions of case-5, it is observed that the MG frequency response is improved with the presence of PHEVs in the SFC loop (DEGs and PHEVs are well coordinated with an MPID controller) rather than in the PFC loop.

5.4.2 Stability Analysis of MG

The linear analysis tool from the Simulink Control Design toolbox of MATLAB/Simulink is used in the present work to demonstrate the stability analysis of the MG for various operating situations together with root locus plots [86] and eigenvalues of the system's linearized transfer function model [87]. Table 5.7 displays the eigen values for various cases. Fig. 5.18 displays the root locus plots for cases 1 and 2. It can be observed that from the eigenvalues and root locus plots, all the closed loop poles lie to the left half of the complex s-plane thereby confirming the stable operation of the MG system. If the gain of the linearized transfer function model of the MG system is greater than 4.3 *(k > 4.3),* then two closed loop poles traverse to the negative half of the complex s-plane making the system unstable which can be seen in the zoomed view of Fig. 5.18.

Table 5.7 Eigen values of MG system for different operating conditions

Case-1	**Cases-2, 3, 4**
-69.50 + j2949.60	-71.20 + j3231.40
-69.50 + j2949.60	-71.20 - j3231.40
-40 + j0	-40 + j0
-1 + j0.40	-1 + j0.40
-1 – j0.40	-1 – j0.40
-0.30 + j0	-0.30 + j0
-0.50 + j0	-0.50 + j0

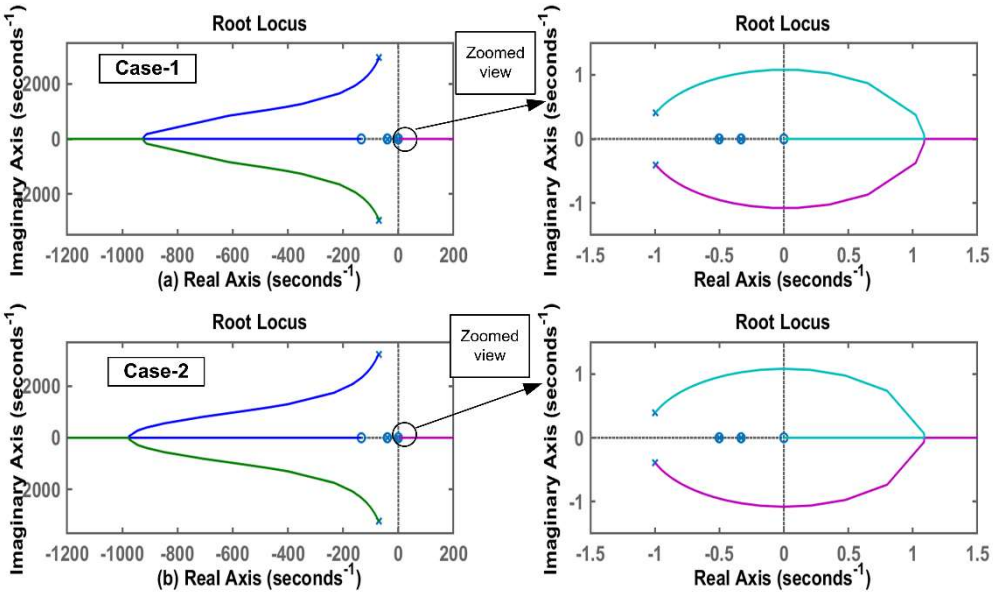

Fig. 5.18 Root locus plots for case-1 and case-2

5.4.3 Comparison with Earlier Reported Works

Table 5.8 Comparison with earlier reported works

Comparison term		**Reference**			
		[87]	**[84]**	**[85]**	**Proposed**
Multiple-step load perturbation response	ST (*s*)	-	5	4	5
	ITAE	-	0.000596	-	0.000190
Simultaneous changes in RES power, load, and parametric uncertainties	ITAE	0.7276	0.000135492	0.006	0.0002384
Controller and optimization techniques		MPID and hybrid whale optimization and pattern search algorithms	Fuzzy-tuned MPID and grass hopper optimization algorithm	Adaptive fuzzy-tuned fractional order MPID and future search algorithm	MPID and MFO
No. of controller parameters optimized		4	11	35	5
No. of algorithm-specific parameters		5	3	0	1
PHEVs considered (Yes/No)		No	No	No	Yes
Stability analysis (Yes/No)		No	No	No	Yes

The comparison of the suggested approach with earlier reported works for islanded MG frequency control employing an MPID controller regarding settling time, ITAE, and controller optimization technique is presented in Table 5.8. Table 5.8 reveals that the performance of the proposed controller is better and nearly on par with the other reported methods, demonstrating optimal results in both ITAE value and settling time. A qualitative comparison of computational burden can be assessed as high/low depending on the count of controller parameters optimized, the count of optimization techniques employed and their algorithm-specific parameters. The computational burden required for optimizing more controller parameters with one or more techniques would be comparatively more.

5.5 Summary

In this chapter, the MFO algorithm is applied to find the optimal gains of the MPID controller. The standalone MG had been subjected to load, solar and wind power disturbances. To expose the supremacy of the proposed MPID controller, the frequency response of the MG during various operating conditions is contrasted with the outcomes of the MFO-PID controller. The dynamic responses confirm the predominant execution of the proposed MPID controller when there are load and RES perturbations. Moreover, the proposed MFO-optimized MPID controller offers enhanced frequency dynamic response and an extended level of robustness for MG and PHEV parametric uncertainties. Furthermore, the proposed MFO algorithm has shown its supremacy over recent and well-established optimization techniques in the literature like GOA, TLBO and PSO. On the other hand, the impact of PHEVs on the MG frequency response is also examined. It is found that MG attains better frequency response when PHEVs and DEGs are coordinated as compared to the case when they are not in coordination. Proper coordination is established between DEGs and PHEVs with the proposed MFO-MPID controller. Therefore, the suggested controller stands as a viable solution for dynamic frequency control applications in MG.

******

Chapter 6

Conclusions and Future Scope

6.1 Conclusions

- In the present work, the protection of different transmission lines and frequency control of islanded microgrid are proposed using artificial intelligent techniques.

- A single fuzzy inference system based protection scheme is proposed for the protection of three-phase double circuit transmission lines that identify the faults within one cycle time (20 ms) with fault detection and classification accuracy of 99.75%. This protection scheme is immune to fault parameter variations and typical system operating conditions.

- A single ANN module is proposed for the protection of six-phase transmission lines against 120 types of short circuit faults. The accuracy of fault detection and classification is found to be 99.76% and the faults are identified within one cycle time (16.67 ms). This scheme is also immune to fault parameter variations. For fault location estimation, 11 ANN modules are used whose output is selected based on the fault type suggested by the ANN_FDC module. The performance of the fault location estimation modules is better with the training data (81% of fault cases are within ±1% error range) and nominal performance is observed with the testing data (53% of fault cases are within ±5% error range).

- A protection scheme based on the fuzzy inference system using voltage information of a single bus is proposed for the protection of transmission lines connected to hybrid renewable energy sources (solar photovoltaic and wind turbine farms). The proposed protection scheme detects and classifies the faults within one cycle time (20 ms) and has an FDC accuracy of 99.56%. The proposed protection scheme is immune to fault parameter variations and renewable power intermittencies. A regression based bagged ensemble learner is proposed for the fault location estimation. The proposed fault location estimation module approximates the fault location within ±5% error band. The Chi-square analysis is used to test the reliability of the fault location module (D^2 = 3.0407).

- A moth flame optimization algorithm based multi-stage PID controller is suggested for the frequency control of an islanded microgrid (Bella Coola MG). The MPID controller parameters are optimized using the MFO algorithm. The MG frequency deviations are mitigated effectively with the proposed MFO-MPID controller. The suggested controller's performance is found to be robust even with the load and renewable energy source power fluctuations and also towards parametric uncertainties.

6.2 Future Scope

- The protection of hybrid transmission lines (cable and overhead line) poses protection issues as the impedance characteristics of cable and overhead line differ from each other.
- The FACTS compensated transmission lines also pose protection issues such as underreaching and overreaching of distance relays.
- The protection tasks such as fault detection and classification and fault location estimation would be complicated for the above-mentioned transmission lines connected to renewable energy sources.
- As limited research is explored in the protection of six-phase transmission lines, the research can be further extended to high-phase order systems. Also, the protection schemes for cross-country and evolving faults and multi-location faults can be an opportunity for further research on such lines which have close proximity.
- The scope of the frequency control problem can be extended to multi-microgrid systems. Furthermore, different controller structures can be adopted whose controller's parameters can be optimized with the optimization algorithms viz. Jaya, Enhanced Jaya, Rao-1, and Rao-2 that are free of algorithm-specific parameters.
- Different artificial intelligent techniques can be adopted for the protection tasks of transmission lines viz. fuzzy decision trees, random forest, deep neural networks, and different ensemble learning methods (homogeneous or heterogenous, bagging, boosting, optimizable learning methods).

******

References

[1] International Energy Agency-World Energy Outlook-2022.

[2] I. R. E. Agency, “Renewable capacity statistics 2021,” Renew. Renew. Capacit. Stat., 2021.

[3] Y. G Paithankar and S. R. Bhide, “Fundamentals of power system protection”, PHI Learning Pvt. Ltd., 2nd ed., 2010.

[4] S. Venkata, W. Guyker, W. Booth, J. Kondragunta, Bhatt, and N. Saini, “Eppc-a computer program for six-phase transmission line design,” IEEE Trans. Power Appar. Syst., no.7, pp.1859–1869,1982.

[5] S. Venkata, W. Guyker, W. Booth, J. Kondragunta, N. Saini, and E. Stanek, “138-kv, six-phase transmission system: fault analysis,” IEEE Trans. Power Appar. Syst., no. 5, pp. 1203–1218, 1982.

[6] J. E. Stamp and A. A. Girgis, “Fault location technique for six phase transmission lines with unsynchronized phasors,” 1999 IEEE Transmission and Distribution Conference (Cat. No. 99CH36333), 1999, pp. 663-667 vol.2, doi: 10.1109/TDC.1999.756130.

[7] L. A. Zadeh, “Fuzzy sets”, Information and Control, vol.8, pp. 338-353, 1965.

[8] Timothy J. Ross., “Fuzzy logic with engineering application”, John Wiley and Sons. 3rd ed., 2010.

[9] Martin T. Hagan, Howard B. Demuth, Mark Hudson Beale and Orlando De Jesús, “Neural network design”, PWS Publication Company, 2nd ed.

[10] Jha G.K., “Artificial neural network and its application”, IARI, 2006.

[11] Lior Rokach and Oded Maimon, “Data mining with decision trees theory and applications”, Published by World Scientific Publishing Co. Pte. Ltd, 5 Toh Tuck Link, Singapore 596224, 2nd ed., April 2014.

[12] Dipak V. Patil and R. S. Bichkar, “Issues in optimization of decision tree learning: A survey”, International Journal of Applied Information Systems (IJAIS), Foundation of Computer Science FCS, New York, USA, vol. 3, no. 5, July 2012.

[13] Krzysztof Grabczewski, “Meta learning in decision tree induction”, Springer Cham Heidelberg New York Dordrecht London, Studies in Computational Intelligence, vol. 498, 2014.

[14] Breiman. L., J. Friedman, R. Olshen and C. Stone, “Classification and regression trees”, 1st Ed., Boca Raton, FL: CRC Press, 1984.

[15] A. H. Osman and O. P. Malik, "Protection of parallel transmission lines using wavelet transform," in IEEE Transactions on Power Delivery, vol. 19, no. 1, pp. 49-55, Jan. 2004, doi: 10.1109/TPWRD.2003.820419.

[16] K. K. R. and P. K. Dash, "A New Real-Time Fast Discrete S-Transform for Cross-Differential Protection of Shunt-Compensated Power Systems," in IEEE Transactions on Power Delivery, vol. 28, no. 1, pp. 402-410, Jan. 2013, doi: 10.1109/TPWRD.2012.2221749.

[17] S. K Mishra, L.N Tripathy, S.C Swain, "DWT approach based differential relaying scheme for single circuit and double circuit transmission line protection including STATCOM", Ain Shams Engineering Journal, Volume 10, Issue 1, 2019, Pages 93-102, ISSN 2090-4479, https://doi.org/10.1016/j.asej.2018.02.002.

[18] V. Ashok, Anamika Yadav, Almoataz Y. Abdelaziz, "MODWT-based fault detection and classification scheme for cross-country and evolving faults", Electric Power Systems Research, Volume 175, 2019, 105897, ISSN 0378-7796, https://doi.org/10.1016/j.epsr.2019.105897.

[19] Ashok, V., & Yadav, A. (2019), "A real-time fault detection and classification algorithm for transmission line faults based on MODWT during power swing", International Transactions on Electrical Energy Systems, 30(1), e12164. https://doi.org/10.1002/2050-7038.12164.

[20] Yadav, A., & Swetapadma, A. (2015), "Enhancing the performance of transmission line directional relaying, fault classification and fault location schemes using fuzzy inference system", IET Generation, Transmission & Distribution, vol. 9, no. 6, pp. 580-591, Apr. 2015. https://doi.org/10.1049/iet-gtd.2014.0498.

[21] Yadav, A., & Swetapadma, A. (2014), "Improved first zone reach setting of artificial neural network-based directional relay for protection of double circuit transmission lines", in IET Generation, Transmission & Distribution, vol. 8, no. 3, pp. 373-388, March 2014. https://doi.org/10.1049/iet-gtd.2013.0239.

[22] Ashok V, Yadav A. "A protection scheme for cross-country faults and transforming faults in dual-circuit transmission line using real-time digital simulator: a case study of chhattisgarh state transmission utility", Iran Journal of science and Technology – Transactions on Electrical Engineering, vol. 43, pp. 941–967, 2019.

[23] Koley, E., Shukla, S. K., Ghosh, S., & Mohanta, D. K. (2017), "Protection Scheme for Power Transmission Lines Based on SVM and ANN Considering the Presence of Non-Linear Loads", IET Generation, Transmission & Distribution, vol. 11, Iss. 9, pp. 2333-2341, 2017. https://doi.org/10.1049/iet-gtd.2016.1802.

[24] V. Malathi, N.S. Marimuthu, S. Baskar, K. Ramar, "Application of extreme learning machine for series compensated transmission line protection", Engineering

Applications of Artificial Intelligence, Volume 24, Issue 5, 2011, Pages 880-887, ISSN 0952-1976, https://doi.org/10.1016/j.engappai.2011.03.003.

[25] S. R. Samantaray, "A Data-Mining Model for Protection of FACTS-Based Transmission Line," in IEEE Transactions on Power Delivery, vol. 28, no. 2, pp. 612-618, April 2013, doi: 10.1109/TPWRD.2013.2242205.

[26] Swetapadma, A., & Yadav, A. (2016), "Data-mining-based fault during power swing identification in power transmission system" IET Science, Measurement & Technology, 10(2), 130-139. https://doi.org/10.1049/iet-smt.2015.0169.

[27] Jena, M. K., & Samantaray, S. (2015), "Intelligent relaying scheme for series-compensated double circuit lines using phase angle of differential impedance" International Journal of Electrical Power & Energy Systems, 70, 17-26. https://doi.org/10.1016/j.ijepes.2015.01.035.

[28] Balakrishnan, P., & Gopinath, S. (2020) "A new intelligent scheme for power system faults detection and classification: A hybrid technique", International Journal of Numerical Modelling: Electronic Networks, Devices and Fields, 33(5), e2728. https://doi.org/10.1002/jnm.2728.

[29] Ray, P., & Mishra, D. P. (2016) "Support vector machine based fault classification and location of a long transmission line", Engineering Science and Technology, an International Journal, 19(3), 1368-1380. https://doi.org/10.1016/j.jestch.2016.04.001.

[30] Upendar J, Gupta CP, Singh GK, and Ramakrishna G., "PSO and ANN-based fault classification for protective relaying", IET Gener Transm Distrib. Volume 4, Issue 10, October 2010, p. 1197 – 1212. DOI: 10.1049/iet-gtd.2009.0488.

[31] Patel, U., Chothani, N., & Bhatt, P. (2021), "Supervised relevance vector machine based dynamic disturbance classifier for series compensated transmission line", International Transactions on Electrical Energy Systems, 31(10), e12663. https://doi.org/10.1002/2050-7038.12663.

[32] M. Abasi, M. Joorabian, A. Saffarian, and S. G. Seifossadat, "A comprehensive review of various fault location methods for transmission lines compensated by facts devices and series capacitors," J. Oper. Autom. Power Eng., vol. 9, no. 3, pp. 213–225, 2021.

[33] H. Shad, M. Gandomkar, and J. Nikoukar, "An improved optimal protection coordination for directional overcurrent relays in meshed distribution networks with dg using a novel truth table," J. Oper. Autom. Power Eng., vol. 11, no. 3, pp. 151–161, 2023.

[34] P. Venkata, V. Pandya, and A. Sant, "Data mining model based differential microgrid fault classification using svm considering voltage and current distortions," J. Oper. Autom. Power Eng., vol. 11, no. 3, pp. 162–172, 2023.

[35] S. Tiwari, G. K. Singh, and A. B. Saroor, “Multiphase power transmission research—a survey,” Electr. Power Syst. Res., vol. 24, no. 3, pp. 207–215, 1992.

[36] N. B. Bhatt, S. S. Venkata, W. C. Guyker, and W. H. Booth, “Six-phase (multi-phase) power transmission systems: fault analysis,” IEEE Trans. Power Appar. Syst., vol. 96, no. 3, pp. 758–767, 1977.

[37] S. Venkata, W. Guyker, W. Booth, J. Kondragunta, N. Saini, and E. Stanek, “138-kv, six-phase transmission system: fault analysis,” IEEE Trans. Power Appar. Syst., no. 5, pp. 1203–1218, 1982.

[38] G. C. Sekhar and P. Subramanyam, “Protection of six phase transmission system of allegheny power system, usa against shunt faults,” in 2014 International Conference on Smart Electric Grid (ISEG), pp. 1–7, IEEE, 2014.

[39] E. Koley, A. Yadav, and A. Thoke, “Six phase to ground fault detection and classification of transmission line using ann,” Int. J. Comput. Appl., vol. 41, no. 4, 2012.

[40] E. Koley, A. Jain, A. Thoke, A. Jain, and S. Ghosh, “Detection and classification of faults on six phase transmission line using ann,” in 2011 2nd International Conference on Computer and Communication Technology (ICCCT-2011), pp. 100–103, IEEE, 2011.

[41] R. Kumar, E. Koley, A. Yadav, and A. Thoke, “Fault classification of phase to phase fault in six phase transmission line using haar wavelet and ann,” in 2014 International Conference on Signal Processing and Integrated Networks (SPIN), pp. 5–8, IEEE, 2014.

[42] E. Koley, A. Yadav, and A. Thoke, “Artificial neural network based protection scheme for one conductor open faults in six phase transmission line,” Int. J. Comput. Appl., vol. 101, no. 4, pp. 42–46, 2014.

[43] E. Koley, A. Yadav, and A. S. Thoke, “A new single-ended artificial neural network-based protection scheme for shunt faults in six-phase transmission line,” Int. Trans. Electr. Energy Syst., vol. 25, no. 7, pp. 1257–1280, 2015.

[44] E. Koley, K. Verma, and S. Ghosh, “A modular neuro-wavelet based non-unit protection scheme for zone identification and fault location in six-phase transmission line,” Neural Comput. Appl., vol. 28, pp. 1369–1385, 2017.

[45] S. K. Shukla, E. Koley, S. Ghosh, and D. K. Mohanta, “Enhancing the reliability of six-phase transmission line protection using power quality informatics with real-time validation,” Int. Trans. Electr. Energy Syst., vol. 29, no. 9, p. e12048, 2019.

[46] A. Yadav and V. Ashok, “A relaying scheme for detection and classification of shunt faults in six-phase transmission system based on dft-fis approach,” J. Power Technol., vol. 98, no. 2, p. 202, 2018.

[47] M. Verma, E. Koley, and S. Ghosh, “Application of fuzzy logic for fault detection and classification in six phase transmission line,” in 2017 IEEE Int. Conf. Comput. Intell. Comput. Res. (ICCIC), pp. 1–5, IEEE, 2017.

[48] Li, X., & Lu, Y. (2023), “Pilot protection of lines emanating from DFIG-based wind farms during balanced faults”, International Journal of Electrical Power & Energy Systems, 151, 109186. https://doi.org/10.1016/j.ijepes.2023.109186.

[49] V. Chakeri, H. Seyedi and M. Tarafdar Hagh, "A New Approach to Transmission Line Pilot Protection in the Presence of Inverter-Interfaced Distributed Generators," in IEEE Systems Journal, vol. 15, no. 4, pp. 5383-5392, Dec. 2021, doi: 10.1109/JSYST.2020.3041203.

[50] Z. Hu et al., "Fast Distance Protection Scheme for Wind Farm Transmission Lines Considering R-L and Bergeron Models," in Journal of Modern Power Systems and Clean Energy, vol. 11, no. 3, pp. 840-852, May 2023, doi: 10.35833/MPCE.2021.000423.

[51] K. Ma, H. K. Høidalen, Z. Chen and C. L. Bak, "Improved Zone 1 Top-line Tilting Scheme for Polygonal Distance Protection in the Outgoing Line of Type-4 Wind Parks," in CSEE Journal of Power and Energy Systems, vol. 9, no. 1, pp. 172-184, January 2023, doi: 10.17775/CSEEJPES.2021.07870.

[52] S. Paladhi and A. K. Pradhan, "Adaptive Distance Protection for Lines Connecting Converter-Interfaced Renewable Plants," in IEEE Journal of Emerging and Selected Topics in Power Electronics, vol. 9, no. 6, pp. 7088-7098, Dec. 2021, doi: 10.1109/JESTPE.2020.3000276.

[53] Saber, A., Shaaban, M., & Zeineldin, H. (2022), “A new differential protection algorithm for transmission lines connected to large-scale wind farms”, International Journal of Electrical Power & Energy Systems, 141, 108220. https://doi.org/10.1016/j.ijepes.2022.108220.

[54] Aboshady, F., Saber, A., Khera, F., & Zobaa, A. F. (2023), “High frequency directional-based protection scheme for transmission lines emanating from large scale wind farms”, Electric Power Systems Research, 225, 109904. https://doi.org/10.1016/j.epsr.2023.109904.

[55] Li B, Liu J, Wang X, Zhao L., “Fault Studies and Distance Protection of Transmission Lines Connected to DFIG-Based Wind Farms”, Applied Sciences. 2018; 8(4):562. https://doi.org/10.3390/app8040562.

[56] Li, B., Sheng, Y., He, J., Li, Y., Xie, Z., & Cao, Y. (2023), “Improved distance protection for wind farm transmission line based on dynamic frequency estimation”, International Journal of Electrical Power & Energy Systems, 153, 109382. https://doi.org/10.1016/j.ijepes.2023.109382.

[57] Ghorbani, A., & Mehrjerdi, H. (2023), “Distance protection with fault resistance compensation for lines connected to PV plant”, International Journal of Electrical Power & Energy Systems, 148, 108976. https://doi.org/10.1016/j.ijepes.2023.108976.

[58] Chowdhury, A., Paladhi, S., & Pradhan, A. K. (2023), “Local positive sequence component based protection of series compensated parallel lines connecting solar photovoltaic plants”, Electric Power Systems Research, 225, 109811. https://doi.org/10.1016/j.epsr.2023.109811.

[59] S. Singh, P. K. Nayak, S. Sarangi and S. Biswas, "Improved Protection Scheme for High Voltage Transmission Lines Connecting Large-Scale Solar PV Plants," 2022 22nd National Power Systems Conference (NPSC), New Delhi, India, 2022, pp. 118-123, doi: 10.1109/NPSC57038.2022.10069457.

[60] Liang Y, Xu G, Zha W, Wang C., “Adaptability Analysis of Fault Component Distance Protection on Transmission Lines Connected to Photovoltaic Power Stations”, Energies. 2019; 12(8):1578. https://doi.org/10.3390/en12081578.

[61] Yoldas YB, Yumurtacı R., “Improvement of Distance Protection with SVM on PV-Fed Transmission Lines in Infeed Conditions”, Energies. 2023; 16(6):2587. https://doi.org/10.3390/en16062587.

[62] Noureldeen, O., Hamdan, I. & Hassanin, B. “Design of advanced artificial intelligence protection technique based on low voltage ride-through grid code for large-scale wind farm generators: a case study in Egypt”, SN Appl. Sci. 1, 515 (2019). https://doi.org/10.1007/s42452-019-0538-9.

[63] S. K. Mohanty, P. K. Nayak, P. K. Bera and H. H. Alhelou, "An Enhanced Protective Relaying Scheme for TCSC Compensated Line Connecting DFIG-Based Wind Farm," in IEEE Transactions on Industrial Informatics, doi: 10.1109/TII.2023.3306575.

[64] A. A. Alrashdan, E. A. Feilat and M. A. Haj-Ahmed, "Protection of Transmission Lines Emanating from DFIG-Based Wind Farms During Symmetrical Faults," 2021 IEEE Industry Applications Society Annual Meeting (IAS), Vancouver, BC, Canada, 2021, pp. 1-6, doi: 10.1109/IAS48185.2021.9677091.

[65] Biswas, S., Nayak, P. K., Panigrahi, B. K., & Pradhan, G. (2023), “An intelligent fault detection and classification technique based on variational mode decomposition-CNN for transmission lines installed with UPFC and wind farm”, Electric Power Systems Research, 223, 109526. https://doi.org/10.1016/j.epsr.2023.109526.

[66] Mohanty, S. K., Santra, S. B., & Siano, P. (2023), "Faulty phase identification and ground detection in TCSC compensated lines integrated with wind farms", International Journal of Electrical Power & Energy Systems, 153, 109383. https://doi.org/10.1016/j.ijepes.2023.109383.

[67] Prasad, C., & Biswal, M. (2020)., "Swarm intelligence-based differential protection scheme for wind integrated transmission system", Computers & Electrical Engineering, 86, 106709. https://doi.org/10.1016/j.compeleceng.2020.106709.

[68] Prasad, C. D., Biswal, M., & Abdelaziz, A. Y. (2020), "Adaptive differential protection scheme for wind farm integrated power network", Electric Power Systems Research, 187, 106452. https://doi.org/10.1016/j.epsr.2020.106452.

[69] D. C. Das, A. K. Roy, and N. Sinha (2012), "GA based frequency controller for solar thermal–diesel–wind hybrid energy generation/energy storage system", Int J. Electr. Power Energy Syst., vol. 43, no. 1, pp. 262–279, 2012.

[70] Shashi, K.P., and Soumya, R. (2014), "Frequency regulation in hybrid power systems particle swarm optimization and linear matrix inequalities based robust controller design", Proc.Elsevier, vol 63, pp. 887-900, 2014.

[71] A. A. El-Fergany and M. A. El-Hameed (2017), "Efficient frequency controllers for autonomous two-area hybrid microgrid system using social-spider optimiser", IET Gener. Transm. Distrib., vol. 11, no. 3, pp. 637–648, 2017.

[72] C. Sreenivasaratnam, C. Yammani, and S. Maheswarapu (2019), "Load Frequency Control of Multi-microgrid System considering Renewable Energy Sources Using Grey Wolf Optimization", Smart Science, vol. 7, no. 3, pp. 198–217, Jul. 2019.

[73] P. K. Ray and A. Mohanty (2018), "A robust firefly–swarm hybrid optimization for frequency control in wind/PV/FC based microgrid", Applied Soft Computing, vol. 85, p. 105823, 2018.

[74] G. Shankar, and V. Mukherjee (2016), "Load frequency control of an autonomous hybrid power system by quasi oppositional harmony search algorithm", Int J. Electr. Power Energy Syst., vol. 78, pp. 715–734, 2016.

[75] S. C., C. Yammani and S. Maheswarapu (2019), "Frequency control of Autonomous Hybrid Multi-Microgrid System", 2019 National Power Electronics Conference (NPEC), Tiruchirappalli, India, 2019, pp. 1-6.

[76] A. Annamraju and S. Nandiraju (2018), "Frequency Control in an Autonomous Two-area Hybrid Microgrid using Grasshopper Optimization based Robust PID Controller", 2018 8th IEEE India International Conference on Power Electronics (IICPE), JAIPUR, India, 2018, pp. 1-6.

[77] A. Latif A. Pramanik D. C. Das I. Hussain and S. Ranjan (2018), "Plug-in hybrid vehicle-wind-diesel autonomous hybrid power system: frequency control using FA and CSA optimized controller", International Journal of System Assurance Engineering and Management, vol. 9, no. 5, pp. 1147-1158, 2018.

[78] H. Bevrani, F. Habibi, S. Shokoohi (2013), "ANN-based self-tuning frequency control design for an isolated microgrid", Meta-Heuristics Optimization Algorithms in Engineering, Business, Economics, and Finance. P. Vasant (Ed), Chapter 12, IGI Global, USA, pp. 357-385, 2013.

[79] Khooban, M.H., Taher Niknam, Frede Blaabjerg, et.al (2016), "A robust adaptive load frequency control for microgrids", Proc. Elsevier, vol 65, pp. 220-229, 2016.

[80] Bevarani, H., and Habibi.F. (2012), "Intelligent frequency control in an AC microgrid: online PSO based fuzzy tuning approach", Proc. IEEE, vol 3, no 4, pp. 1935-1944, 2012.

[81] A. Annamraju and S. Nandiraju (2018), "Robust Frequency Control in an Autonomous Microgrid: A Two-Stage Adaptive Fuzzy Approach", Electr. Power Components Syst., vol. 46, no. 1, pp. 83–94, Jan. 2018.

[82] Prakash K. Ray, & Asit Mohanty (2019), "A robust firefly–swarm hybrid optimization for frequency control in wind/PV/FC based microgrid" Applied Soft Computing, Volume 85, Dec. 2019, 105823. https://doi.org/10.1016/j.asoc.2019.105823.

[83] Khadanga RK, Padhy S, Panda S, and Kumar A. (2018), "Design and analysis of multi-stage PID controller for frequency control in an islanded micro-grid using a novel hybrid whale optimization-pattern search algorithm", International Journal of Numerical Modelling, vol. 31, no.5, e2349, 2018, DOI: https://doi.org/10.1002/jnm.2349.

[84] Annamraju A and Nandiraju S., (2020), "A novel fuzzy tuned multistage PID approach for frequency dynamics control in an islanded microgrid", International Transactions on Electrical Energy Systems, vol. 30, no.12, Dec. 2020, e12674, https://doi.org/10. 1002/2050-7038.12674.

[85] Annamraju A, Bhukya L, and Nandiraju S., (2021), "Robust frequency control in a standalone microgrid: An adaptive fuzzy based fractional order cascade PD-PI approach", Advanced Control for Applications: Engineering and Industrial Systems, vol. 3, no. 3, pp. 1–18 Sep. 2021, https://doi.org/10.1002/adc2.72.

[86] Khokhar, B., Dahiya, S. & Parmar, K.P.S. (2021), "A Novel Hybrid Fuzzy PD-TID Controller for Load Frequency Control of a Standalone Microgrid", Arabian Journal for Science and Engineering, 46, 1053–1065 (2021). https://doi.org/10.1007/s13369-020-04761-7

[87] Bhuvnesh Khokhar, Surender Dahiya, and K. P. Singh Parmar (2020), "A Robust Cascade Controller for Load Frequency Control of a Standalone Microgrid Incorporating Electric Vehicles", Electric Power Components and Systems, vol. 48, Iss. 6-7, 711-726, Aug.2020, DOI: 10.1080/15325008.2020.1797936

[88] Phadke AG, Thorp JS. Computer relaying for power systems. 2nd ed. Chichester: John Wiley & Sons; 2009.

[89] D. J. Spoor and J. Zhu, "Intercircuit faults and distance relaying of dual-circuit lines," in IEEE Transactions on Power Delivery, vol. 20, no. 3, pp. 1846-1852, July 2005, doi: 10.1109/TPWRD.2004.833899.

[90] Borăscu IC, Iliescu SS. "Influence of the zero sequence mutual impedance to the distance protection," U.P.B. Sci Bull Ser. C. vol. 77, Iss. 4, pp. 69–80, 2015.

[91] Bhide SR, "Digital power system protection", Delhi: PHI Learning Private Limited; 2014.

[92] P. K. Nayak, A. K. Pradhan and P. Bajpai, "A Fault Detection Technique for the Series-Compensated Line During Power Swing," in IEEE Transactions on Power Delivery, vol. 28, no. 2, pp. 714-722, April 2013, doi: 10.1109/TPWRD.2012.2231886.

[93] S., P. M., Nayak, P. K., & Pradhan, G. (2018), "Detection of three-phase fault during power swing using zero frequency filtering", *International Transactions on Electrical Energy Systems*, *29*(1), e2700. https://doi.org/10.1002/etep.2700.

[94] A. E. Emanuel, D. Cyganski, J. A. Orr, S. Shiller and E. M. Gulachenski, "High impedance fault arcing on sandy soil in 15 kV distribution feeders: contributions to the evaluation of the low frequency spectrum," in IEEE Transactions on Power Delivery, vol. 5, no. 2, pp. 676-686, April 1990, doi: 10.1109/61.53070.

[95] Lai, T., Snider, L., & Lo, E. (2006), "Wavelet transform based relay algorithm for the detection of stochastic high impedance faults" *Electric Power Systems Research*, *76*(8), 626-633. https://doi.org/10.1016/j.epsr.2005.12.021

[96] Premalatha J, Pradhan AK, "Detection of high impedance faults", in IEEE International Conference, Jan, 2012.

[97] V. Ashok and A. Yadav, "Fault Diagnosis Scheme for Cross-Country Faults in Dual-Circuit Line With Emphasis on High-Impedance Fault Syndrome," in IEEE Systems Journal, vol. 15, no. 2, pp. 2087-2097, June 2021, doi: 10.1109/JSYST.2020.2991770.

[98] CT saturation and DC offset current lecture notes. (n. d.) Available at: https://Nptel.Ac.in/Content/Storage2/ Courses/108101039/Download/Lecture-7.Pdf

[99] AsghariGovar, S., & Seyedi, H. (2016), "Adaptive CWT-based transmission line differential protection scheme considering cross-country faults and CT saturation", *IET Generation, Transmission & Distribution*, *10*(9), 2035-2041. https://doi.org/10.1049/iet-gtd.2015.0847

[100] Shukla, S. K., Koley, E., & Ghosh, S. (2019), "DC offset estimation-based fault detection in transmission line during power swing using ensemble of decision tree," *IET Science, Measurement & Technology*, *13*(2), 212-222. https://doi.org/10.1049/iet-smt.2018.5071

[101] R. Godse and S. Bhat, "Mathematical Morphology-Based Feature-Extraction Technique for Detection and Classification of Faults on Power Transmission Line," in IEEE Access, vol. 8, pp. 38459-38471, 2020, doi: 10.1109/ACCESS.2020.2975431.

[102] Fahim, S. R., Sarker, S. K., Muyeen, S., Das, S. K., & Kamwa, I. (2021), "A deep learning based intelligent approach in detection and classification of transmission line faults", *International Journal of Electrical Power & Energy Systems*, *133*, 107102. https://doi.org/10.1016/j.ijepes.2021.107102

[103] Vyas, B. Y., Maheshwari, R., & Das, B. (2021), "Versatile relaying algorithm for detection and classification of fault on transmission line", *Electric Power Systems Research*, *192*, 106913. https://doi.org/10.1016/j.epsr.2020.106913

[104] N. B. Bhatt, S. S. Venkata, W. C. Guyker, and W. H. Booth, "Six-phase (multi-phase) power transmission systems: fault analysis," IEEE Trans. Power Appar. Syst., vol. 96, no. 3, pp.758–767,1977.

[105] E. Koley, A. Yadav, and A. Thoke, "Six phase to ground fault detection and classification of transmission line using ann," Int. J. Comput. Appl., vol. 41, no. 4, 2012.

[106] Li, Q., Li, Y., Rowland, S., Hu, J., Cotton, I., & Jiang, X. (2022), "Audible noise evaluation for six-phase overhead lines transformed from existing three-phase double circuit infrastructures with uprated voltages", *High Voltage*, *7*(5), 866-876. https://doi.org/10.1049/hve2.12246

[107] Shen, S., Cao, B., Crossley, P., Wang, Z., & Ding, X. (2022), "Transformation of a three-phase double-circuit overhead transmission line into a six-phase feeder to increase power transfer capability", *IET Generation, Transmission & Distribution*, *16*(23), 4663-4671. https://doi.org/10.1049/gtd2.12545

[108] J. Stewart and I. Grant, "High phase order-ready for application," IEEE Trans. Power Appar. Syst., no. 6, pp. 1757–1767, 1982.

[109] Valsan, S. P., & Swarup, K. (2009), "Wavelet transform based digital protection for transmission lines", *International Journal of Electrical Power & Energy Systems*, *31*(7-8), 379-388. https://doi.org/10.1016/j.ijepes.2009.03.024

[110] Hajjar, A. A. (2013), "A high speed noncommunication protection scheme for power transmission lines based on wavelet transform", *Electric Power Systems Research*, *96*, 194-200. https://doi.org/10.1016/j.epsr.2012.10.018

[111] Adly, A. R., Aleem, S. H. E. A., Algabalawy, M. A., Jurado, F., & Ali, Z. M. (2020), "A novel protection scheme for multi-terminal transmission lines based on wavelet transform", *Electric Power Systems Research*, *183*, 106286. https://doi.org/10.1016/j.epsr.2020.106286

[112] Valabhoju, A., Yadav, A., Pazoki, M. *et al.,* "Optimized ensemble of regression tree-based location of evolving faults in dual-circuit line", *Neural Comput & Applic* **33**, 8795–8820 (2021). https://doi.org/10.1007/s00521-020-05628-6

[113] H. Mustafidah, S. Hartati, R. Wardoyo, and A. Harjoko, "Selection of most appropriate backpropagation training algorithm in data pattern recognition," arXiv preprint arXiv:1409.4727, 2014.

[114] D. W. Marquardt, "An algorithm for least-squares estimation of nonlinear parameters," Journal of the society for Industrial and Applied Mathematics, vol. 11, no. 2, pp. 431–441, 1963.

[115] M. T. Hagan and M. B. Menhaj, "Training feedforward networks with the marquardt algorithm," IEEE trans. neural netw., vol. 5, no. 6, pp. 989–993, 1994.

[116] M. Akke and J. T. Thorp, "Some improvements in the three phase differential equation algorithm for fast transmission line protection," IEEE Trans. Power Deliv., vol. 13, no. 1, pp. 66–72, 1998.

[117] Shukla, S.K., Koley, E. & Ghosh, S., "A hybrid wavelet–APSO–ANN-based protection scheme for six-phase transmission line with real-time validation", *Neural Comput & Applic* **31**, 5751–5765 (2019). https://doi.org/10.1007/s00521-018-3400-x

[118] Tirupathi Rao Althi, Ebha Koley, Subhojit Ghosh & Sunil Kumar Shukla (2023), "Six Phase Transmission Line Protection Using Bat Algorithm Tuned Stacked Sparse Autoencoder," Electric Power Components and Systems, 51:2, 113-130, DOI: 10.1080/15325008.2022.2163519

[119] A. Hooshyar, R. Iravani, "Microgrid Protection," Proc. IEEE. 105 (2017) 1332–1353. https://doi.org/10.1109/JPROC.2017.2669342.

[120] J.C. Quispe, E. Orduña, "Transmission line protection challenges influenced by inverter-based resources: a review," Prot. Control Mod. Power Syst. 7 (2022) 1–17. https://doi.org/10.1186/s41601-022-00249-8.

[121] A.F. Tazay, A.M.A. Ibrahim, O. Noureldeen, I. Hamdan, "Modeling, control, and performance evaluation of grid-tied hybrid pv/wind power generation system: Case study of gabel el-zeit region, egypt," IEEE Access. 8 (2020) 96528–96542. https://doi.org/10.1109/ACCESS.2020.2993919.

[122] L. Wang, Q.S. Vo, A.V. Prokhorov, "Stability Improvement of a Multimachine Power System Connected With a Large-Scale Hybrid Wind-Photovoltaic Farm Using a Supercapacitor," IEEE Trans. Ind. Appl. 54 (2018) 50–60. https://doi.org/10.1109/TIA.2017.2751004.

[123] L. Breiman, "Bagging predictors," Mach. Learn. 24 (1996) 123–140. https://doi.org/10.1023/A:1018054314350.

[124] R. Polikar, "Ensemble based systems in decision making," IEEE Circuits Syst. Mag. 6 (2006) 21–44. https://doi.org/10.1109/MCAS.2006.1688199.

[125] MATLAB, Tree Baggers Document, (n.d.). https://in.mathworks.com/help/stats/treebagger.html.

[126] W.-Y. Loh, "Classification and Regression Trees," Wiley Interdiscip. Rev. Data Min. Knowl. Discov. 1 (2010) 14–23. https://doi.org/https://doi.org/10.1002/widm.8.

[127] E. Koley, S.K. Shukla, S. Ghosh, D.K. Mohanta, "Protection scheme for power transmission lines based on SVM and ANN considering the presence of non-linear loads," IET Gener. Transm. Distrib. 11 (2017) 2333–2341. https://doi.org/10.1049/iet-gtd.2016.1802.

[128] A. Srivastava, S.K. Parida, "A Robust Fault Detection and Location Prediction Module Using Support Vector Machine and Gaussian Process Regression for AC Microgrid," IEEE Trans. Ind. Appl. 58 (2022) 930–939. https://doi.org/10.1109/TIA.2021.3129982.

[129] M. Manohar, E. Koley, S. Ghosh, "Stochastic Weather Modeling-Based Protection Scheme for Hybrid PV-Wind System with Immunity against Solar Irradiance and Wind Speed," IEEE Syst. J. 14 (2020) 3430–3439. https://doi.org/10.1109/JSYST.2020.2964990.

[130] M.N. Uddin, N. Rezaei, M.S. Arifin, "Hybrid Machine Learning-Based Intelligent Distance Protection and Control Schemes With Fault and Zonal Classification Capabilities for Grid- Connected Wind Farms," IEEE Trans. Ind. Appl. 59 (2023) 7328–7340. https://doi.org/10.1109/TIA.2023.3302836.

[131] S. Biswas, P.K. Nayak, "A New Approach for Protecting TCSC Compensated Transmission Lines Connected to DFIG-Based Wind Farm," IEEE Trans. Ind. Informatics. 17 (2021) 5282–5291. https://doi.org/10.1109/TII.2020.3029201.

[132] J. Dekker, M. Nthontho, S. Chowdhury, and S. P. Chowdhury (2012) “Economic analysis of PV/diesel hybrid power systems in different climatic zones of South Africa.” Int. J. Electr. Power Energy Syst., vol. 40, no. 1, pp. 104–112, Sep. 2012.

[133] "IEEE Guide for Design, Operation, and Integration of Distributed Resource Island Systems with Electric Power Systems", in *IEEE Std 1547.4-2011*, pp. 1-54, 20 July 2011.

[134] Z. A. Obaid, L. M. Cipcigan, L. Abrahim, and M. T. Muhssin (2019) “Frequency control of future power systems: reviewing and evaluating challenges and new control methods.” Journal of Modern Power Systems and Clean Energy, vol. 7, no. 1, pp. 9–25, 2019.

[135] H. Bevrani, M. R. Feizi and S. Ataee (2016), “Robust Frequency Control in an Islanded Microgrid: H_∞ and μ Synthesis Approaches”, IEEE Transactions on Smart Grid, vol. 7, no. 2, pp. 706-717, March 2016.

[136] A. H. Hajimiragha and M. R. D. Zadeh (2013), “Research and development of a microgrid control and monitoring system for the remote community of Bella Coola: Challenges, solutions, achievements and lessons learned” in 2013 IEEE International Conference on Smart Energy Grid Engineering (SEGE), 2013, pp. 1–6.

[137] Papathanassiou, S.A., and Papadopoulos, M.P. (2001) “Dynamic characteristics of autonomous wind-diesel systems”, Proc.Elsevier, vol. 23, pp. 293–311, 2001.

[138] Dong-Jing, L., and Li, W. (2008) “Small-signal stability analysis of an autonomous hybrid renewable energy power generation/energy storage system part I: Time domain simulations”, IEEE Trans. on energy conversion, Vol. 23, No. 1, pp. 311-320, 2008.

[139] M. A. El-Hameed and A. A. El-Fergany (2016), “Water cycle algorithm-based load frequency controller for interconnected power systems comprising non-linearity”, IET Generation, Transmission & Distribution, vol. 10, no. 15, pp. 3950-3961, 17 11 2016, doi: 10.1049/iet-gtd.2016.0699.

[140] A. Annamraju and S. Nandiraju (2018), “Robust Frequency Control in an Autonomous Microgrid: A Two-Stage Adaptive Fuzzy Approach”, Electr. Power Components Syst., vol. 46, no. 1, pp. 83–94, Jan. 2018.

[141] S. Izadkhast, P. Garcia-Gonzalez and P. Frías (2015), “An Aggregate Model of Plug-In Electric Vehicles for Primary Frequency Control”, IEEE Transactions on Power Systems, vol. 30, no. 3, pp. 1475-1482, May 2015.

[142] S. Mirjalili (2015), “Moth-Flame Optimization Algorithm: A Novel Nature-inspired Heuristic Paradigm”, Knowledge-Based Systems, vol. 89, pp. 228-249, 2015.

[143] S. Debbarma and A. Dutta (2017), "Utilizing Electric Vehicles for LFC in Restructured Power Systems Using Fractional Order Controller", IEEE Transactions on Smart Grid, vol. 8, no. 6, pp. 2554-2564, Nov. 2017.

[144] L. Huang, B. Yang, X. Zhang, L. Yin, T Yu and Z Fang (2019), "Optimal power tracking of doubly fed induction generator-based wind turbine using swarm moth–flame optimizer", Transactions of the Institute of Measurement and Control., vol. 41, no. 6, pp. 1491-1503, 2019.

[145] S. Reddy, L. Panwar, B. Panigrahi and R. Kumar (2018), "Solution to unit commitment in power system operation planning using binary coded moth flame optimization algorithm: a flame selection based computational technique", Journal of Computational Science, vol. 25, pp. 298-317, 2018, https://doi.org/10.1016/j.jocs.2017.04.011.

[146] S. Izadkhast, P. Garcia-Gonzalez and P. Frías (2015), "An Aggregate Model of Plug-In Electric Vehicles for Primary Frequency Control", IEEE Transactions on Power Systems, vol. 30, no. 3, pp. 1475-1482, May 2015.

[147] S. Saremi S. Mirjalili and A. Lewis (2017), "Grasshopper Optimisation Algorithm: Theory and application", Adv. Eng. Softw. vol. 105, pp. 30-47, 2017.

[148] P. Savsani, R. L. Jhala and V. J. Savsani (2016), "Comparative Study of Different Metaheuristics for the Trajectory Planning of a Robotic Arm.", IEEE Systems Journal, vol. 10, no. 2, pp. 697-708, June 2016, doi: 10.1109/JSYST.2014.2342292.

******

Publications

List of Published Papers

1) Gotte Vikram Raju & Nandiraju Venkata Srikanth (2023), "Single fuzzy inference based fault detection and classification protection scheme for different types of short circuit faults on double circuit transmission lines", International Journal of Modelling and Simulation, DOI: 10.1080/02286203.2023.2193912. (Taylor and Francis) [ESCI Indexed, Impact factor = 3.1].
2) Vikram Raju, G., & Venkata Srikanth, N. (2024), "Mono ANN Module Protection Scheme and Multi ANN Modules for Fault Location Estimation for a Six-Phase Transmission Line Using Discrete Wavelet Transform", Journal of Operation and Automation in Power Engineering, Volume 12, Issue 4, Pages 337-351, December 2024, DOI: 10.22098/JOAPE.2023.11690.1874. (University of Mohaghegh Ardabili, Iran) [Scoupus Indexed].

List of Communicated Papers

1) Gotte Vikram Raju & Nandiraju Venkata Srikanth, "A Novel Protection Scheme for Transmission Lines Connected to Solar Photovoltaic and Wind Turbine Farms using Fuzzy Logic Systems and Bagged Ensemble Learning" is communicated to "Electrical Engineering" (Springer Nature), (Status: Under Review, R1 Submitted)
2) Gotte Vikram Raju & Nandiraju Venkata Srikanth, "Frequency Control of an Islanded Microgrid with Multi-stage PID Control Approach Using Moth Flame Optimization Algorithm" is communicated to Electrical Engineering, {Special Issue on "Design and Control of Hybrid Energy System and Energy Storage for Sustainable Energy Solutions"} (Springer Nature). (Status: Under Review).

*****

Appendices

Appendix – I

Power system operating conditions and system parameters

Source data at both sending and receiving ends of the line.		**Transmission line parameter data (Transmission line length: 300 km (divided into three equal sections))**				
Nominal source voltage and system frequency	400 kV and 50 Hz	Parameter	Positive	Negative	Zero	Mutual zero
Pre-fault power flow angle of the system	15°	Resistance (Ω/km)	0.0275	0.0275	0.275	0.21
Short circuit capacity	1.25 GVA	Inductance (H/km)	1.002e-03	1.002e-03	3.268e-03	2.0e-03
Base voltage	400 kV	Capacitance (F/km)	13e-09	13e-09	8.5e-09	-5.0e-09
X/R ratio	10					

Appendix – II

Six-phase transmission line parameters

Resistance matrix (ohm/km):

0.1960	0.1241	0.1186	0.1185	0.1238	0.1338
0.1241	0.1766	0.1104	0.1103	0.1150	0.1238
0.1186	0.1104	0.1675	0.1060	0.1103	0.1185
0.1185	0.1103	0.1060	0.1675	0.1104	0.1186
0.1238	0.1150	0.1103	0.1104	0.1766	0.1241
0.1338	0.1238	0.1185	0.1186	0.1241	0.1960

Inductance matrix (H/km):

1.9717e-03	8.2710e-04	7.0988e-04	6.5597e-04	6.7658e-04	7.0263e-04
8.2710e-04	2.0228e-03	8.6436e-04	7.1351e-04	6.9801e-04	6.7658e-04
7.0988e-04	8.6436e-04	2.0475e-03	7.7846e-04	7.1351e-04	6.5597e-04
6.5597e-04	7.1351e-04	7.7846e-04	2.0475e-03	8.6436e-04	7.0988e-04
6.7658e-04	6.9801e-04	7.1351e-04	8.6436e-04	2.0228e-03	8.2710e-04
7.0263e-04	6.7658e-04	6.5597e-04	7.0988e-04	8.2710e-04	1.9717e-03

Capacitance matrix (F/km):

8.5463e-09	-1.5037e-09	-5.9333e-10	-3.4736e-10	-4.8782e-10	-7.6412e-10
-1.5037e-09	8.5282e-09	-1.4971e-09	-4.9062e-10	-4.7051e-10	-4.8782e-10
-5.9333e-10	-1.4971e-09	8.4771e-09	-8.1902e-10	-4.9062e-10	-3.4736e-10
-3.4736e-10	-4.9062e-10	-8.1902e-10	8.4771e-09	-1.4971e-09	-5.9333e-10
-4.8782e-10	-4.7051e-10	-4.9062e-10	-1.4971e-09	8.5282e-09	-1.5037e-09
-7.6412e-10	-4.8782e-10	-3.4736e-10	-5.9333e-10	-1.5037e-09	8.5463e-09

Appendix – III

Data of transmission line parameters (200 km line length)		
Parameter	**Positive and negative**	**Zero**
Resistance (Ω/km)	0.0275	0.275
Inductance (H/km)	1.002e-03	3.268e-03
Capacitance (F/km)	13e-09	8.5e-09

Appendix – IV

PV Data		**Module Specifications**	
Rated power	50 MW (1 MW units)	PV module type	1Soltech 1STH-350-WH
L_B	1.7 mH	Rated power	349.59 W
Switching frequency	2.1 kHz	Open circuit voltage (V_{oc})	51.5 V
$R_{filter1}$	0.0015 pu	Short circuit current (I_{sc})	9.4 A
$L_{filter1}$	0.15 pu	Voltage at max. power point	43 V
$Q_{filter1}$	0.1 pu	Current at max. power point	8.13 A
V_{dc1}	1200 V	Temperature coefficient of V_{oc}	-0.36% /°C
DC link capacitor	16.45 mF	Temperature coefficient of I_{sc}	0.09% /°C
Voltage regulator (PI-1)	K_p = 7 and K_i = 800		
Current regulator (PI-2)	K_p = 0.3 and K_i = 20		

Appendix – V

DFIG based wind farm data			
Rated power of wind farm	50 MW	No. of pole pairs (p)	3
Rated power of wind turbine	1.5 MW	DC link voltage (V_{dc2})	1150 V
Wind turbine inertia constant (H_t)	4.32 s	$R_{filter2}$	0.003 pu
Nominal power generator	1.5/0.9 MW	$L_{filter2}$	0.3 pu
Inertia constant (H_g)	0.685 s	$Q_{filter2}$	0.08 pu
Nominal stator voltage	575 V	Switching frequency (GSC)	2.7 kHz
Nominal rotor voltage	1975 V	PI-3 (GSC)	K_p = 8 and K_i = 400
Stator resistance (R_s)	0.023 pu	PI-4 (GSC)	K_p = 0.83 and K_i = 5
Rotor resistance (R_r)	0.016 pu	Switching frequency (RSC)	1.62 kHz
Stator inductance (L_s)	0.18 pu	Voltage regulator (RSC)	K_p = 5 and K_i = 20
Rotor inductance (L_r)	0.16 pu	PI-5 (RSC)	K_p = 0.6 and K_i = 8
Magnetizing inductance (L_m)	2.9 pu		

Appendix – VI

Optimization Data		
S. No.	Optimization Algorithm	Data
1.	MFO [145]	No. of moths = 100, No. of iterations = 50
2.	GOA [147]	Population size = 100, No. of iterations = 50, Adaptation factor (c) = [0.0001 – 4], Attraction factor (f) = 0.5, Attractive length scale (l) = 1.5
3.	TLBO [148]	Population size = 100, No. of iterations = 50, TF = [2 – 1
4.	PSO [70]	Population size = 100, No. of iterations = 50, Inertia weight (w) = 0.65, Cognitive factors (C_1, C_2) = 2

Appendix – VII

PHEV Data

$SOC_1 = 0.1$, SOC_2= 0.2, SOC_3=0.8, SOC_4=0.9, N_{EV} = 600, T_{PHEV}=0.1 s, R_{av}=2.4 Hz/puMW, P_{Max} (Individual EV) = 5 kw, Δf_L= 0.1 Hz, Δf_U= 0.1 Hz.

*****